THERMODYNAMIC ANALYSIS AND OPTIMIZATION OF ORGANIC RANKINE CYCLES USING 1-BUTYLPYRIDINIUM TETRAFLUOROBORATE AS A GEOTHERMAL FLUID

SHABNAM KAZEMI

FACULTY OF ENGINEERING
UNIVERSITY OF MALAYA
KUALA LUMPUR

2020

THERMODYNAMIC ANALYSIS AND OPTIMIZATION OF ORGANIC RANKINE CYCLES USING 1-BUTYLPYRIDINIUM TETRAFLUOROBORATE AS A GEOTHERMAL FLUID

SHABNAM KAZEMI

THESIS SUBMITTED IN FULFILMENT OF THE REQUIREMENTS FOR THE DEGREE OF MASTER OF ENGINEERING SCIENCE

FACULTY OF ENGINEERING
UNIVERSITY OF MALAYA
KUALA LUMPUR

2020

UNIVERSITY OF MALAYA

ORIGINAL LITERARY WORK DECLARATION

Name of Candidate: **SHABNAM KAZEMI**

Matric No: **KGA160049**

Name of Degree: **MASTER OF ENGINEERING SCIENCE**

Title of Project Paper/Research Report/Dissertation/Thesis ("this Work"):

THERMODYNAMIC ANALYSIS AND OPTIMIZATION OF ORGANIC RANKINE CYCLES USING 1-BUTYLPYRIDINIUM TETRAFLUOROBORATE AS A GEOTHERMAL FLUID

Field of Study: **HEALTH, SAFETY & ENVIRONMENT (CHEMICAL PROCESS)**

I do solemnly and sincerely declare that:

(1) I am the sole author/writer of this Work;
(2) This Work is original;
(3) Any use of any work in which copyright exists was done by way of fair dealing and for permitted purposes and any excerpt or extract from, or reference to or reproduction of any copyright work has been disclosed expressly and sufficiently and the title of the Work and its authorship have been acknowledged in this Work;
(4) I do not have any actual knowledge nor do I ought reasonably to know that the making of this work constitutes an infringement of any copyright work;
(5) I hereby assign all and every rights in the copyright to this Work to the University of Malaya ("UM"), who henceforth shall be owner of the copyright in this Work and that any reproduction or use in any form or by any means whatsoever is prohibited without the written consent of UM having been first had and obtained;
(6) I am fully aware that if in the course of making this Work, I have infringed any copyright whether intentionally or otherwise, I may be subject to legal action or any other action as may be determined by UM.

Candidate's Signature Date: 10 August 2020

Subscribed and solemnly declared before,

Witness's Signature Date:

Name:

Designation:

THERMODYNAMIC ANALYSIS AND OPTIMIZATION OF ORGANIC RANKINE CYCLES USING 1-BUTYLPYRIDINIUM TETRAFLUOROBORATE AS A GEOTHERMAL FLUID

ABSTRACT

Organic Rankine cycle (ORC) is a promising technology for electricity generation by utilizing heat sources at low to moderate temperature that ranges between 80-350° C. In the present work, an ionic liquid (1-butylpyridinium tetrafluoroborate, $C_9H_{14}NBF_4$), a known green chemical and non-volatile compound with good thermal and chemical stability, significant heat capacity, low vapor pressure and a wide liquid temperature range (25 to 459 °C), is utilized as a geothermal fluid. Simulation and optimization were conducted for a basic organic Rankine cycle (basic ORC), a regenerative organic Rankine cycle (RORC) and a two-stage evaporative organic Rankine cycle (TSORC) by maximizing exergy efficiency and minimizing specific investment cost. The operating parameters considered in the optimization exercise were evaporative and regenerative temperatures, pinch point temperature difference of evaporators and the degree of superheat. Peng Robinson equation of state was used, and isobutane (R-600a) and butane (R-600) were selected as working fluids. Comparisons were made between the performance of ORCs when $C_9H_{14}NBF_4$ and water were individually used as a geothermal fluid. Utilization of an ionic liquid improved the performance of the three ORC configurations with the best performance generated from a basic ORC with exergy efficiency of 82.35% (R-600) and 87.70 %(R-600a). From an economic viewpoint, the amount of specific investment cost (SIC) is comparatively lower when ionic liquid is used as a geothermal fluid.

Keywords: ionic liquid, geothermal, organic Rankine cycle, optimization, thermo-economic analysis

ANALISIS TERMODINAMIK DAN PENGOPTIMUMAN KITARAN RANKINE ORGANIK DENGAN MENGGUNAKAN 1-BUTYLPYRIDINIUM TETRAFLUOROBORATE SEBAGAI CECAIR GEOTHERMAL

ABSTRAK

Kitaran Rankine Organik (ORC) adalah teknologi yang menjana elektrik dengan menggunakan sumber haba antara berjulat rendah ke sederhana (80 – 350 °C). Dalam kajian ini, cecair ionik (1-butilpyridinium tetrafluoroborate, $C_9H_{14}NBF_4$), sebatian kimia hijau yang tidak mudah meruap dengan kestabilan terma dan kimia yang baik, kapasiti haba yang ketara, tekanan wap rendah dan julat suhu cecair yang besar (25 hingga 459 °C), digunakan sebagai cecair geothermal. Simulasi dan pengoptimuman dijalankan untuk kitaran Rankine organik asas (ORC asas), kitaran Rankine organik regeneratif (RORC) dan kitaran Rankine organik penguapan dua tahap (TSORC) dengan memaksimumkan kecekapan tenaga dan meminimumkan kos pelaburan spesifik. Parameter operasi yang dipertimbangkan dalam pengoptimuman adalah suhu penyejatan dan regeneratif, perbezaan suhu titik cubit pemeluap dan tahap pemanasan lampau. Persamaan Peng- Robinson digunakan dan isobutana (R-600a) dan butana (R-600) dipilih sebagai cecair kerja. Prestasi ORC apabila $C_9H_{14}NBF_4$ digunakan sebagai cecair geotermal, dibandingkan dengan prestasi ORC apabila air digunakan. Penggunaan cecair ionik didapati meningkatkan prestasi ketiga-tiga konfigurasi ORC dengan prestasi terbaik terhasil dari ORC asas dengan keberkesanan eksergi 82.35% (R-600) dan 87.70% (R-600a). Dari sudut pandangan ekonomi, jumlah kos pelaburan spesifik (SIC) adalah lebih rendah apabila cecair ionik digunakan sebagai cecair geoterma.

kata kunci: cecair ionik, geotermal, kitaran Rankine organik, pengoptimuman, analisis thermo-ekonomi

ACKNOWLEDGEMENTS

The success of this project required a lot of guidance and assistance from many people, and I am extremely privileged to have got this all guidance and assistance along my long journey. All that I have done is only due to such supervision and assistance, and I would not forget to thank them.

I wish to express my gratitude to my dear supervisors, encik Mohamad Iskandar Mohammad Noor and Dr. Teoh Wen Hui for providing me an opportunity to do the project work in such a reputable University and giving me all the support and guidance, which made me complete the project duly. I am extremely thankful to Dr. Teoh Wen Hui for providing such unconditional support and believing in me throughout the research.

I am grateful to thank my parents for staying patient, and finally, I would like to express my loving appreciation to my husband, Pouya Darvish, and my sister, Neda Kazemi, who were with me and for me, especially during the tenure of my MEng study. To them, I humbly dedicate this piece of study.

TABLE OF CONTENTS

LIST OF FIGURES

LIST OF TABLES

LIST OF SYMBOLS AND ABBREVIATIONS

A_{HX}	:	heat exchangers' surface area (m^2)
B_1, B_2	:	constant parameters of equipment in bare module cost
C_1, C_2, C_3	:	constant parameters of equipment in bare module cost
$C_{0,t}$	:	initial cost of the turbine ($/W)
$C_{0,P}$	:	initial cost of the pump ($/W)
C_{HX}	:	costs of the heat exchangers ($/W)
cond	:	condenser/condensation
csi, cso	:	heat sink (cooling fluid) inlet/outlet
d_i , d_o	:	inner and outer diameter of the tube
$D.S$	:	degree of superheat (K)
evap	:	evaporator/evaporation
$\dot{Ex}$	:	exergy flow rate (kW)
$\dot{EX}_p$	:	exergy flow rate in the pump (kW)
$\dot{EX}_h, \dot{Ex}_{available}$	:	exergy flow rate in the heat source (kW)
$\dot{EX}_{wf,evap}$	:	exergy flow rate in the evaporator (kW)
$\dot{Ex}_{wf,cond}$	:	exergy flow rate in the condenser (kW)
$\dot{EX}_t$	:	available exergy in the expansion process (kW)
$\dot{Ex}_{cond}$	:	available exergy in the condensation process (kW)
$F_{P,HX}$	:	heat exchangers' pressure factor
$F_{M,HX}$	:	heat exchangers' material factor
$F_{M,t}$	:	material factor of the turbine
$F_{M,P}$	:	material factor of the pump
$F_{P,P}$	:	pump's pressure factor

F_S	:	correction factor of overhead cost
F	:	Heat exchangers' correction factor
f	:	friction factor
gen	:	generator
h	:	specific enthalpy (kJ kg^{-1})
$h_{p,out}^{is}$	:	isentropic enthalpy of the outlet fluid from the pump (kJ kg^{-1})
$h_{p,in}$, $h_{p,out}$	:	actual inlet/outlet enthalpy of the working fluid in pumping process (kJ kg^{-1})
$h_{wf,in}^{evap}$, $h_{wf,out}^{evap}$	:	actual enthalpy of the working fluid to/from the evaporator (kJ kg^{-1})
h_{hsi} , h_{hso}	:	enthalpy of geothermal fluid to/from the evaporator (kJ kg^{-1})
$h_{t,in}$, $h_{t,out}$	:	enthalpy of the vapor to/from the turbine (kJ kg^{-1})
$h_{t,out}^{is}$	:	isentropic enthalpy of the outlet vapor from the turbine (kJ kg^{-1})
h_{wf}^{cond}	:	enthalpy of the operating fluid in the condenser (kJ kg^{-1})
$h_{wf,in}^{cond}$, $h_{wf,out}^{cond}$	:	enthalpy of the internal and external working fluid in the condensation process (kJ kg^{-1})
h_{csi} , h_{cso}	:	enthalpy of internal and external cooling fluid (kJ kg^{-1})
h_h , h_c	:	enthalpy of geothermal fluid and cooling fluid (kJ kg^{-1})
$h_{wf,in}^{reg}$, $h_{wf,out}^{reg}$	:	enthalpy of the inlet/outlet operating fluid to/from the regenerative (kJ kg^{-1})
h_i , h_o	:	heat transfer coefficient inside/outside of the tube (W m^{-2} K^{-1})
hsi, hso	:	heat source (geothermal fluid) inlet/outlet
h/c	:	heat source/heat sink or hot/cold
ILs	:	ionic liquid solvent
IHX	:	internal heat exchanger
in/out	:	inlet/outlet
i/o	:	inside/outside
is	:	isentropic
K_1, K_2, K_3	:	constants parameters of equipment in bare module cost

K	:	conductive heat transfer coefficient in heat exchangers (W m^{-2} K^{-1})
$\dot{m}$	:	mass flow rate (kg s^{-1})
$\dot{m}_{wf}$	:	working fluid mass flow rate (kg s^{-1})
$\dot{m}_h$, $\dot{m}_c$	:	mass flow rate of geothermal fluid and cooling fluid (kg s^{-1})
Nu	:	Nusselt number
ORC	:	organic Rankine cycle
p	:	pump
P	:	pressure (bar)
P_C	:	critical pressure (bar)
P_{HX}	:	surface pressure of the heat exchangers (bar)
Pr	:	Prandtl number
PPTD	:	pinch point temperature difference (K)
$\dot{Q}$	:	heat transfer flow rate (kW)
$\dot{Q}_{h,evap}$, $\dot{Q}_h$	:	heat transfer flow rate in the evaporator (kW)
$\dot{Q}_c$	:	heat transfer flow rate in the condenser (kW)
$\dot{Q}_{reg}$	:	heat transfer flow rate in the regenerative (kW)
Q_{hx}	:	heat transfer flow rate by the heat exchangers (W)
R	:	universal gas constant ($J.K^{-1}.mol^{-1}$)
$R_{f,i}$, $R_{f,o}$	:	internal / external sediment resistance factor of the pipe
Re	:	Reynolds number
RC	:	Rankine cycle
RORC	:	regenerative organic Rankine cycle
reg	:	regenerative
S	:	specific entropy (kJ kg^{-1} K^{-1})
SIC	:	specific investment cost ($ W^{-1})

$s_{p,in}$, $s_{p,out}$	:	entropy of the inlet/outlet fluid to/from the pump (kJ kg^{-1} K^{-1})
$s_{wf,in}^{evap}$, $s_{wf,out}^{evap}$	:	entropy of the inlet/outlet working fluid to/from the evaporator (kJ kg^{-1} K^{-1})
s_{hsi}, s_{hso}	:	entropy of the inlet/outlet of a geothermal fluid to/from the evaporator (kJ kg^{-1} K^{-1})
$s_{t,in}$, $s_{t,out}$	:	entropy of the inlet/outlet vapor in the turbine (kJ kg^{-1} K^{-1})
s_{csi}, s_{cso}	:	entropy of the inlet/outlet cooling fluid in the condenser (kJ kg^{-1} K^{-1})
T, Temp.	:	temperature (K)
T_h , T_L	:	temperature of geothermal fluid/cooling fluid (K)
$T_{h,in}$, $T_{h,out}$	:	inlet / outlet temperature of a geothermal fluid (K)
T_C	:	critical temperature/pressure (K)
$T_{c,in}$, $T_{c,out}$		inlet /outlet temperature of the cooling fluid (K)
T_r	:	reduced temperature
T_0	:	ambient temperature (K)
TC_B	:	total bare module cost
TSORC	:	two stage evaporative organic Rankine cycle
t	:	turbine
ΔT_{Lm}	:	logarithmic mean temperature difference (K)
U	:	overall heat transfer coefficient in heat exchangers (W m^{-2} K^{-1})
$\dot{W}$	:	output/input power (kW)
$\dot{W}_p$	:	input power of the pump (kW)
$\dot{W}_p^{elec}$	:	motor output power of the pump (kW)
$\dot{W}_t$	:	turbine output power/ useful exergy (kW)
$\dot{W}_t^{elec}$	:	generator output power (kW)
$\dot{W}_{net}$, $\dot{Ex}_{useful}$	:	net mechanical output power (kW)
wf	:	working fluid
X	:	vapor quality

β	:	coefficient of linear weighted evaluation function
α	:	coefficient of linear weighted evaluation function
η	:	efficiency (%)
η_{is}^{p}	:	pump isentropic efficiency (%)
η_{motor}	;	motor efficiency of the pump (%)
η_{is}^{t}	:	turbine isentropic efficiency (%)
η_{th}	:	first-law efficiency /thermal efficiency (%)
η_{ex}	:	second-law efficiency /exergy efficiency (%)

CHAPTER 1: INTRODUCTION

1.1 Background

Energy is one of the indispensable factors for economic growth. However, energy conversion and transformation can contribute to the degradation of the environment. The consumption of fossil fuels and the encroachment on the environment from greenhouse gas (GHG) emissions in recent decades has led to global warming, depletion of the ozone layer and the contamination of water bodies. The onward march for sustainability has led to the development and use of renewable energy sources. Despite that, more than 75% of the world's energy need is supplied from fossil fuels (Lee et al., 2016).

For many decades, a large amount of electricity was generated efficiently and economically by central power stations consists of a large-scale hydro (Weiyao Tang et al., 2018). In large-scale hydropower, the power is generated in internal combustion engines by burning fossil fuels or nuclear reactors then sent to the load centers. Despite the advantages of centralized power stations in power production, there are not cost-effective due to the long-distance transmission (Moran et al., 2018). Nowadays, power production and energy consumption have become more severe as time passes, and the demand for energy production is increasing due to population growth compared to the past. Therefore, modern power stations for electricity generation on a large scale have been designed and commercialized (Moran et al., 2018).

The most common systems used for converting renewable heat into electricity are Rankine cycles (RCs), (Kazemi & Samadi, 2016). A Rankine cycle is a thermodynamic cycle consisting of four main components: the feed pump, a vaporizer, a turbine, and a condenser connected via a working fluid in a closed-loop to generate electricity by heat conversion (thermal energy) into useful work (electrical energy), (Kazemi & Samadi, 2016). Typically, for a low to medium-grade heat temperature ranging between 80 ^{o}C and

350 ºC, an organic Rankin cycle (ORC) is utilized (Kazemi & Samadi, 2016; Taylor et al., 2013).

As the ORC cycles are compatible with different renewable heat sources (e.g., geothermal energy, solar energy, wind, biomass energy, and industrial process waste heat), these have captured the interest of researchers recently (Ashouri et al., 2017; Karimi & Mansouri, 2018; Kazemi & Samadi, 2016; Kazemi et al., 2020; Lin et al., 2017; Navarro-Esbrí et al., 2019). Energy sources such as wind energy can be harnessed using wind turbines. However, wind turbines are very noisy and can cause the destruction of landscapes (Deshmukh et al., 2019). Solar energy, on the other hand, has a time limitation for utilization (Wang et al., 2019). Geothermal power, a significant renewable energy source, can be employed, independent of season and time of day (Samadi & Kazemi, 2020).

Generally, geothermal power has been classified into three categories; these being, low temperature (<90°C), medium temperature (90 °C – 150 °C) and high temperature (>150 °C), (Dai & Chen, 2008; Sui et al., 2019). In addition, geothermal energy is clean, renewable and permanent, cost-effective, and has no constructional problems that are observed in the build-up of other energy sources, such as the need for creating a tunnel, open pits, rubbish clusters or having to deal with oil spills (DiPippo, 2008c; Sui et al., 2019). This ground source of energy could be utilized in many applications. It can be tapped into residential places to supply the necessary power for heating and cooling water or in businesses for electricity generation. In the case of heating residential homes, pipes are designed and buried into a geothermal reservoir at a depth where the earth's temperature remains constant, which is usually several meters below ground.

1.2 Problem statement

In recent decades, the impact of various operating conditions having significant effects on the performance of different ORC configurations was employed by many researchers (Hærvig et al., 2016; Saloux et al., 2018; Sun et al., 2017; Vescovo & Spagnoli, 2017; Xu et al., 2018). These studies include the selection of working fluids, studies on heat source temperatures and operating pressures, and the addition of external equipment such as the inclusion of regeneration or extra heat exchanger to a basic ORC (Braimakis & Karellas, 2017, 2018; Li, Zhang, et al., 2015; Wang et al., 2017; Zeynali et al., 2019). In this regard, optimal fluids selections are highly dependent on the heat source characteristic (Bao & Zhao, 2013; Chen et al., 2010; Martínez-Gomez et al., 2017; Saleh et al., 2007). Moreover, each fluid has different thermodynamic properties which could directly affect the efficiency of a cycle. The difference in fluid properties such as molecular structures plays a crucial role in increasing an ORC efficiency (Zhai et al., 2014) while other properties such as critical temperature are not vital for performance improvement (Liu et al., 2004).

In the initial modifications to the basic ORCs such as the inclusion of extra heat exchanger (regeneration or evaporator) and the use of various working fluids, thermodynamic performances tended to improve. However, as more and more changes (inclusion of extra heat exchanger and the use of various working fluids), were made to the basic ORC, the costs of the cycle increase; rendering the changes uneconomical. With a ceiling in cycle's performances (energy and exergy efficiencies), even with various modifications to the ORCs, the next improvement may come from the heat sources. In the case of a geothermal heat source, thermodynamic improvements may be derived from a higher energy density being carried from the geothermal source into the ORC system, requiring mayhap, a change in a geothermal fluid. Hence, the present work aims to

explore the use of an alternate geothermal fluid and look into its influence on the thermodynamic performances of various ORC systems.

1.3 Objectives

The objectives of the present study are as follows:

- Evaluate the thermodynamic performances of a basic ORC, RORC, and TSORC in terms of energy and exergy efficiencies with ionic liquid and water as geothermal fluids and R-600 and R-600a as working fluids.
- Conduct optimization on a basic ORC, RORC and TSORC based on thermo-economic objective function by maximizing the second law of thermodynamics (exergy efficiency) and minimizing the specific investment cost (SIC).
- Determine the effect of ionic liquid as a geothermal fluid on the performances of ORC configurations in comparison with water.

1.4 Scope

The present work aims to explore the use of an alternate geothermal fluid and cooling fluid, 1-butylpyridinium tetrafluoroborate, $C_9H_{14}NBF_4$, an ionic liquid (IL), and look into its influence on three ORC configurations; basic ORC, RORC and TSORC from thermodynamic (energy and exergy efficiency), economic (SIC) and thermo-economic (multi-objective functions) perspectives. Peng Robinson equation of state (PR EOS) and bare module cost will be used to evaluate the thermodynamic and economic behavior of cycles. Besides, a linear weighted evaluation function will be employed to investigate the thermodynamic and economical performance of the cycles simultaneously. In addition, the performances of considered cycles with water as a geothermal fluid are going to be evaluated, and the outcomes of optimization will be compared between IL and water under the same circumstances.

CHAPTER 2: LITERATURE REVIEW

In recent decades, fossil fuels consumption and greenhouse gas (GHG) emissions have been the significant causes of environmental issues such as global warming, ozone layer depletion and water contamination. Therefore, the replacement of fossil fuels with renewable energy resources could be a vital step in reducing harmful environmental impacts. This chapter will define the nature of geothermal energy and its pros and cons. Different types of geothermal power plants and their applications in ORCs are also discussed.

The previous investigations of the ORCs in terms of operating temperatures and pressures, cycle's architectures, working fluid nomination, and additional cycle's equipment (regenerative and/evaporator) are compared. Additionally, the properties of the proposed geothermal fluid (1-butylpyridinium tetrafluoroborate, $C_9H_{14}NBF_4$) is explained broadly.

2.1 Renewable energy

Renewable energies are the types of energies re-created or renewed by the environment in a short period of time (Harjanne & Korhonen, 2018). In recent years, due to the fact that non-renewable energy sources (fossil fuels) are running out, the utilization of renewable resources (e.g. geothermal, solar, wind, hydrothermal, and etc.) are more significant (Harjanne & Korhonen, 2018; Tiwari et al., 2017).

In 2006, 18.4% of the world's energy was generated by renewable energy, especially geothermal energy (Abolhosseini et al., 2014). Table 2. 1 demonstrates the comparison of four different renewable energies according to the annual electricity production by each source. As can be seen, geothermal energy was by far the most significant energy source

in electricity generation (Abolhosseini et al., 2014; Holm et al., 2010; Signanini & Giancarlo, 2001).

Table 2. 1: The annual contribution of renewable energies (Holm et al., 2010)

Types of renewable energy	*Installed capacity*		*Generated energy per year*	
	(MW)	**(%)**	**(GWh/Y)**	**(%)**
Geothermal	6.456	61	37.976	86
Wind	3.517	33	4.878	11
Solar	0.366	3	0.897	2
Tide	0.261	3	0.601	1
Total	10.600	100	44.352	100

2.2 Geothermal Energy

2.2.1 Definition of Geothermal

Geothermal is made up of two parts of geo, and therme. Geo derived from the Greek word means the earth, and therme implies for the heat (Lukawski et al., 2018; Rypkema, 2018). Up to 4000 kilometres under the earth's surface, two core layers with an estimated temperature between 5000 and 11000 Fahrenheit (ºF) consisting of extremely hot molten iron is surrounded by a solid iron centre. Near the earth's core, the mantle is located with the thickness of 1800 miles, containing stone and a large amount of magma. After mantle, earth and insulating crust covered the outermost layer where the sheet rock is not continuous and is broken into pieces called plates (Lukawski et al., 2018; Rypkema, 2018).

Plate tectonics is a process that happens because of pushing and drifting apart (about one inch) of slab continent and ocean per year. As a result of plate tectonics process, the crust is broken and allows the plumes magma reaching the surface in the form of volcanoes. Around 1000 to 1 million years could be taken for magmas to be cooled down (Rypkema, 2018). Typically, magma remains under the surface and heats up the

surrounding stones and water, a typical source of water in the ground is rainwater that has penetrated deep into the earth. Some of the heated water flows through the faults and breakdowns to the surface and then known as hot springs and waterfalls. However, a large amount of water is trapped underground between fractures and porous rocks, forming geothermal reservoirs (Dye, 2012; Rypkema, 2018)

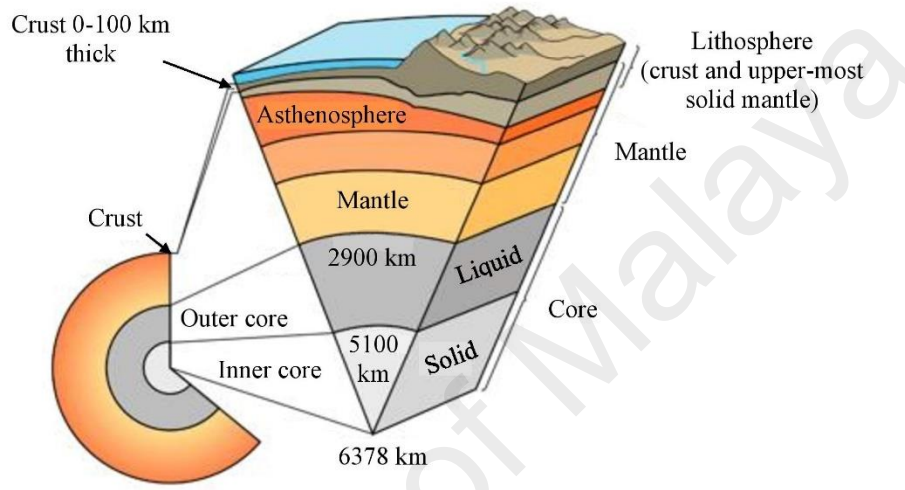

Figure 2. 1: The earth's crust, mantle

2.2.2 Advantages and disadvantages of geothermal energy

Geothermal heat is independent of season and time of day and has been proven to be clean due to reduced production of hydrogen sulfide (H_2S) at over 99.9%, reduced CO_2 emissions, being renewable and permanent, cost-effective, having fewer construction problems for a power plant and without additional challenges such as having to create tunnels and open pits or having to deal with rubbish clusters and oil spills (DiPippo, 2008c; Lukawski et al., 2018). Moreover, the price of electricity generates by geothermal power plants is predictable compared to burning fuel, and therefore, it remains stable over the life of the project. Table 2.2 compares the effect of geothermal energy with other thermal energies from an environmental viewpoint. As can be seen, data shows that geothermal power plants emit less air pollution than all other thermal energy sources. To

be precise, the total emission of non-condensable gas (NO_x, SO_2, CO_2, and particulate matter) from geothermal resources is less than five percent of the total steam emitted.

Table 2.2: Comparing the environmental impacts of geothermal emissions with other thermal energies (Kagel et al., 2005)

	TYPES OF AIR EMISSIONS			
Environmental Effects	**Nitrogen Oxide (NO_x)**	**Sulfur Dioxide (SO_2)**	**Carbon Dioxide (CO_2)**	**Particulate Matter(PM)**
	-lung irritation -coughing -smog formation -water quality deterioration	-Wheezing chest tightness -Respiratory illness -Eco-system damage	-Rising sea levels -Flood risks -Glacial melting -Global warming	-Asthma -Bronchitis -Cancer -Atmospheric deposition -Visibility impairment
All Types (Ib/MWh) **Flash Steam** **Binary-** **Flash/Binary**	0 0 0	0 - 0.35 0.35 0	0-88.8 60 0	0 0 negligible
Coal Emissions (Ib/MWh)	4.31	10.39	2191	2.23
Oil Emissions (Ib/MWh)	4	12	16.72	not available
Natural Gas	2.96	0.22	1212	0.14
Emissions offset by Geothermal utilization (annually)	32×10^3 tons	78×10^3 tons	16×10^6 tons	17×10^3 tons

There are several potential environmental impacts from geothermal plants demonstrated in Table 2. 3. These environmental impacts include water contamination, air and noise pollution, greenhouse gases, etc. In terms of air pollution, geothermal steam contains non-condensable gases (e.g., hydrogen sulfide, H_2S, carbon dioxide, CO_2, methane, CH_4). Under normal conditions, the gases are isolated in a condenser, drawn into ejectors, and treated before release to the atmosphere (DiPippo, 2016g).

Reinjection of the waste brine into the reservoir could be the prominent way to prevent water contamination. The noise pollution is mainly attributed to well drilling and the testing of wells (DiPippo, 2016a). Cyclone silencers and rock mufflers are effective methods that could abate the geothermal steam noise. Land subsidence might happen

when large quantities of subsurface water are removed (e.g., Wairakei, New Zealand, over the 45 years of exploitation), (Bošnjaković et al., 2019; DiPippo, 2016f, 2016g).

Table 2. 3: Environmental concerns of geothermal power plant (DiPippo, 2016g)

Possible impact	***Details***	***Abatement Techniques***
Air Pollution	H_2S emissions	Several effective commercial systems in use
Water pollution	Surface discharge of waste brine; groundwater contamination	Reinjection
Noise pollution **Visual pollution**	Drilling; well testing Unsightly pipes and buildings in pristine areas	Rock mufflers; silencers Use low-level structures, paint equipment in blending colours
Land usage	Well pads, pipe routes, powerhouse, and substation	Much lower impact than conventional plants
Water usage **Land subsidence**	Cooling tower makeup (for binary plants only) Liquid removal from subsurface can lead to surface depressions	Use air-cooled condensers Rare, most dramatic at Wairakei, New Zealand
Greenhouse gases	CO_2 emissions	Very low emissions relative to conventional fossil plants
Loss of natural wonders	Thermal manifestations may disappear, e.g., the geysers at Beowawe and Steamboat Springs, Nevada	Do not develop resources in or adjacent to national parks

2.3 Suitable places for utilization of geothermal energy

Geothermal heat can only be used in areas where a continuous volcano or earthquake caused by heat transfer of a fluid such as steam, hot water or both to the Earth's surface (Lukawski et al., 2018). The areas with hot springs and geysers are the first areas where geothermal energy has been exploited and developed. Currently, almost all the geothermal energy is supplied from such places. Therefore, geothermal energy is formed where geological processes allow magma to reach the earth's surface, or to flow like lava as follows (Dye, 2012; Zheng & Chen, 2016).

- Oceanic-continental encounter (subduction) where two sheets collide, driven under other sheets that lead to destroying the shell (e.g., the ring of fire in the Pacific Ocean).
- Divergent sheets where melting materials come out and make a new crust (e.g., Great Rift Valley in Africa).
- Extremely hot spots in the earth, where the magma continuously shifted from the mantle to the surface of the earth (forming volcanoes).

In recent decades, geothermal energy has been used in many countries such as China, America, Russia, Iceland, Mexico, Italy, Philippines, France (Karimi & Mansouri, 2018; Nyambura., 2016; Rudiyanto et al., 2017; Yue-feng et al., 2015). Figure 2.2 shows the electricity generates by geothermal energy in different countries.

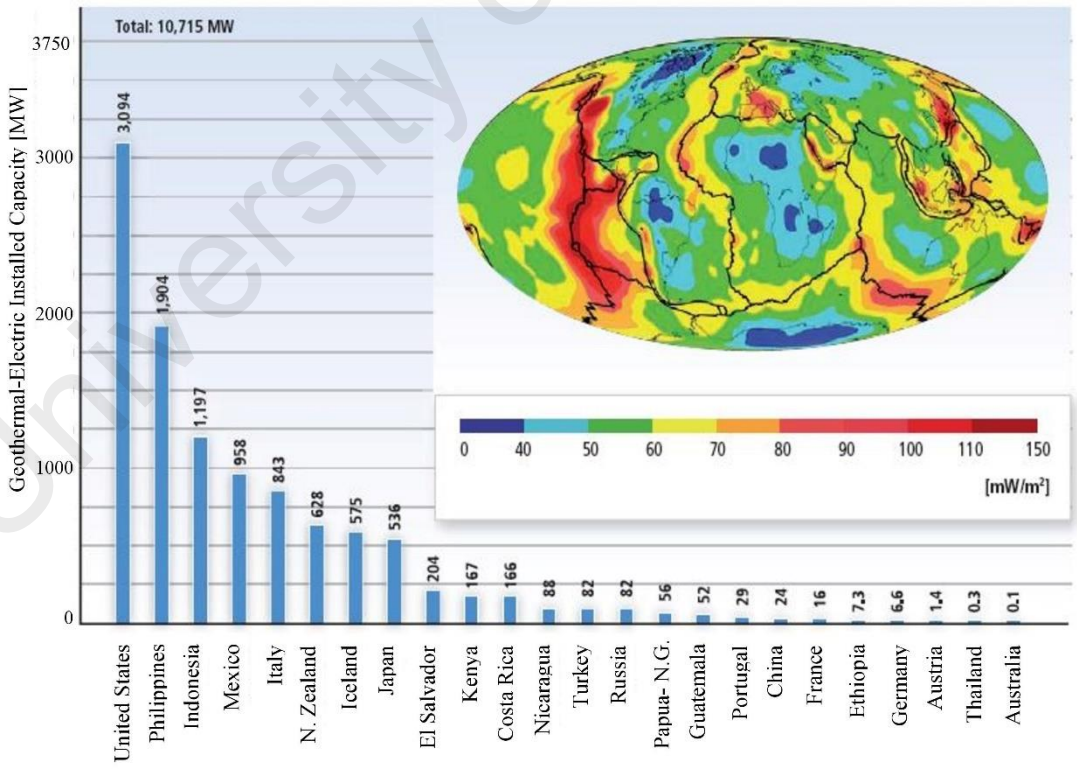

Figure 2.2: Electricity generation by geothermal energy in different countries (Holm et al., 2010)

2.4 Types of Geothermal power plants

The technology of geothermal power generation can be classified based on different types of geothermal power plants such as dry steam, flash steam and binary cycle power generation (El Haj Assad et al., 2017). The classification of geothermal power plants is highly dependent on the temperature of the reservoir (Gitonga., 2017).

- High temperature (>200 °C): suitable for commercial production of electricity by utilizing dry stream and flash stream systems.
- Low to medium temperature (<200 °C): more than 70% of the geothermal resources available in the world are classified in this group (Franco & Vaccaro, 2012; Kanoglu & Bolatturk, 2008).

Considering the importance of the locations of geothermal power plants in supplying the required hot brine, power plants need to be built on-site of geothermal reservoirs (El Haj Assad et al., 2017; Gitonga., 2017).

2.4.1 Dry steam

Dry steam power generation is the first type of high temperature, a vapor-dominant geothermal power plant that plays a vital role in the commercial production of electricity (DiPippo, 2016d; El Haj Assad et al., 2017). In dry steam plants, the extremely high-temperature steam above 235 ºC (455 ºF) is directly applied to spin generator (see Figure 2. 3). However, the application of dry steam power generation is limited due to a few vapor-dominant hydrothermal resources (Yue-feng et al., 2015). Approximately 26% of the total geothermal capacity worldwide is supplied from dry steam plants (DiPippo, 2016d). Dry-steam plants have simple cycle configurations, and they are more economical than flash-steam and binary cycles (Hanbury & Vasquez, 2018).

The vapor is used as the working fluid in dry-steam cycles which have a higher enthalpy compared to that of fluids used in other types of geothermal power plants (flash-steam and binary cycles). A 45 MW of power could be generated by a dry steam cycle unit which is considerably higher than electrical power generated by flash steam (30 MW) or binary cycles (5 MW), (Bertani, 2012). This is because of using vapor as the working fluid, which leads to an increase in the cycle's power output (Chamorro et al., 2012).

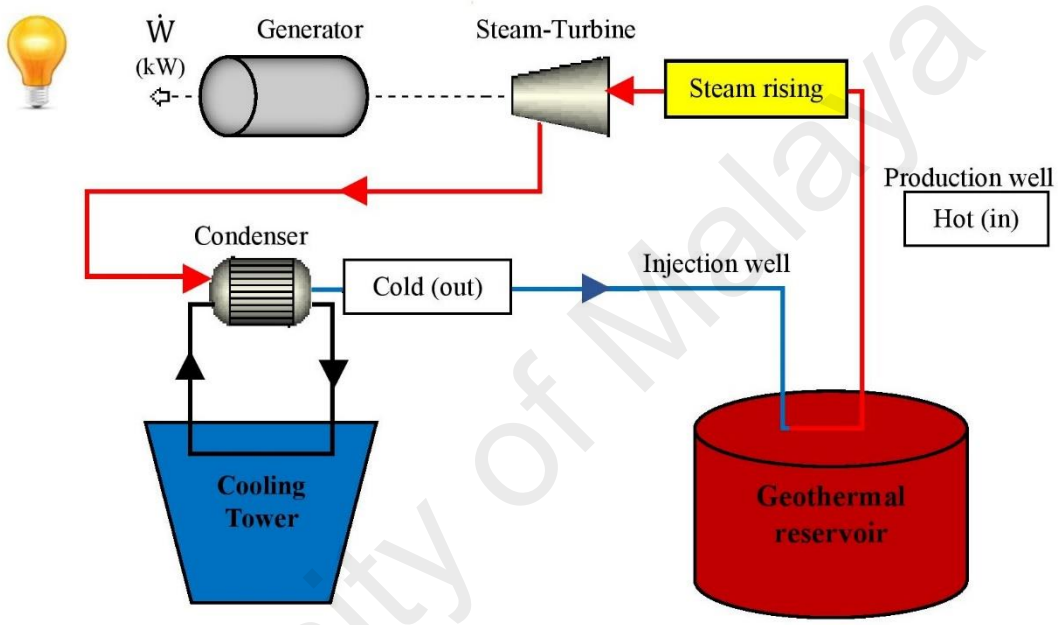

Figure 2. 3: Dry steam power plant

2.4.2 Flash steam

Flash steam power generation is the second type of geothermal power plants, and classified into two main systems being single flash (SF), and double flash (DF), (El Haj Assad et al., 2017). When a liquid-dominant mixture is produced at the wellhead of the geothermal reservoir, flash steam power plants are applied. In flash steam power plants, the liquid-dominant mixture from the wellhead is separated into vapor and liquid phases in the flash vessel where the vapor is sent to the generator for generating electricity (single flash). The separated liquid-phase (waste brine) is then sent to the secondary level flash vessel to obtain more steam at a lower pressure, and the steam enters low-pressure turbine

to produce more electricity (double flash), (DiPippo, 2016b, 2016c; El Haj Assad et al., 2017).

The single flash is often the first kind of liquid-dominated geothermal field with the temperature above 182 ºC (360 ºF), and it consists of 32% of all geothermal power plants. However, the improved design of a single flash is known as double flash power generation producing 15-25% more output power for the same conditions of geothermal fluid. Compared to single flash, double flash steam cycles are more complicated and expensive. However, the extra power output usually seems a reasonable justification for installing such a plant (DiPippo, 2013, 2016b, 2016c; Jalilinasrabady, 2012; Pambudi et al., 2015; Shokati et al., 2015; Unverdi & Cerci, 2013; Zhao et al., 2017).

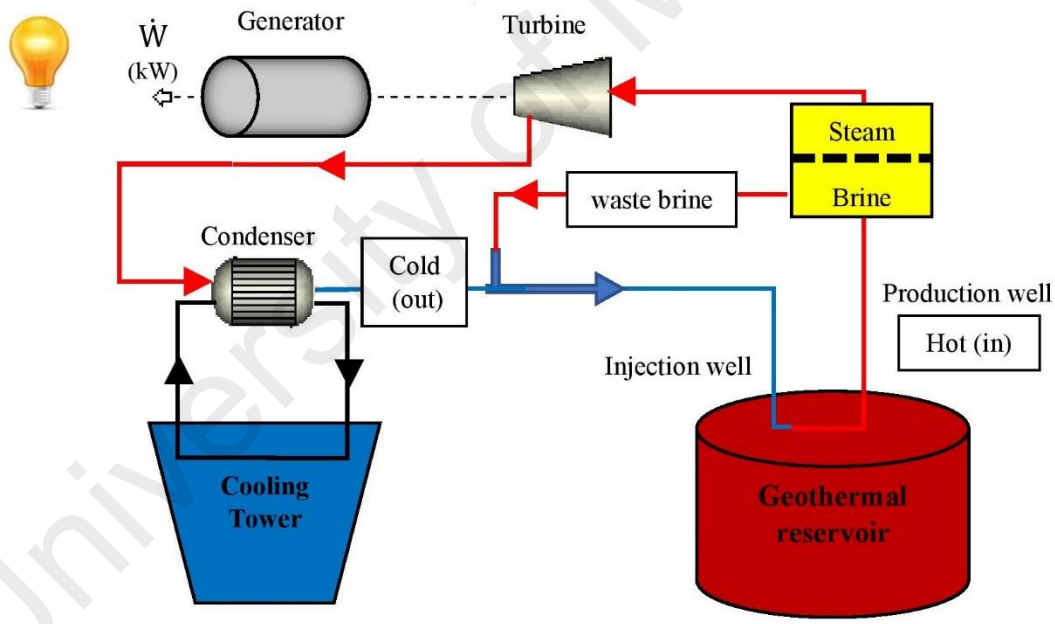

Figure 2. 4: Flash steam power plant

2.4.3 Binary power generations

The last but not least type of geothermal technology is known as binary cycles. Binary power plants are classified as a simple or moderate temperature ranged plants, ranging between 107 ºC and 182 ºC (225 ºF and 360 ºF). In recent years, binary plants have gained increased interest from researchers as the most usable geothermal power plant (Aneke et

al., 2011; Astolfi et al., 2014b; El Haj Assad et al., 2017; Franco & Villani, 2009; Karimi & Mansouri, 2018; Kazemi & Samadi, 2016; Kazemi et al., 2020).

Compared to dry steam and flash steam cycles, binary geothermal power generation performs differently, see Figure 2. 5. As can be seen in Figure 2. 5, in brine power plants, by heat transferring between the hot brine (geothermal fluid) and secondary liquid (working fluid), with lower boiling point and higher vapor pressure, the working fluid is vaporized and the necessary power for rotating the turbine is supplied. Then, the cooled geothermal fluid is reinjected to the ground for recharging the storage (DiPippo, 2008b). The operation happens in the closed-loop process. According to the wide variety of binary power plants applications, they have been the most type of geothermal power plants employed in the Rankine cycle (Astolfi et al., 2014a, 2014b; Franco & Villani, 2009; Györke et al., 2018; Heberle et al., 2016; Kazemi & Samadi, 2016; Kazemi et al., 2020; Yue-feng et al., 2015).

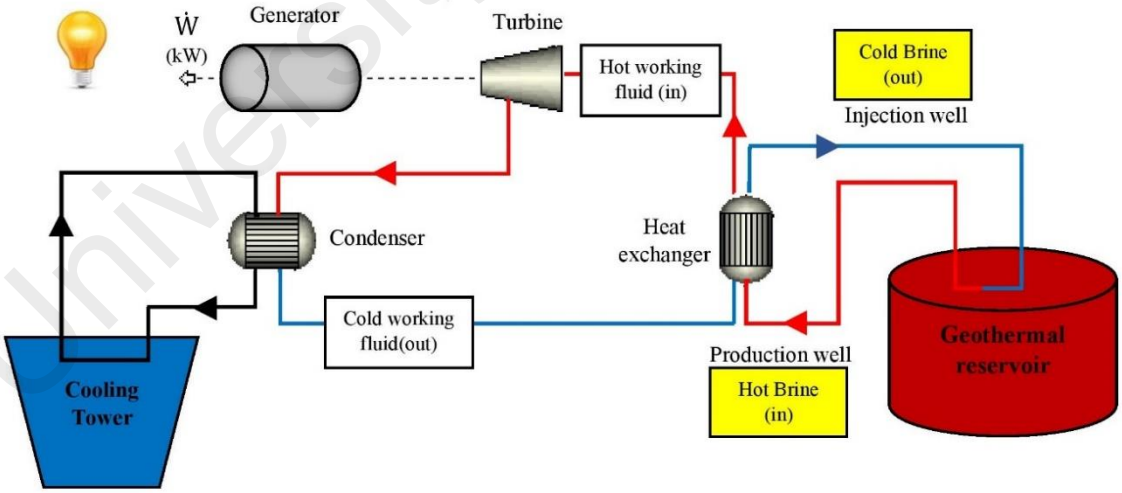

Figure 2. 5: Binary cycle power plant

2.5 Geothermal energy applications

Based on records (Nyambura., 2016; Sircar, 2009; Yadav & Sircar, 2019), geothermal energy was directly utilized in heating, agriculture, animal husbandry, and industrial applications. Geothermal water was generally fed to the heat exchanger, and the extracted heat was applied for home heating, cooking, vegetable drying and therapeutic purposes. For example, the Romans used this water to treat skin and eye diseases. In Mumbai, it was applied to heat homes. Native Americans also used geothermal water for cooking and medicinal purposes.

In the year 1300, it was the first-time geothermal water was used for heating purposes (e.g., heating the environment) in Iceland. The initial measurements of the Earth's temperature were in France done by the thermometer in 1740. More than one century later, in 1870, the thermal behavior of the earth with the advanced scientific methods was studied, and in 1800, geothermal energy was widely studied by Kent Francesco Delider. In 1897, the first mechanical transducer was built in Larderlo, Italy (DiPippo, 2016e), to heat the boiler, rotating a small steam engine. Then in 1904, the first attempt to generate electricity by a generator was carried out with the ability to illuminate four lamps. (DiPippo, 2008a, 2016e). Until 1950, the application of geothermal energy has not extended considerably. However, from 1950 to 1973, due to the unprecedented rise in oil prices, the usage of alternative energy sources, especially geothermal energy, were taken into account by all countries (DiPippo, 2016h).

In recent decades, geothermal energy has been applied to supply the energy required to rotate the generator-turbine for generating electricity (Lukawski et al., 2018). As mentioned in section 1.1, Organic Rankine cycles (ORCs) are by far the most common cycles employed for the conversion of geothermal heat into electricity. In ORCs, organic fluids with high critical temperature and low vapor pressure are nominated while in RCs,

water vapor is utilized (Kazemi et al., 2020; Samadi & Kazemi, 2020). Selection of the working fluid plays a vital role in the system's performance. Working fluids with low boiling points are compatible to be utilized at low-grade heat. For instance, chlorofluorocarbons and hydrocarbons (e.g., isobutane). The fluid is required to have suitable properties such as high critical temperature, and high specific enthalpy, which allows the fluid to absorb more heat without reaching the critical temperature (Dincer, 2018).

Compared to water vapor in RCs, organic fluids in ORCs have lower specific enthalpy drop in the turbine. In other words, an efficient ORC could be as small as 25 kW single stage turbo-expanders whereas, the system with the same efficiency when water vapor used require three to four stage turbine (Fakeye & Oyedepo, 2018).

The effect of various fluids, including pure fluids and zeotropic mixtures, were investigated in Rankine cycles. Degree of superheat, expander intake temperature, working fluid mass flow rate, volumetric flow, and exergy destruction were selected as cycle's operating conditions. In the same operating conditions, working fluids with high critical temperature indicated higher exergy efficiencies (Guo et al., 2015).

Within the ORC process, the heated geothermal fluid is pumped to the evaporator to transfer the heat to the working fluid. Then the saturated/superheated working fluid is expanded through the turbine to generate electricity. Remained vapor is cooled by the condenser to liquify and pumped to the evaporator to complete the cycle (Kazemi & Samadi, 2016; Kazemi et al., 2020; Tchanche et al., 2011).

In recent decades, the impact of various operating parameters including different working fluids, various heat source temperatures, operating pressures, and the addition of external heat exchanger (e.g., regenerative and/or evaporator) having significant effects

on the performance of ORCs have been investigated (Braimakis & Karellas, 2017, 2018; Hærvig et al., 2016; Karimi & Mansouri, 2018; Kazemi et al., 2020; Saloux et al., 2018; Samadi & Kazemi, 2020; Sun et al., 2017; Vescovo & Spagnoli, 2017; Wang et al., 2017; Xu et al., 2018; Zeynali et al., 2019).

Working fluid nomination is highly dependent on the heat source characteristic and various evaluation criteria (Bao & Zhao, 2013; Chen et al., 2010; Martínez-Gomez et al., 2017; Saleh et al., 2007). Each fluid has different thermodynamic properties which could directly affect the cycle's efficiency. For example, working fluid molecular structures increase the exergy efficiency. To be precise, working fluids with double-bonds (e.g., propylene) or cyclic structures (e.g., benzene) enhance the cycle's efficiency (Zhai et al., 2014). While, other fluid's properties such as critical temperature is a weak function for the improvement of the cycle's thermal efficiency (Liu et al., 2004).

The effect of heat source temperature and isobutane/isopentane mixture were revealed in dual-pressure evaporation ORC. 100–200 °C was applied for the heat source temperature. Results showed that the system's net power output was improved by 11.9% with increasing heat source temperature (Li et al., 2019). Liu et al. (2016) determined the optimal heat source temperature for supercritical ORC. The exergetic efficiency was maximized when the difference between optimal heat source temperature and heat source temperature was minimized. Additionally, R236fa performed as the optimum fluid with the highest efficiency of 83.87% and turbine inlet temperature of 129.1 ºC.

Extra regenerative or /a heat exchanger has been shown to further improve the system's efficiency over a simple cycle. Braimakis and Karellas (2018) optimized the thermodynamic aspects of the three regenerative ORCs. The results determined that recuperative and regenerative ORCs influenced the performances of the dry fluids greatly. Le et al. (2014) employed a genetic algorithm to maximize the efficiency of the system

by nominating different fluids. As a result, the recuperative cycle with R152a outperformed the basic configuration in terms of the cycle's efficiency.

The thermodynamic performances of the ORCs enhanced with the two-stage evaporators, in parallel (PTORC) and in series (STORC), were investigated (Li, Zhang, et al., 2015). R245fa and water (90–120) °C were employed as the operating and geothermal fluids, respectively. A significant reduction in the cycle's power output was observed for the ORC coupled with the two-stage evaporator in parallel (PTORC).

A two-stage organic Rankine cycle enhanced with the regenerative was proposed to improve the thermodynamic cycle's efficiency (Li et al., 2018). Four working fluids consisting of toluene, benzene, cyclohexane, and R245fa were nominated. Toluene, benzene, cyclohexane were examined for the high-temperature cycle (absorbing the exhaust heat for the first time), and R245fa was selected for the low-temperature cycle (absorbing the exhaust heat for the second time). Thermal efficiency, exergy efficiency, and net output power was chosen as the research objective functions. Research outcomes showed that the addition of regenerative increased the net output power with cyclohexane and the thermal efficiency with benzene were improved up to 10.76 kW and 7.85%, respectively

In a similar study, the thermodynamic optimization of ORC using two-stage evaporation with R245a as the operating fluid was evaluated (Li, Wang, et al., 2015). The optimization results indicated that with increasing geothermal water inlet temperature (GWIT)and different evaporating temperatures, the cycle's irreversibility reached the minimum losses.

In a study carried out by Braimakis and Karellas (2017), the thermo-economic objective function was employed to optimize the regenerative ORC (RORC). The

optimization was evaluated by integrating different energy heat sources and heat capacities. As a part of their research outcome, the RORC configuration was the optimal cycle under the economic analysis with R-600 as the best performer among selected working fluids. Yang and Yeh (2015) conducted the numerical thermo-economic optimization of the RORC to recover waste heat from large marine diesel engines. R245fa, R1234yf, R1234ze, R152a, and R-600a were nominated as their research operating fluids. Among selected fluids, R1234yf performed as the optimal candidate in thermo-economic optimization.

The Genetic Algorithm (GA) optimization was employed to optimize the system's second law of thermodynamics (exergy efficiency) (Dai et al., 2009). Turbine inlet temperature and pressure were considered as operating parameters in optimization. R236EA with the highest exergy efficiency (35.43%) and thermal efficiency (12.37%) was nominated as the optimum fluid.

The exergoeconomic analysis of Isobutane/Isopentane as zeotropic mixture on the new proposed ORC was conducted by Samadi and Kazemi (2020). Multi-objective functions (thermodynamic, economic, and thermo-economic) were employed to optimize the temperatures of two series evaporators and regenerative, pinch point temperature difference, and degree of superheating. Results indicated that by increasing the mole fraction of isobutane up to 0.5 in isobutane/isopentane mixture, the cycle's efficiency decreased significantly. However, the cycle's improvement was enhanced with increasing the pureness of Isobutane.

2.6 Geothermal fluid

Thermal energy can be derived from various types of geothermal resources which include convective hydrothermal resources (vapor or hot water dominated), other hydrothermal resources (sedimentary basin, geopressured or radiogenic) and hot rock

resources (hot dry rock or magma). Geothermal energy can be found at various depths in the Earth's crust with an estimated 5.4 billion EJ of thermal energy content (Özkaraca et al., 2017). In a power plant where the geothermal source temperature is typically between 110 °C and 180 °C, a binary power plant is required. A binary power plant operates with a geothermal fluid providing the thermal input into the ORC via a pressurized working fluid. A geothermal fluid is defined as the fluid that carries the thermal energy between a geothermal reservoir and the ORC power plant. A geothermal fluid, in this case, is in contact with high-temperature water/brine from the geothermal production well through a heat exchanger, in a closed-loop flow.

Water is the most typical geothermal fluid used in a power plant on the reasons that its heat capacity is sufficiently high, and that water is easily available and relatively cheap. However, depleting surface water resources, and a growing world population with unsustainable groundwater being pumped out faster than it is replenished, is contributing to the rapidly shrinking amount of assessable freshwater. As such, the replacement of water in industrial processes is warranted. Hence, the present work puts into consideration the replacement of water with a green solvent that has sufficiently high heat capacity (Ionic Liquids).

Ionic Liquid solvents (ILs)

Ionic liquids (ILs) are organic salts and considered as green solvents due to the very low vapor pressure and high thermal stability. Hence, ILs are relatively non-volatiles and therefore, do not emit harmful volatile organic compounds (VOCs) (Mallakpour & Dinari, 2012). Due to thermal-physical properties, ILs are possible candidates for utilization as HTFs (Heat Transfer Fluids) for medium to high-temperature processes. The thermo-physical properties of ILs include having a relatively low viscosity (Mun & Sim, 2012), a wide liquid temperature range (25 °C - 459 °C), good thermal conductivity,

low vapor pressure (Bier & Dietrich, 2010; Ravula et al., 2019), high chemical stability, density and heat capacity (Aparicio et al., 2010; Brennecke & Edward, 2001; Domańska, 2006; Fredlake et al., 2004; G. Montalbán et al., 2017; Goswami, 2004; Muhammad et al., 2008; Ravula et al., 2019; Reddy et al., 2003; Valkenburg et al., 2005). The physical properties of the ionic liquid ($C_9H_{14}NBF_4$) considered in the present work are shown in Table 2. 4.

Table 2. 4: Properties of $C_9H_{14}NBF_4$ (Mun & Sim, 2012)

PROPERTIES	M_W (g/mol)	T_B (K)	T_C (K)	P_C (bar)	ω
$C_9H_{14}NBF_4$	223.02	459.9	674	25.8	0.3468

CHAPTER 3: CYCLES DESCRIPTION, THERMODYNAMIC AND ECONOMIC ANALYSIS AND OPTIMIZATIONS

The present study focuses on three ORC configurations consisting of a basic ORC, a regenerative ORC (RORC) and a two-stage evaporative ORC (TSORC). Two pure organic fluids, R-600 and R-600a, were nominated. 1-butylpyridinium tetrafluoroborate ,$C_9H_{14}NBF_4$, was proposed as the alternate fluid in both evaporation (geothermal fluid) and condensation (cooling fluid) processes. Peng Robison equation of state (PR-EoS) is applied to evaluate the thermodynamic aspects of the cycles, and bare module cost is employed to estimate the cycle's total costs. Also, a linear weighted function is taken to monitor the thermo-economic operation of the ORCs.

3.1 Rankine cycle (RC)

Figure 3. 1 shows a thermodynamic Rankine cycle consisting of four main equipment. The Rankine cycle operates by conversion of thermal energy supplied by fuels such as coal, oil or natural gas into useful work (electrical energy). Approximately 80% of electrical power around the world is generated by the Rankine cycle.

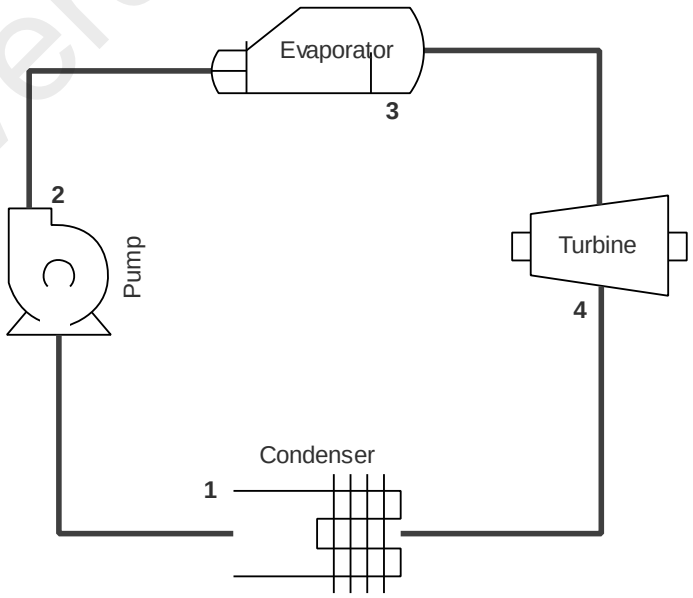

Figure 3. 1:Schematic of Rankine cycle

3.2 Basic organic Rankine cycle (basic ORC)

In reference to sections 1.1 and 2.5, the ORC is made up of four principal components linked via R-600/R-600a as an operating fluid in the closed-loop cycle. 1-butylpyridinium tetrafluoroborate ($C_9H_{14}NBF_4$), an alternate geothermal fluid, is applied in both evaporator and condenser as the HTF and cooling fluid respectively,

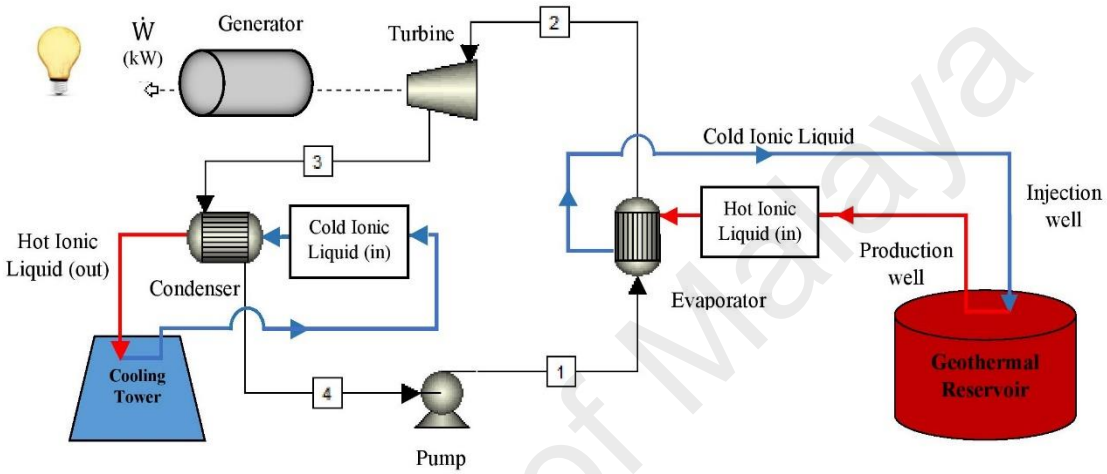

Figure 3. 2: Schematic of basic ORC

As can be seen in Figure 3. 2, 1-butylpyridinium tetrafluoroborate ($C_9H_{14}NBF_4$) is injected into a reservoir to absorb heat from the ground layers. The heated $C_9H_{14}NBF_4$ is then pumped to the evaporator to transfer the required heat to the R-600/R-600a. The saturated/superheated R-600/R-600a is then expanded through the turbine for electricity generation. The rest of the expanded vapor in the turbine is cooled by the condenser to liquify and pump to the evaporator to complete the cycle.

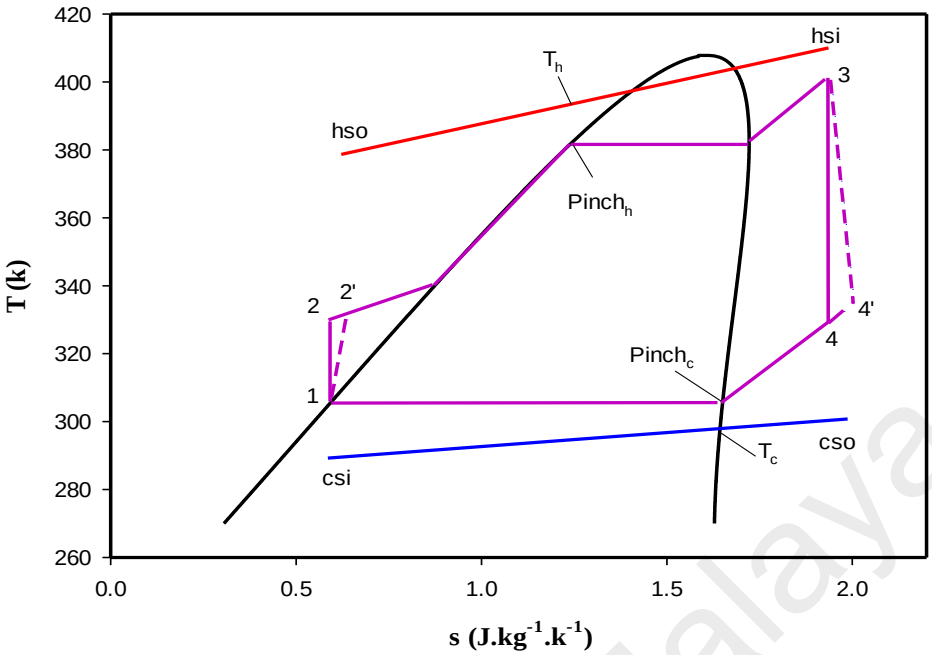

Figure 3. 3: T-S diagram of basic ORC

According to the temperature-entropy diagram (T-S diagram), Figure 3.3, four following processes are identified.

•**Process 1-2:** The working fluid is pumped from low pressure to high pressure. As the fluid is liquid at this stage, the pump requires little input energy (Reversible adiabatic pumping process in the pump).

•**Process 2-3:** A high-pressure liquid enters the boiler where it is heated at constant pressure by an external heat source to become saturated/superheated vapor (heat transfer at constant pressure in the evaporator).

•**Process 3-4:** The saturated/superheated vapor expands through the turbine, generating power. This decreases the temperature and pressure of the vapor, and some condensation may occur (Reversible adiabatic expansion in the turbine).

•**Process 4-1:** The superheated vapor then enters the condenser where it is condensed at a constant pressure to become a saturated liquid (heat transfer at constant pressure in the condenser).

If the pump and turbine are isentropic, the Rankine cycle will be an ideal cycle and processes 1-2 and 3-4 would be represented by lines 1-2' and 3-4' (Figure 3.3). In other words, no entropy would be generated by the pump and the turbine so that the output power is maximized. However, due to the cycle's irreversibility due to the heat losses in the cycle's equipment, the total output power is decreased.

3.3 Regenerative organic Rankine Cycle (RORC)

The basic ORC has a plain configuration which makes it more affordable. However, due to its irreversibility (entropy changes at various stages of the cycle), the cycle tends to have a lower thermal efficiency. One way of reducing the irreversibility is through the inclusion of regenerative or the evaporator to the cycle's configuration.

In the regenerative organic Rankine cycle (RORC), a feed heater and a pump are added, to the basic ORC, Figure 3. 4. By adding regenerative to the basic ORC, an exhaust vapor from the turbine (superheated vapor) is used to preheat the outlet fluid from pump 1 (subcooled fluid). In this cycle, the amount of working fluid is taken between two stages of expansion and used as a required heat source of regeneration before entering to the evaporator (process 3-3''), T-S diagram. As a result, the amount of heat that the evaporator received and the outlet work done by the turbine would reduce.

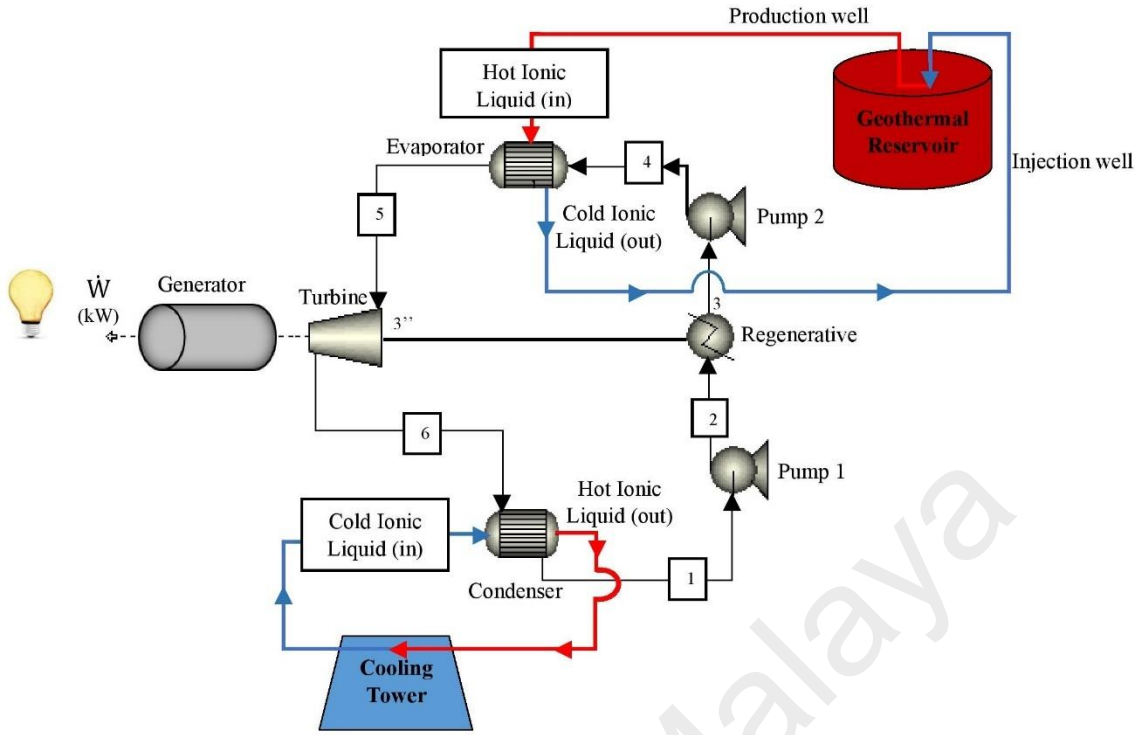

Figure 3. 4: Schematic of RORC

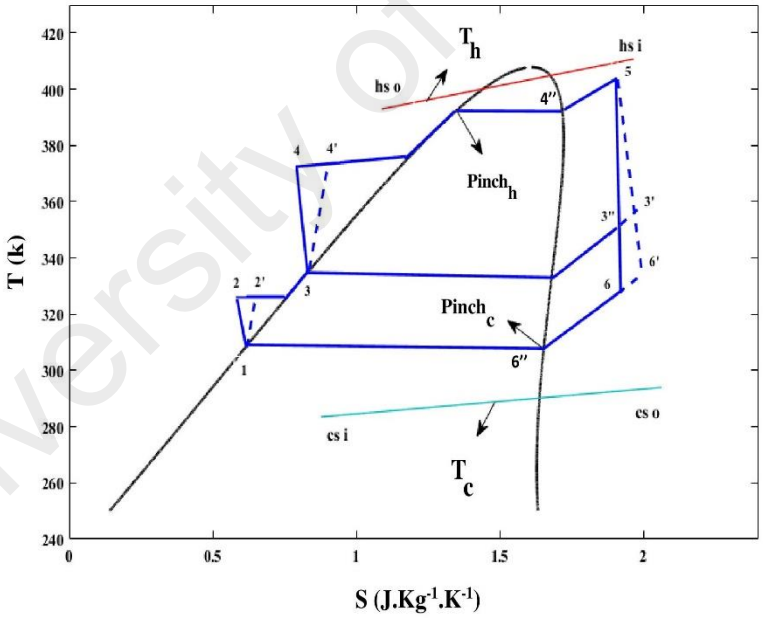

Figure 3. 5: T-S diagram of RORC

3.4 Two-Stage-Evaporative ORC (TSORC)

In TSORC, an additional evaporator, either in series or parallel, is usually applied to the configuration of the basic ORC. In the present work, ORC is enhanced with two evaporators in series due to its higher efficiency compared to the parallel configuration. The added evaporator generates a higher mass flow rate of a vaporized working fluid due

to a larger amount of heat received from the heat source. There is thus, an increase in the generation of electricity.

In TSORC, Figure 3. 6, high-pressure liquid is pumped from pump 1 to evaporator 2. A portion of the working fluid in evaporator 2 absorbs heat from a geothermal fluid (line B) and converts the working fluid to the saturated liquid phase. A portion of the working fluid is then vaporized and enters a turbine [process (3-3" in Figure 3. 7)]. Meanwhile, the rest of the working fluid in evaporator 2 is pumped to evaporator 1 to absorb heat from a geothermal fluid (line A). The working fluid from evaporator 1 is then expanded through the turbine. The discharging vapor from the turbine outlet is liquefied by the cooling ionic liquid ($C_9H_{14}NBF_4$) in the condenser, and the cycle is repeated.

The flow of a geothermal fluid is shown by the red line (ABC) in Figure 3. 6. A geothermal fluid first enters evaporator 1, where some of its heat is transferred to the working fluid in evaporator 1. Then, it is allowed to flow into evaporator 2 to heat up a portion of the working fluid. The exited geothermal fluid from the evaporator 2 is then entered via line C into the underground reservoir to absorb heat, and the cycle for a geothermal fluid is repeated.

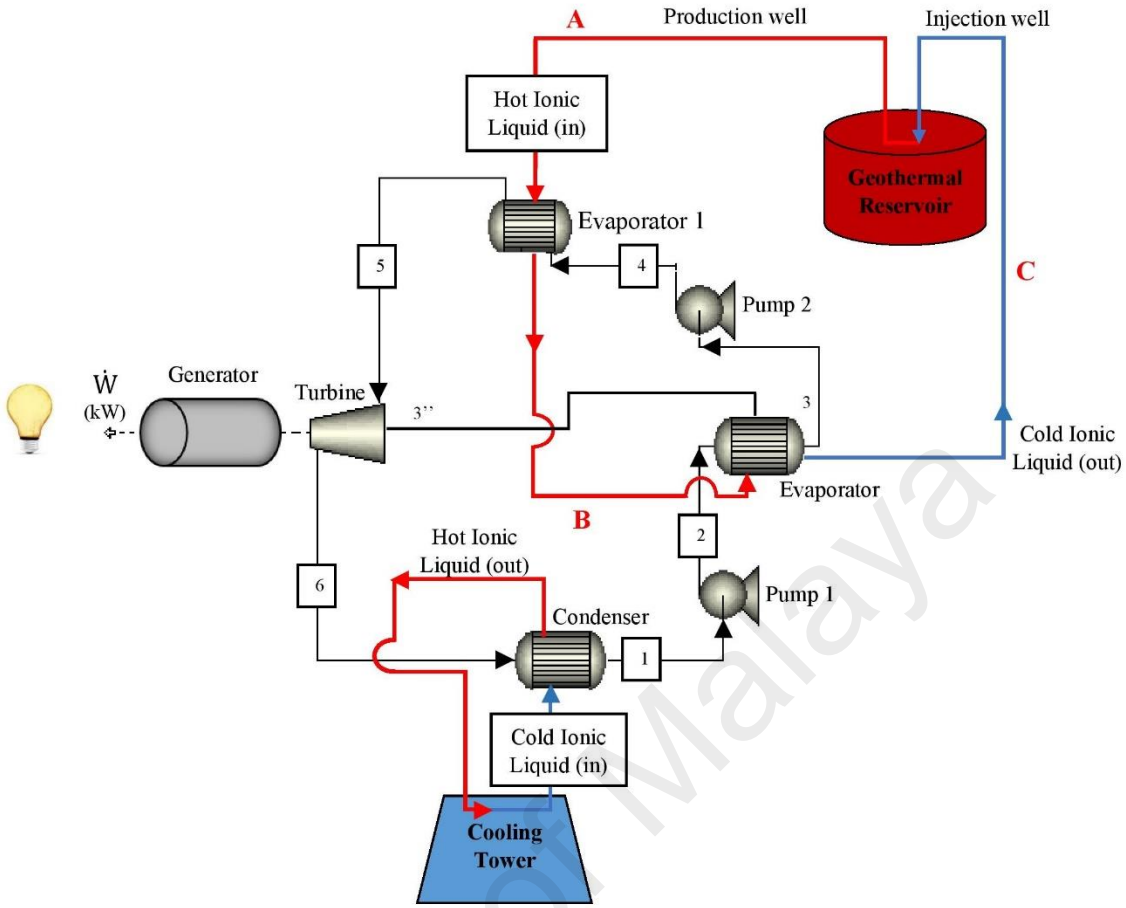

Figure 3. 6: Schematic of TSORC

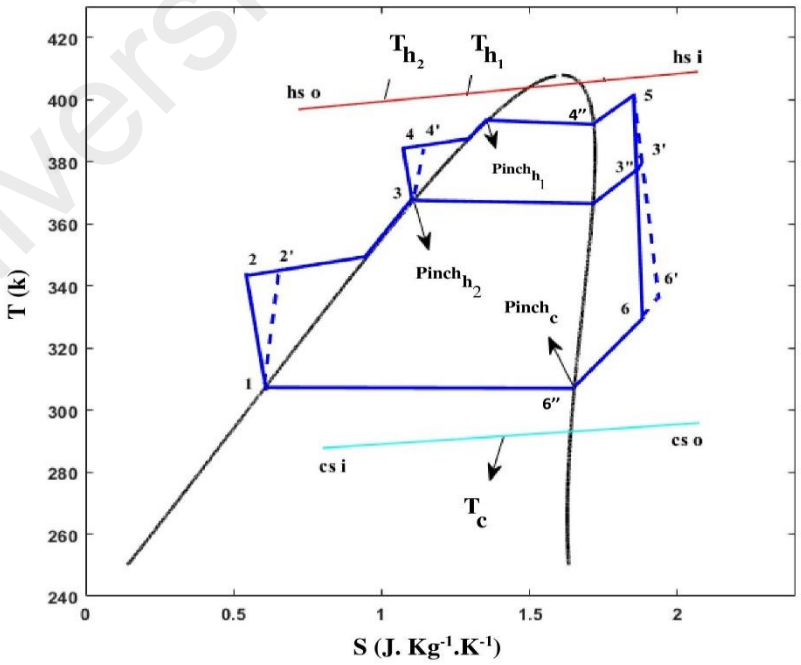

Figure 3. 7: T-S diagram of TSORC

3.5 Working Fluid

The selection of working fluid for the organic Rankine cycle is usually performed carefully by considering the safety and environmental properties of the working fluid. These properties include atmospheric lifetime (ALT), ozone depletion potential (ODP), and global warming potential (GWP). Low toxicity and high chemical stability, high flash point, low specific heat, high latent heat, and high thermal conductivity are the other factors required to consider for fluids nomination.

Added to the above elements, as mentioned earlier, all working fluids used in ORCs must be classified under the organic groups. The slope of the saturation vapor line of the organic working fluid, determined by the slope of the temperature-entropy diagram, is also essential, Figure 3. 8. As can be seen in Figure 3. 8, organic fluids are categorized into three groups as dry, wet, and isentropic. Isentropic and dry fluids stop the formation of the liquid droplet

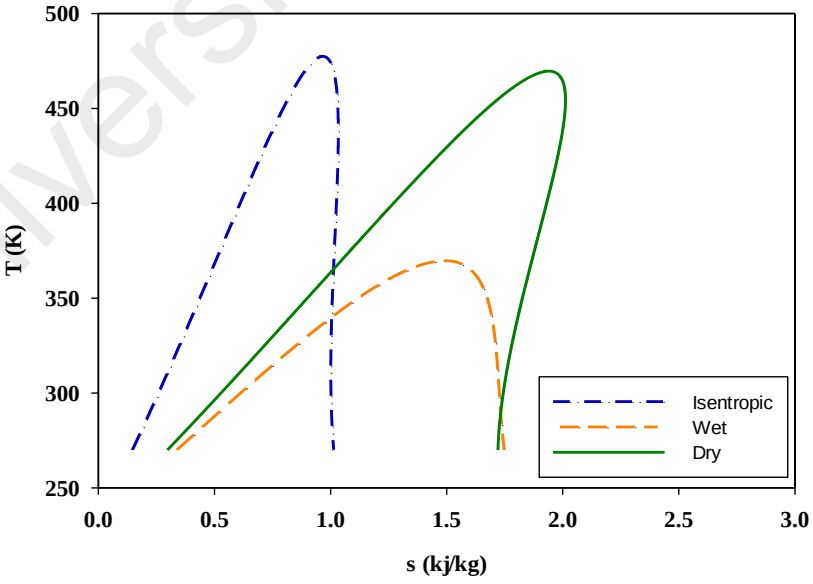

Figure 3. 8: The T-S diagram of working fluid (dry, wet, and isentropic)

In this study, R-600 (dry) and R-600a (isentropic) were selected as two pure organic fluids. Table 3. 1 indicates the thermodynamic properties of R-600 and R-600a.

Table 3. 1: Thermodynamic properties of working fluids (Hung et al., 2010; Lemmon E et al., 2011; Liu et al., 2012)

Substances	Mw (g/mol)	Tc (K)	Pc (bar)	ω
Butane (R-600)	58.123	425.12	37.96	0.20
Isobutane (R-600a)	58.123	407.85	36.40	0.19

3.6 Modelling and optimization

In the present study, to monitor the cycle's efficiency, the first and the second laws of thermodynamics known as the thermal and exergy efficiencies. Specific investment cost (SIC) was applied to assess the economic aspects of the cycles. Additionally, multi-objective function (thermo-economic) was employed to maximize the efficiency of the cycle and minimize the cycle's total costs at the same time.

3.7 Thermodynamic modelling

Thermodynamic efficiency of the ORC system is affected by the operating conditions, types of working fluids, system components, and selection of appropriate objective functions for optimization.

3.7.1 Thermodynamic modelling based on energy

Energy analysis is based on the first law of thermodynamics. This section explains the relations between the work done and the amount of heat exchanged by the ORCs' equipment (pump, evaporator, regenerative, turbine and condenser).

3.7.1.1 Pumping Process

- **Pump isentropic efficiency (η_{is}^{p})**

$$\eta_{is}^{p} = \frac{h_{p,out}^{is} - h_{p,in}}{h_{p,out} - h_{p,in}} \tag{3.1}$$

In this regard, η_{is}^{p} is an indicative of the pump isentropic efficiency, $h_{p,out}^{is}$ indicates the isentropic enthalpy of the outlet fluid from the pump, $h_{p,in}$ and $h_{p,out}$ are the actual

enthalpy of the inlet/outlet working fluid in the pumping process. If the pump and turbine are isentropic, the cycle's net power output is reached the maximum value (Figure 3.3).

Following relations, (3.2) and (3.3), were employed to calculate the real enthalpy of the outlet fluid and output power.

- **Pump input power ($\dot{W}_p$)**

$$\dot{W}_p = \dot{m}_{wf}(h_{p,out} - h_{p,in}) = \frac{\dot{m}_{wf}(h^{is}_{p,out} - h_{p,in})}{\eta^{p}_{is}} \quad (3.2)$$

- **Pump isentropic efficiency or engine input power ($\dot{W}_p^{elec}$)**

$$\dot{W}_p^{elec} = \frac{\dot{W}_p}{\eta_{motor}} \quad (3.3)$$

In the above equations, $\dot{W}_p$ and $\dot{W}_p^{elec}$ are described as the pump's input and output power. Also, η_{motor} denotes the motor efficiency of the pump where it is evaluated by relation (3.4).

- **Pump motor efficiency (η_{motor})**

$$\eta_{motor} = 75 + 11.5 \log_{10}(\dot{W}_p) - 1.5[\log_{10}(\dot{W}_p)]^2 \quad (3.4)$$

3.7.1.2 Heat transfer process

The thermodynamic relations for the heat exchangers (evaporator, regenerative and condenser) are described as follows.

- **Heat transfer process in the evaporator ($\dot{Q}_{h,evap}$)**

$$\dot{Q}_{h,evap} = \dot{m}_{wf}(h^{evap}_{wf,out} - h^{evap}_{wf,in}) = \dot{m}_h(h_{hsi} - h_{hso}) \quad (3.5)$$

$\dot{Q}_{h,evap}$ implies for the transferred heat between a geothermal fluid ($C_9H_{14}NBF_4$ / water) and the operating fluid (R-600 /R-600a). $h^{evap}_{wf,out}$ and $h^{evap}_{wf,in}$ are the actual enthalpy of the internal/external operating fluid to/from the evaporator. Moreover, $\dot{m}_h$ denotes the

mass flow rate of a geothermal fluid where its value considered 50 (kg/s) in all processes. h_{hsi},h_{hso} are the real enthalpy of the internal/external geothermal fluid to/from the evaporator.

3.7.1.3 Regenerative process

$$\dot{Q}_{h,reg} = (1 - X)\dot{m}_{wf}(h^{reg}_{wf,out} - h^{reg}_{wf,in}) \quad (3.6)$$

Equation (3.6) indicates the transferred heat between the superheated vapor leaves the turbine and the cooling fluid ($C_9H_{14}NBF_4$ / water) in the condenser. X is the mass fraction of the operating fluid taken from the turbine.

$$X = \frac{(h_3 - h_2^{'})}{(h_3^{'} - h_2^{'})} \quad (3.7)$$

3.7.1.4 Expansion process

The expansion process happens through the turbine. Turbine isentropic efficiency (η^t_{is}), turbine output power ($\dot{W}_t$) and generator output power ($\dot{W}^{elec}_t$) are defined by equations (3.8), (3.9) and (3.10), respectively. In equation (3.8), $h_{t,in}$, $h_{t,out}$ are the indicative of the of the internal or external saturated/superheated vapor to/from the turbine. $h^{is}_{t,out}$ stands for the isentropic enthalpy of the outlet vapor from the turbine.

- **Turbine isentropic efficiency (η^t_{is})**

$$\eta^t_{is} = \frac{h_{t,in} - h_{t,out}}{h_{t,in} - h^{is}_{t,out}} \quad (3.8)$$

- **Turbine output power ($\dot{W}_t$)**

$$\dot{W}_t = \dot{m}_{wf}(h_{t,in} - h_{t,out}) = \dot{m}_{wf}\,\eta^t_{is}\,(h_{t,in} - h^{is}_{t,out}) \quad (3.9)$$

- **Generator output power ($\dot{W}^{elec}_t$)**

$$\dot{W}^{elec}_t = \eta_{gen}\dot{W}_t \quad (3.10)$$

3.7.1.5 Condensation process

The condensation process takes place in the condenser where the heat is transferred between the superheated vapor that leaves the turbine and the cooling fluid in the condenser. In the following equation, $h_{wf,in}^{cond}$ and $h_{wf,out}^{cond}$ stand for the actual enthalpy of the internal and external working fluid in the condensation process. h_{cso} and h_{csi} are the symbols which denote the enthalpy of internal and external geothermal fluid.

$\dot{m}_{wf}$ and $\dot{m}_c$ are the working fluid and cooling fluid mass flow rates where their relations for basic ORC, RORC and TSORC are given in the sections "3.7.2.1", "3.7.2.2", and "3.7.2.3", respectively.

$$\dot{Q}_c = \dot{m}_{wf}\left(h_{wf,in}^{cond} - h_{wf,out}^{cond}\right) = \dot{m}_c\,(h_{cso} - h_{csi}) \tag{3.11}$$

3.7.1.6 ORC system

Equation (3.12) reveals the first-law efficiency (thermal efficiency(η_{th})) where $\dot{W}_{net}$ is the net mechanical output power (3.13) and $\dot{Q}_h$ is the heat transfer flow rate in the evaporator (3.5).

$$\eta_{th} = \frac{\dot{W}_{net}}{\dot{Q}_h} \tag{3.12}$$

$$\dot{W}_{net} = \dot{W}_t - \dot{W}_p \tag{3.13}$$

3.7.2 Expansion of Energy relations for basic ORC, RORC, and TSORC

In accordance to the thermodynamic relations given for the organic Rankine cycle "3.7.1" and Figures (3.3), (3.5) and (3.7), the relations for the basic ORC, RORC, and TSORC could be extended as follows.

3.7.2.1 Expansion of energy relations for basic ORC

- Pumping process

$$\dot{W}_p = \dot{m}_{wf}\left(h_2^{is} - h_1\right) \Big/ \eta_{is}^{p} \tag{3.14}$$

- Heat transfer process

$$\dot{Q}_{h,evap} = \dot{m}_{wf}(h_3 - h_2) \tag{3.15}$$

- Expansion process

$$\dot{W}_t = \dot{m}_{wf}\,\eta_{is}^{t}\left(h_3 - h_4^{is}\right) \tag{3.16}$$

- Condensation process

$$\dot{Q}_c = \dot{m}_c\,(h_4 - h_1) \tag{3.17}$$

In the equations (3.14) to (3.17), the mass flow rate of operating fluid (R-600/R-600a) and the mass flow rate of cooling fluid in the condenser ($C_9H_{14}NBF_4$ / water) for the basic ORC are as follow.

$$\dot{m}_{wf} = \frac{\dot{m}_h(h_{hsi} - h_h\ |_{\text{at } T_H})}{(h_3 - h_{wf}^{evap}\ |_{\text{at Bubble point}})} \tag{3.18}$$

$$\dot{m}_c = \frac{\dot{m}_{wf}(h_{wf}^{cond}\ |_{\text{at Dew point}} - h_1)}{(h_c\ |_{\text{at } T_L} - h_{csi})} \tag{3.19}$$

3.7.2.2 Expansion of energy relations for RORC

- Pumping process

$$\dot{W}_{p_1} = (1 - X)\,\dot{m}_{wf}\,(h_2^{is} - h_1) \Big/ \eta_{is}^{p_1} \tag{3.20}$$

$$\dot{W}_{p_2} = \dot{m}_{wf}\,(h_4^{is} - h_3) \Big/ \eta_{is}^{p_2} \tag{3.21}$$

- Regenerative process

$$\dot{Q}_{reg} = (1 - X)\dot{m}_{wf}\,(h_3 - h_{2'}) = X\,\dot{m}_{wf}(h_3 - h_{3''}) \quad (3.22)$$

- Heat transfer process

$$\dot{Q}_{h,evap} = \dot{m}_{wf}(h_5 - h_{4'}) \quad (3.23)$$

- Expansion process

$$\dot{W}_t = \dot{m}_{wf}\,\eta_{is}^{t}\,(h_5 - h_{3''}) + (1 - X)\,\eta_{is}^{t}\,(h_{3''} - h_6) \quad (3.24)$$

- Condensation process

$$\dot{Q}_c = \dot{m}_c\,(h_{6'} - h_1) \quad (3.25)$$

In equations (3.18) to (3.25), the vapor quality of the operating fluid (X) is calculated by equation (3.7) and $\dot{m}_{wf}$, $\dot{m}_c$ are describes as below.

$$\dot{m}_{wf} = \frac{\dot{m}_h(h_{hsi} - h_h|\ \text{at } T_H)}{(h_5 - h_{wf}^{evap}\ |\ \text{at Bubble point})} \quad (3.26)$$

$$\dot{m}_c = \frac{\dot{m}_{wf}\,(1 - X)\,(h_{wf}^{cond}\ |\ \text{at Dew point} - h_1)}{(h_c\ |\ \text{at } T_L\ - h_{csi})} \quad (3.27)$$

3.7.2.3 Expansion of Energy relations for TSORC

- Pumping process

$$\dot{W}_{p_1} = (\dot{m}_{wf_1} + \dot{m}_{wf_2})(h_2^{is} - h_1)/\eta_{is}^{p_1} \quad (3.28)$$

$$\dot{W}_{p_1} = \dot{m}_{wf_1}(h_4^{is} - h_3)/\eta_{is}^{p_2} \quad (3.29)$$

- Heat transfer process

$$\dot{Q}_{h,evap2} = \dot{m}_{wf_1}(h_3 - h_2{}') = \dot{m}_{wf_2}(h_3{}' - h_3) \quad (3.30)$$

$$\dot{Q}_{h,evap1} = (\dot{m}_{wf_1} + \dot{m}_{wf_2})((h_5 - h_4{}') \quad (3.31)$$

- Expansion process

$$\dot{W}_t = \dot{m}_{wf_1}\eta_{is}^{t}\,(h_5 - h_3{}'') + \dot{m}_{wf_2}\,\eta_{is}^{t}\,(h_3{}'' - h_6) \quad (3.32)$$

- Condensation process

$$\dot{Q}_c = \dot{m}_c\,(h_6' - h_1) \tag{3.33}$$

Likewise, $\dot{m}_{wf_1}$, $\dot{m}_{wf_2}$ and $\dot{m}_c$ in the TSORC are evaluated by the following equations.

$$\dot{m}_{wf_1} = \frac{\dot{m}_h(h_{hsi}^{evap_1} - h_h\big|\ \text{at } T_{H_1})}{(h_5 - h_{wf}^{evap_1}\ \big|\ \text{at Bubble point})} \tag{3.34}$$

$$\dot{m}_{wf_2} = \frac{\dot{m}_h(h_{hsi}^{evap_2} - h_h\big|\ \text{at } T_{H_2})}{(h_3' - h_{wf}^{evap_2}\ \big|\ \text{at Bubble point})} \tag{3.35}$$

$$\dot{m}_c = \frac{\dot{m}_{wf}\,(h_{wf}^{cond}\ \big|\ \text{at Dew point} - h_1)}{(h_c\ \big|\text{at } T_L\ - h_{csi})} \tag{3.36}$$

3.7.3 Thermodynamic modelling based on exergy

Exergy is a thermodynamic term which is also known as the second law efficiency and refers to the most useful work that can be obtained from a system in an equilibrium process. However, the conversion of thermal energy into useful work (e.g., electricity) leads to energy losses in which the loss in a cycle could not be investigated by the first law of thermodynamics due to its incapability to convert low-grade heat into electricity. Consequently, to evaluate the maximum useful work in a thermodynamic process, exergy efficiency needs to be evaluated. The second law of thermodynamics relations for the ORCs' equipment is given in this section.

3.7.3.1 Pumping process

$$\dot{Ex}_p = \dot{m}_{wf}\left[h_{p,out} - h_{p,in} - T_0\,(s_{p,out} - s_{p,in})\right] \tag{3.37}$$

$\dot{Ex}_p$ in the above equation indicates the useful exergy (exergy received by the fluid) for the pumping process. Ambient temperature (T_0) is considered at 25 °C in the standard condition. $s_{p,out}$, and $s_{p,in}$ stand respectively for the mass flow rate of operating fluid,

the enthalpy and entropy of the inlet and outlet fluid. The supplied exergy (pump power input), $\dot{W}_p$, generated by the pump is calculated via equation (3.38).

$$\dot{W}_p = \dot{m}_{wf}(h_{p,out} - h_{p,in}) \quad (3.38)$$

3.7.3.2 Heat Transfer process

Exergy supplied by the heat source (exergy change in the heat source), $E\dot{X}_h$, is attained by equation (3.39) and exergy received by the working fluid, $E\dot{X}_{wf,evap}$, is computed by equation (3.40).

$$E\dot{x}_h = \dot{m}_h[h_{hsi} - h_{hso} - T_0(s_{hsi} - s_{hso})] \quad (3.39)$$

In this respect, $E\dot{x}_h$ stands for the exergy obtained in the evaporator by geothermal fluid and $\dot{m}_h$ is the mass flow of geothermal fluid (50 kg/s). The enthalpy and entropy of the inlet and outlet of a geothermal fluid in the evaporation process are shown by h_{hsi}, h_{hso} and s_{hsi}, s_{hso} .

$$E\dot{x}_{wf,evap} = \dot{m}_{wf}\left[h_{wf,ot}^{evap} - h_{wf,in}^{evap} - T_0\left(s_{wf,out}^{evap} - s_{wf,in}^{evap}\right)\right] \quad (3.40)$$

Parameters $h_{wf,in}^{evap}$, $h_{wf,out}^{evap}$ and $s_{wf,in}^{evap}$, $s_{wf,out}^{evap}$ are indicatives of the enthalpy and the entropy of the fluid exited /entered the evaporator.

3.7.3.3 Expansion process

The thermodynamic relations for the available exergy ($E\dot{X}_t$) and the useful exergy ($\dot{W}_t$) happened through the turbine are shown.

$$E\dot{x}_t = \dot{m}_{wf}\left[h_{t,in} - h_{t,out} - T_0\left(s_{t,in} - s_{t,out}\right)\right] \quad (3.41)$$

$$\dot{W}_t = \dot{m}_{wf}\left(h_{t,in} - h_{t,out}\right) \quad (3.42)$$

*The subscript (t) denotes the processes take place in the turbine.

3.7.3.4 Condensation process

Similar to the evaporators, the amount of exergy obtained in the condenser is provided by the cooling fluid and by the operating fluid

$$\dot{Ex}_{cond} = \dot{m}_c \left[h_{cso} - h_{csi} - T_0 \left(s_{cso} - s_{csi}\right)\right] \quad (3.43)$$

In equation (3.43), $\dot{Ex}_{cond}$ denotes the received exergy by the cooling fluid. h_{csi}, h_{cso} and s_{csi}, s_{cso} are respectively imply for the enthalpy and entropy of the inlet and outlet cooling fluid. The received exergy by the working fluid in the condenser is calculated as below.

$$\dot{Ex}_{wf,cond} = \dot{m}_{wf}\left[h_{wf,in}^{cond} - h_{wf,out}^{cond} - T_0\left(s_{wf,in}^{cond} - s_{wf,out}^{cond}\right)\right] \quad (3.44)$$

3.7.3.5 ORC system

The second law efficiency (exergy efficiency) of the ORC systems can be assessed via the following equation.

$$\eta_{ex} = \frac{\dot{Ex}_{useful}}{\dot{Ex}_{available}} \quad (3.45)$$

$\dot{Ex}_{useful}$ is the net mechanical output power of the system shown by equation (3.13) and the available exergy of the ORC is considered to be the exergy change in the heat source,(3.39). Therefore, the exergy efficiency relation is extended as equation (3.46).

$$\eta_{ex} = \frac{\dot{Ex}_{useful}}{\dot{Ex}_{available}} = \frac{\dot{W}_{net}}{\dot{Ex}_h} = \frac{\dot{W}_t - \dot{W}_p}{\dot{m}_h[h_{hsi} - h_{hso} - T_0(s_{hsi} - s_{hso})]} \quad (3.46)$$

3.8 Calculation of the thermodynamic properties

For the calculation of energy and exergy efficiencies, certain thermodynamic parameters such as enthalpy, entropy, vapor pressure, $\dot{m}_{wf}$, $\dot{m}_c$ and X (3.7) are necessary to be determined. PR-EoS was utilized for calculating enthalpy (3.47) and entropy (3.48),

and the modified Wagner equation was used to obtain the vapour pressures of each fluid (3.49), (Peng & Robinson, 1976; Perry Robert et al., 1997).

3.8.1 Peng-Robinson equation of state (PR- EoS)

The Peng Robinson equation is a cubic equation which can be used to study the thermodynamic behavior of materials in various phases.

$$p = \frac{RT}{V - b} - \frac{(a\alpha)}{V(V + b) + b\,(V - b)} \tag{3.47}$$

In the above equation, the parameter 'a' represents the size of the intermolecular gravity forces, and parameter 'b' is used to indicate the volume of molecules.

$$a = \Omega_a \frac{R^2 T_C^2}{P_C} \tag{3.47.1}$$

$$b = \Omega_b \frac{RT_C}{P_C} \tag{3.47.2}$$

where $\Omega_a = 0.45724$ and $\Omega_b = 0.07780$ and T_C, P_C and R are the critical temperature, critical pressure, and gas constant, respectively. Also, 'α' is obtained from the following equation.

$$\alpha = (1 + m\,(1 - \sqrt{T_r}))^2$$

$$m = 0.3796 + 1.54226\,\omega - 0.2699\,\omega^2 \tag{3.48}$$

In the above equation, T_r denotes for reduced temperature. The Peng Robinson equation of state offers a modified relation for 'm' for heavier components with centrifugal coefficient or ω > 0.49,

$$m = 0.379642 + 1.48503\,\omega - 0.1644\,\omega^2 + 0.016667\,\omega^3 \tag{3.49}$$

By applying changes into equation (3.47) with respect to the compressibility coefficient (z), the modified Peng Robinson is rearranged as below.

$$Z^3 + (B-1)Z^2 + (A - 3B^2 - 2B)Z - (AB - B^2 - B^3) = 0 \quad (3.50)$$

In this equation (3.50), for the prediction of the phases and the volumetric behavior of the mixtures, the critical pressure, P_C, the critical temperature, T_C , and the compressibility coefficient, Z, must be known for each component in the mixture. For pure components, the necessary properties are known and well defined. The value of B and A for pure components are defined as follow.

$$B = \frac{bP}{RT} \quad , \quad A = \frac{(a\alpha)P}{(RT)^2} \quad (3.51)$$

3.8.2 Enthalpy calculation

Enthalpy is the total heat content of a system, and it is a function of pressure and volume. Absolute enthalpy is not measurable, and only the enthalpy differences could be calculated. To check the energy balance, the calculation of the enthalpy is needed. $\left(\frac{\partial H}{\partial P}\right)$ indicates the ratio of enthalpy changes to pressure changes at a constant temperature. Therefore, the enthalpy changes relative to the reference enthalpy is shown in equation (3.52).

$$[H_p - H_{p_0}]_T = -\int_{P_0}^{P} [\frac{\partial H}{\partial P}]_T \, dp \quad (3.52)$$

In this respect, H_p is the enthalpy (kJ / kmol) at pressure P (bar), H_{p_0} denotes the enthalpy (kJ / kmol) at reference pressure P_0 (bar) , and T shows the temperature (K).

The equation below is given for the enthalpy changes based on pressure changes:

$$(\partial H/\partial P)_r = V - T\,(\partial V/\partial T)_p \quad (3.53)$$

Therefore,

$$(\partial V/\partial T)_p = [\frac{\partial}{\partial T}\left(\frac{ZRT}{P}\right)]_p = \frac{R}{P}\,[Z + T\,(\frac{\partial Z}{\partial T})_P] \tag{3.54}$$

Where 'Z' and 'R' are compressibility coefficient and constant of gases, respectively, by combining equations (3.52) to (3.54), the enthalpy deviation at pressure 'P' and reference pressure 'P_0' could be evaluated.

$$[H_p - H_{p_0}]_T = -\int_{P_0}^{P} [\frac{RT^2}{P}(\frac{\partial Z}{\partial P})_P]_T \; dp \tag{3.55}$$

$$[H_p - H_{p_0}]_T = RT\,(Z-1) + \frac{T\,(da/dT) - a}{2\sqrt{2b}} \times \ln\,[\;\frac{Z + (1+\sqrt{2})B}{Z + (1-\sqrt{2})B}\;] \tag{3.56}$$

where,

$$B = \frac{bP}{RT} \quad , \quad da/dT = -0.45724\frac{R^2.T_C^{\,2}}{P_C}K\sqrt{\frac{\alpha}{T.T_C}} \tag{3.57}$$

As mentioned earlier, the PR-EoS is compatible with predicting the behavior of liquid and vapor phases (3.56). According to the previous researches, this cubic equation (PR EoS) is more accurate and reliable for prediction of the vapor phase condensation coefficient compared to the liquid phase. Figure 3. 9 illustrates the function of enthalpy deviation.

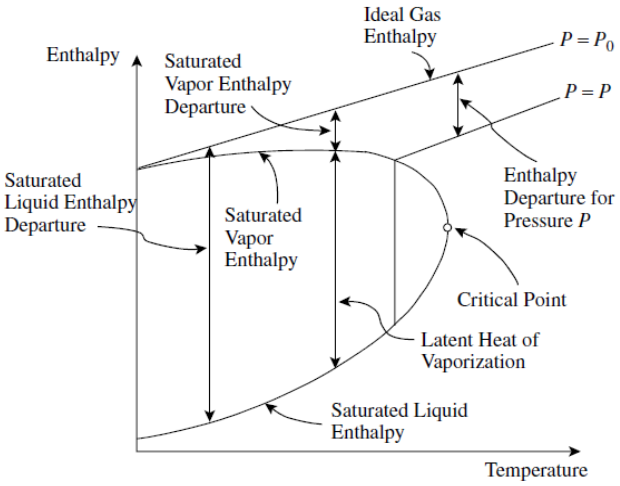

Figure 3. 9: Enthalpy deviation function (Smith, 2005)

3.8.3 Reference Enthalpy

A reference enthalpy is an enthalpy defined at temperature 'T' and reference pressure 'P_0'. At zero pressure, fluids in the gas phase are ideal so that their enthalpy is independent of pressure. The enthalpy of the ideal gases can be evaluated according to its heat capacity.

$$H_T^0 = H_{T_0}^0 + \int_{T_0}^{T} C_P^0 \, dT \tag{3.58}$$

In this equation (3.58), H_T^0 stands for enthalpy (kJ/kmol) at pressure 'P' and temperature 'T', $H_{T_0}^0$ is an enthalpy (kJ/kmol) at reference pressure 'P_0' and temperature 'T_0', T is a temperature (K) and C_P^0 is an enthalpy of the ideal gas (kJ/kmol.K) at reference pressure 'P_0' (bar) calculated by equation (3.59).

3.8.4 Enthalpy of ideal gases

Enthalpy of an ideal gas is defined as a function of temperature (3.59). The value of $\alpha_0, \alpha_1, \alpha_2, \alpha_3$ and α_4 are constants , (Cox & Chapman, 2001), and their values are different for different components.

$$\frac{C_P^0}{R} = \alpha_0 + \alpha_1 T + \alpha_2 T^2 + \alpha_3 T^3 + \alpha_4 T^4 \tag{3.59}$$

3.8.5 Entropy calculation

Entropy is evaluated to investigate the expansion and condensation processes. Usually, in ideal processes, isentropic turbine and condenser are employed.

$$[S_P - S_{P_0}]_T = \int_{P_0}^{P} \left(\frac{\partial S}{\partial P}\right)_T dP \tag{3.60}$$

S_P and S_{P_0} are the entropies at the pressure 'P' and the pressure 'P_0'.

According to the Maxwell equation, the change in entropy of a system is determined as below.

$$(\frac{\partial S}{\partial P})_T = -(\frac{\partial V}{\partial T})_P \quad (3.61)$$

Considering the relations (3.56), (3.58) and (3.61) the entropy equation is rearranged as follows.

$$[S_P - S_{P_0}]_T = -\int_{P_0}^{P} [\frac{RZ}{P} + \frac{RT}{P}(\frac{\partial Z}{\partial P})_P]_T \, dp \quad (3.62)$$

whereby the value of integral is calculated by the PR-EoS.

3.8.6 Reference Entropy

Contrary to enthalpy, entropy is not measurable at P_0 due to the fact that the entropy of gases at P_0 is infinity. Consequently, usually at low pressures, P_0 is considered 1 bar or 1 atm as a reference pressure.

$$S_T = S_{T_0} + \int_{T_0}^{T} \frac{C_P^0}{T} \, dT \quad (3.63)$$

S_T shows the entropy at the temperature 'T' and pressure 'P', and S_{T_0} is the entropy in the reference temperature (T_0) and pressure (P_0). To calculate the entropy of liquid or gas at temperature 'T' and pressure 'P', PR-EoS is evaluated. Entropy deviation function is shown in Figure 3. 10.

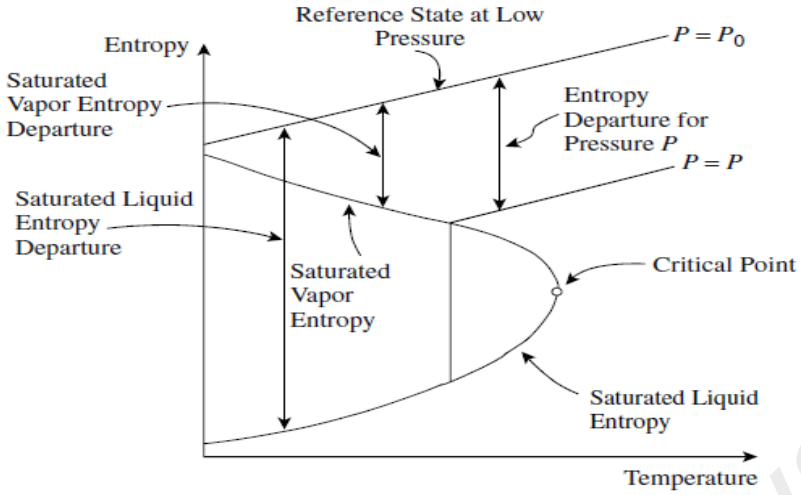

Figure 3. 10: Entropy deviation function (Smith, 2005)

3.8.7 Saturated vapor pressure calculation

The modified Wagner equation, (Perry et al., 1997), is employed for the calculation of the saturated vapor pressure. It is worth mentioning that one of the most significant specifications of this equation is calculating the exact value of vapor pressure at the critical points.

$$\ln P_r = aX_1 + bX_2 + cX_3 + dX_4 \tag{3.64}$$

$$T_r = \frac{T^{sat}}{T_C} \quad , \quad P_r = \frac{P^{sat}}{P_C} \tag{3.65}$$

$$P^{sat} = P_C \,.\exp(aX_1 + bX_2 + cX_3 + dX_4) \tag{3.66}$$

where,

$$\mathbf{X_4} = \frac{(\mathbf{1} - \mathbf{T_r})^{\mathbf{5}}}{\mathbf{T_r}} \quad , \quad \mathbf{X_3} = \frac{(\mathbf{1} - \mathbf{T_r})^{\mathbf{2.5}}}{\mathbf{T_r}} \tag{3.66.1}$$

$$\mathbf{X_2} = \frac{(\mathbf{1} - \mathbf{T_r})^{\mathbf{1.5}}}{\mathbf{T_r}} \quad , \quad \mathbf{X_1} = \frac{(\mathbf{1} - \mathbf{T_r})}{\mathbf{T_r}}$$

In the above relations, T_r stands for the reduced temperature, T_C is the critical temperature, and T^{sat} is the saturated temperature. Also, P_r shows the reduced pressure, P_C stands for the critical pressure and the P^{sat} is the saturated pressure.

Besides, for calculation of the a, b, c and d coefficients, the following relations were employed (Forero & J, 2011). ω is an acentric factor, and its value for different components are different.

$$a = -0.9687\,\omega^2 - 4.895\,\omega - 5.9677 \quad (3.66.2)$$
$$b = 2.8882\,\omega^2 + 0.8663\,\omega + 1.27761$$
$$c = -4.9542\,\omega^2 - 5.1381\,\omega - 0.5428$$
$$d = 2.8913\,\omega^2 - 6.9855\,\omega - 1.2417$$

$\Delta T_{PP,eva}$, $\Delta T_{PP,cond}$ are determined according to Figure 3.5 as follows.

The pinch point temperature difference in the evaporator, $\Delta T_{PP,eva}$, can be expressed to consider the minimum temperature difference between a geothermal fluid ($C_9H_{14}NBF_4$/water) and the working fluid (R-600/R-600a) in the evaporation process.

$$PPTD = \Delta T_{PP,eva} = T_{h,pp} - T_{4''} \quad (3.67)$$

Accordingly, the pinch point temperature difference in the condenser, $\Delta T_{PP,cond}$, is the minimum temperature difference between the rest of the vapor leaving the turbine and the cooling fluid ($C_9H_{14}NBF_4$/water) in the condenser.

$$PPTD = \Delta T_{PP,cond} = T_{6''} - T_{C,pp} \quad (3.68)$$

Followings are the relations of $\dot{m}_{wf}$ and $\dot{m}_c$ in general. It is a note of interest that $\dot{m}_{wf}$ and $\dot{m}_c$ for each cycle are explained in the sections “3.7.2.1” to “3.7.2.3”.

$$\dot{m}_{wf} = \frac{\dot{m}_h (h_{si} - h_h \mid \text{at } T_L)}{(h_{wf,out}^{evap} - h_{wf}^{evap} \mid \text{at Bubble point})} \quad (3.69)$$

$$\dot{m}_c = \frac{\dot{m}_{wf}(h_{wf}^{cond} \mid \text{at Dew point} - h_{wf,out}^{cond})}{(h_c \mid \text{at } T_L - h_{csi})} \quad (3.70)$$

3.9 Economic and thermo-economic evaluation

In addition to the thermodynamic optimization, economic optimization is evaluated. Also, the thermo-economic optimization was employed to distinguish the cycle's performances thermodynamically and economically.

The term thermo-economics is defined as the combination of exergy and economical to enhance the design and operation of the thermal processes. Thermo-economics is sometimes known as exergo-economics.

3.9.1 Economic relations to calculate the cost of components in the cycle

In the following section, the economic relations for the utilized equipment in the cycles are given. Accordingly, in order to estimate the cost of each equipment in the ORC cycle, the bare module method (Imran et al., 2014) was selected.

3.9.1.1 Cost of heat exchangers (C_{HX})

Following equations are given for assessing the cost of heat exchangers including the evaporator, regenerative and condenser.

$$C_{HX} = \frac{603.1}{397} \times C_{0,HX} \times \left[B_{1,HX} + \left(B_{2,HX} \times F_{M,HX} \times F_{P,HX}\right)\right] \quad (3.71)$$

$$\log C_{0,HX} = [\, K_{1,HX} + K_{2,HX} (\log A_{HX}) + K_{3,HX} (\log A_{HX})^2 \quad (3.72)$$

$$\log F_{P,HX} = [\, C_{1,HX} + C_{2,HX} (\log P_{HX}) + C_{3,HX} (\log P_{HX})^2] \quad (3.73)$$

C_{HX} shows the heat exchangers' costs, $F_{P,HX}$ is the heat exchangers' pressure factor, P_{HX} implies for the surface pressure, A_{HX} stands for a surface area and $F_{M,HX}$ is the heat exchangers material factor. By using equation (3.72), the primary cost of heat exchangers is determined.

3.9.1.2 Cost of turbine (C_t)

$$C_t = \frac{603.1}{397} \times C_{0,t} \times F_{M,t} \quad (3.74)$$

$$\log C_{0,t} = [K_{1,t} + K_{2,t} (\log W_t) + K_{3,t} (\log W_t)^2] \quad (3.75)$$

where $C_{0,t}$ and $F_{M,t}$ indicate the initial cost and material factor of the turbine, respectively.

3.9.1.3 Cost of pump (C_P)

For the investigation of the costs of the pump, the following relations are applied.

$$C_P = \frac{603.1}{397} \times C_{0,P} \times [B_{1,P} + (B_{2,P} \times F_{M,P} \times F_{P,P})] \quad (3.76)$$

$$\log C_{0,P} = [K_{1,P} + K_{2,P} (\log W_P) + K_{3,P} (\log W_P)^2] \quad (3.77)$$

$$\log F_{P,P} = [C_{1,P} + C_{2,P} (\log P_P) + C_{3,P} (\log P_P)^2] \quad (3.78)$$

In this regard, $C_{0,P}$ is the initial pump cost, $F_{M,P}$ shows the material factor of the pump , and $F_{P,P}$ stands for the pump's pressure factor. B_1, B_2, K_1, K_2, K_3, C_1, C_2 and C_3 in equations (3.76) to (3.77) are constant parameters of the equipment shown in Table 3. 2. Besides, 603.1 and 397 are chemical engineering plant cost indexes for the year 2018 and 2001, respectively (Peters et al., 1968).

Table 3. 2: bare module constant parameters (Kazemi & Samadi, 2016; Turton et al., 2009)

	Equipment of ORCs		
Constants	**Heat exchanger**	**pump**	**turbine**
K_1	4.3247	3.3892	2.2476
K_2	-0.3030	0.0536	1.4965
K_3	0.1634	0.1538	-0.1618
C_1	0.03881	-0.3935	-
C_2	-.01127	0.3957	-
C_3	0.0818	-0.0023	-
B_1	1.6300	1.8900	-
B_2	1.6600	1.3500	-
F_M	1.0000	1.6000	3.5000
F_S	1.7000	1.7000	1.7000

It is worth mentioning that in this study, all pumps were selected from centrifuge type and equipment was made of carbon steel.

3.10 specific investment cost (SIC)

To evaluate the total costs of the ORC cycle (cost produced by each equipment in the cycle), the specific investment cost (SIC) was employed.

$$SIC = F_S \times \frac{TC_B}{\dot{W}_{net}} \tag{3.79}$$

where F_S and TC_B respectively stand for the correction factor of overhead cost and the total bare module cost. The value of F_S is shown in Table 3. 2, and TC_B is obtained by equation (3.80).

$$TC_B = \sum_{i=1}^{n} C_i \tag{3.80}$$

In the present work, the cost of geothermal energy (heat source) and working fluids are considered to be minute in comparison to the costs of the power plant.

3.11 Selection of heat exchanger

To calculate heat exchangers' cost, the type of heat exchanger should be determined. The heat exchanger is the substantial cycle' equipment, and it needs to be selected wisely considering the cycle's operating parameters and its heat surface area. The plate heat exchangers are operated if power output capacity ($\dot{W}_{net}$) is lower than 10 kW. Otherwise, for production higher than 100 kW, shell and tube heat exchangers are employed (Li, Wang, et al., 2015). In this research, the shell and tube heat exchangers were selected, see **Figure 3. 11**.

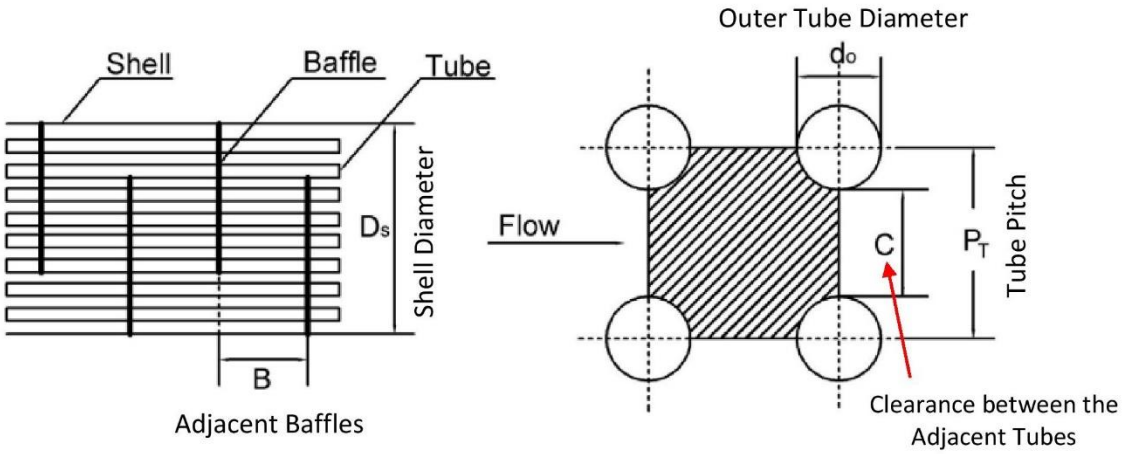

Figure 3. 11: Schematic diagram of shell and tube heat exchanger (Le, Kheiri, et al., 2014)

The specification of the shell and tube heat exchanger coupled with the ORCs with flow in the tube and liquid in the shell are shown in table below.

Table 3. 3: Shell and tube data (Le, Kheiri, et al., 2014)

Inner tube diameter, d_i (mm)	Outer tube diameter, d_o (mm)	Tube Pinch, P_T (mm)	Refrigerant fouling factor, ($m^2{}^oC/w$),(Tubular Exchanger Manufacturers, 1999)	Pressure drop (bar)
10.92	12.70	19.05	0.0003522	**Tube:** 0.2
				Shell: 0.5

3.12 Heat exchanger surface area

To calculate the cost of heat exchangers, the surface areas of evaporator, condenser and regenerative are required. In this research, Kern's method, (Kazemi & Samadi, 2016; Kern, 1986), is applied to determine the heat transfer surface area of heat exchangers.

$$A_{hx} = \frac{Q_{hx}}{UF\ (\Delta T_{Lm})} \tag{3.81}$$

Q_{hx} stands for the transferred heat by the heat exchangers, and its relation for the evaporator, regenerative, and condenser are described in equations (3.5), (3.6) and (3.11). U is the overall heat transfer coefficient, and it is evaluated by the relation (3.80). F

implies for the correction factor and ΔT_{Lm} denotes for the logarithmic mean temperature difference.

Therefore,

$$U = \left[\frac{d_o}{h_i d_i} + \frac{R_{f,i} d_o}{d_i} + \frac{d_o \ln(d_o/d_i)}{2k} + R_{f,o} + \frac{1}{h_o}\right]^{-1} \quad (3.82)$$

$$F = \frac{1}{RF - 1} \log\left(\frac{1 - PF}{1 - (PF \times RF)}\right) \quad (3.83)$$

$$\Delta T_{Lm} = \frac{(T_{h,out} - T_{c,in}) - (T_{h,in} - T_{c,out})}{\ln\left[(T_{h,out} - T_{c,in})/(T_{h,in} - T_{c,out})\right]} \quad (3.84)$$

In equation (3.82), the heat transfer coefficient of inside and outside of the tube is denoted by h_i and h_o. d_i and d_o stand for the inner and outer diameter of the tube, $R_{f,i}$ and $R_{f,o}$ are the internal and external sediment resistance factor of the pipe and K is the conductive heat transfer coefficient. Accordingly, RF and PF are calculated as follows.

$$RF = \frac{(T_{h,in} - T_{h,out})}{(T_{c,out} - T_{c,in})} \quad (3.85)$$

$$PF = \frac{(T_{c,out} - T_{c,in})}{(T_{h,in} - T_{c,in})} \quad (3.86)$$

where, $T_{h,in}$ and $T_{h,out}$ are the inlet and outlet temperatures of a geothermal fluid, $T_{c,in}$ and $T_{c,out}$ denote the inlet and outlet temperatures of the cooling fluid.

According to the relation (3.82), to analyze the overall heat transfer coefficient (U), the value of inside and outside heat transfer coefficient of the tube (h_i and h_o) are needed. Gnielinski's method is used to evaluate the value of h_i.

$$h_i = Nu \frac{k_i}{d_i} \quad (3.87)$$

Nu denotes the Nusselt number and its value for the fluid inside the tube is equal to:

$$\mathrm{Nu} = \frac{(\mathrm{f}/8)(\mathrm{Re} - 1000)\mathrm{Pr}}{1 + 12.7(\mathrm{f}/8)^{0.5}(\mathrm{Pr}^{2/3} - 1)} \tag{3.88}$$

Where f, Re and Pr are indicators of friction factor, Reynolds number and Prandtl number, respectively.

(a) Friction factor (f)

The friction factor is defined based on the fluid flows in the pipe into two principal categories.

i. Turbulent flow

$$\mathrm{f} = [0.790\ln(\mathrm{Re}) - 1.64]^{-2} \tag{3.89}$$

ii. Laminar flow

$$\mathrm{f} = 64/\mathrm{Re} \tag{3.90}$$

(b) Reynolds number (Re)

$$\mathrm{Re_i} = \frac{\dot{m}_i d_i}{\mu_i A_i} \tag{3.91}$$

(c) Prandtl number (Pr)

$$\mathrm{Pr_i} = \frac{\mu_i C_{p_i}}{k_i} \tag{3.92}$$

By swapping the above equations in the relations (3.87) and (3.88), the heat transfer coefficient in the tube is calculated.

Then by employing Kern's method, the value of h_o (heat transfer coefficient outside the tube) is obtained as below.

$$h_o = \frac{k_o}{d_o} \times 0.36 \times \left(\frac{d_o \dot{m}_o}{A_o \mu_o}\right)^{0.55} \left(\frac{C_{p_o} \mu_o}{k_o}\right)^{1/3} \tag{3.93}$$

3.13 Optimization

Optimization is an essential tool for many engineering designs and can be realized by using different objective functions By optimization, not only be able to find an optimum design but also, without the examining all possible cases, time of simulation is reduced. To carry out the optimization, the elements, including objective functions for optimization, parameters and boundaries, and mathematical model, are needed to be specified.

3.13.1 Objective function

The selection of an appropriate objective function is substantial in optimizing the operating parameters. In this study, thermodynamic (exergy efficiency relation), economic (SIC relation) and thermo-economic [linear weighted function (Xiao et al., 2015)], were selected for optimization of evaporation temperature (T_{evap}), the temperature of the second evaporator (T_{evap_2}), pinch point temperature difference in the evaporator ($\Delta T_{p.p}$), the degree of superheat (D.S) and the regenerative temperature (T_{reg}).

In the following equations, $F_1(X)$ and $F_2(X)$ are indicators nominated to represent the the thermodynamic and economic objective functions. The aim of nomination of the indicators were to ease and shorthern the calculation steps of the third objective function (thermo-economic) in the optimization.

$$F_1(X) = \text{Maximize}\ (\eta_{ex}) = \frac{\dot{W}_{net}}{E\dot{x}_h} = \frac{\dot{W}_t - \dot{W}_p}{\dot{m}_h[h_{hsi} - h_{hso} - T_0(s_{hsi} - s_{hso})} \quad (3.94)$$

$$F_2(X) = \text{Minimize}\ (SIC) = F_S \times \frac{TC_B}{\dot{W}_{net}} \quad (3.95)$$

$$F(X) = \alpha F_1(X) + \beta F_2(X) \quad (3.96)$$

α and β are weight coefficients, and their values are dependents on the thermodynamic and economic optimizations (3.96.1).

$$\alpha = \frac{(F_2^1 - F_2^2)}{[(F_1^2 - F_1^1) + (F_2^1 - F_2^2)]} \quad , \quad \beta = 1 - \alpha \tag{3.96.1}$$

F_1^1 , F_1^2 , F_2^2 , F_2^1 in (3.96.1) are described as follows.

- F_1^1: the maximum value of F_1
- F_1^2: the value of function F_1 when F_2 obtained a minimum value
- F_2^2: the minimum value of F_2
- F_2^1: the value of function F_2 when F_1 obtained a maximum value

As explained precisely in section "3.7.3", to maximize the efficiency of the system, the output power of the cycle should be increased. According to the relation given for the thermodynamic objective function (3.94), the net output power ($\dot{W}_{net}$) directly influences the system's efficiency. In other words, the more power is generated, the higher efficiency is obtained. Furthermore, according to the section "3.10", to assess the cycle's total costs (3.95), the cost of each equipment in the cycle should be computed. The economic relations for all the equipment (pump, evaporator, turbine, regenerative and condenser) used in the ORC system are given in sections "3.9.1.1" to "3.9.1.3".

3.13.2 Mathematical model

MATLAB programming is applied to optimize the objective functions by genetic algorithm (GA) method, (Xi et al., 2013). The genetic algorithm is based on Darwin's theory of evolution, and it is a random-based algorithm in which gradual changes are made to the values to obtain the best fitness (Saraswat & Sharma, 2013).

The GA conditions in optimization are indicated in Table 3. 4**.** Conditions are selected according to the research investigated by (Karimi & Mansouri, 2018).

Table 3. 4: GA conditions in optimization (Karimi & Mansouri, 2018)

GA operating parameters	*Population size*	*Crossover probability (fraction)*	*Crossover function*	*Elite count*	*Stop generation*	*Plot function*
range/type	20	0.8	scattered	1	100	Best fitness

3.13.3 Optimized variables and boundaries

As one of the necessary steps in GA optimization, the number of parameters going to be optimized should be specified. Several parameters are defined according to the equipment used in each cycle. For example, in the basic ORC, only three parameters T_{evap_1}, $\Delta T_{p.p}$, and D.S are optimized. Table 3. 5 indicates the parameters optimized for each cycle's configuration.

Table 3. 5: Optimization parameters for three selected configurations

	Optimized Parameters				
	$\mathbf{T_{evap_1}}$	$\mathbf{T_{evap_2}}$	$\mathbf{T_{reg}}$	$\mathbf{\Delta T_{p.p}}$	**D.S**
basic ORC	✓			✓	✓
RORC	✓		✓	✓	✓
TSORC	✓	✓		✓	✓

Constraints and bounds of operating parameters are the limitations defined for the cycle to monitor the cycle's behaviour. In other words, without constraints and bounds, the performance of the cycle is out of control. For example, if the pump's pressure is not limited, the pump bursting will probably occur. Therefore, monitoring the cycle's performance could be a vital step from thermodynamic and economic perspectives. Table 3. 6. indicates lower and upper bands defined for the optimization. These bounds are identified according to properties of the operating fluid used in the cycle, heat source temperature and cycle's components (e.g., type of heat exchangers, pump).

Table 3. 6: Constraints and bounds of optimization parameters

Parameters (constraints)	Lower bound	Upper bound
Temperature of evaporator 1 - (T_{evap_1})	320(K)	485(K)
Temperature of evaporator 2 - (T_{evap_2})	320(K)	485(K)
Temperature of regenerative – (T_{reg})	320(K)	485(K)
Degree of superheat - **(D.S)**	0(K)	20(K)
PPTD in evaporator 1	5(K)	20(K)
Pressure of evaporator 1	5(bar)	30(bar)

As part of optimization, some parameters were considered as constant values. These constant parameters were nominated according to the optimization modeling studied by other researchers (Karimi & Mansouri, 2018; Kazemi & Samadi, 2016; Samadi & Kazemi, 2020). Applied constant design parameters in optimization are indicated.

Table 3. 7: Constant design parameters in optimization (Karimi & Mansouri, 2018; Kazemi & Samadi, 2016; Samadi & Kazemi, 2020)

Parameters	*Value*
Isentropic efficiency of the pump, η_{is}^{p} (%)	80
Isentropic efficiency of the turbine, η_{is}^{t} (%)	76
Electrical generator efficiency, η_{gen}^{t} (%)	95
Heat sink inlet temperature, T_{csi} (K)	293.15
Heat source inlet pressure, P_{hsi} (bar)	5
Heat sink inlet pressure, P_{csi} (bar)	2
Temperature of condenser, T_c (K)	308
Pinch point temperature in condenser, T_{pinch}^{c} (K)	5
Heat source mass flow rate, $\dot{m}_h$ (kg/s)	50
Temperature of the environment taken as standard-state value, T_0 (K)	298.15

3.14 Summary

In this chapter, the descriptions of the three selected cycles were presented. The thermodynamic (energy and exergy efficiencies) and economic (specific investment cost) relations for all ORCs' components were given and discussed. Besides, maximization of the cycle's efficiency and minimization of its total costs was applied as the objective function in optimization of evaporation temperature, the temperature of the second evaporator, pinch point temperature difference in the evaporator, the degree of superheat and the regenerative temperature.

CHAPTER 4: RESULTS AND DISCUSSIONS

In this chapter, the optimization results for all ORCs are illustrated and discussed. The outcomes of optimization were compared between $C_9H_{14}NBF_4$ /water (geothermal fluids) and R-600/R-600a (working fluid) under the same circumstances.

4.1 Verification

The exergy efficiency versus evaporating temperature for R-600 obtained from the thermodynamic optimization in the present model was verified with the study carried out by Shengjun et al. (2011), Figure 4. 1. As can be seen, the model presented in this research shows a similar pattern to that of studied by Shengjun et al. (2011).

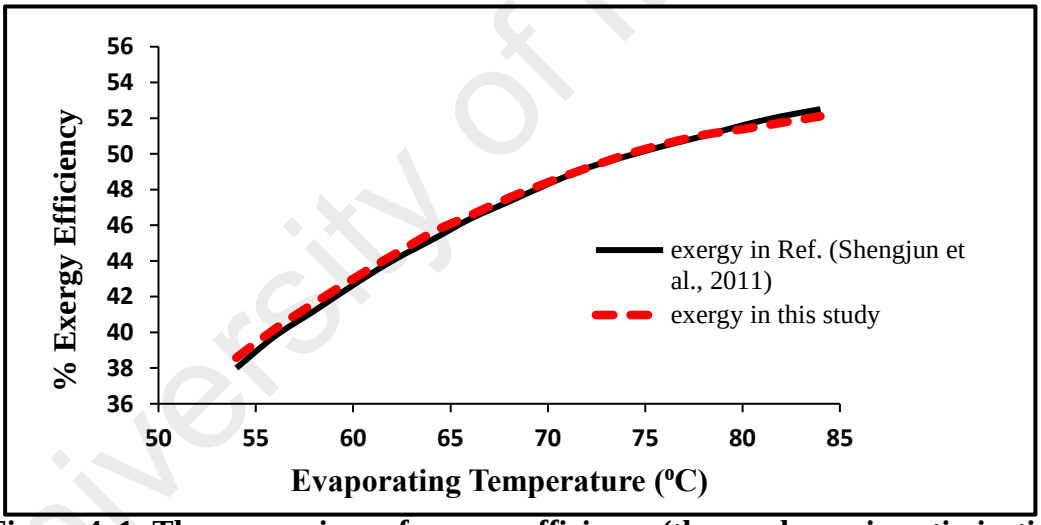

Figure 4. 1: The comparison of exergy efficiency (thermodynamic optimization) in this study and Shengjun et al. (2011)

In addition, the obtained thermal efficiency for the basic ORC from the present work is compared with the work of other authors, and the results are shown in Table 4. 1. It can be seen that the obtained thermal efficiencies are in good agreement with those of efficiencies investigated by other authors. The slight differences (up to 0.24%) observed in the thermal and exergy efficiencies can be due to the optimization conditions and assumptions.

Table 4. 1:Obtained thermal efficiency based on thermodynamic optimization conducted through this study compared to other studies

COMP.	T_{geo} (°C)	T_{Cool} (°C)	T_{evap} (°C)	T_{cond} (°C)	$\Delta P_{p.p,evap}$ (°C)	$\Delta P_{p.p,cond}$ (°C)	D. S (°C)	η_{th}%	Ref.
R-600	120.00	15.00	74.16	25.00	5.00	5.00	0.00	6.52	This work
R-600	120.00	15.00	74.16	25.00	5.00	5.00	0.00	6.44	(Karimi & Mansouri, 2018)
R-600a	150.00	20.00	123.01	35.00	5.064	5.00	8.319	12.04	This work
R-600a	150.00	20.00	123.01	35.00	5.064	5.00	8.319	11.83	(Kazemi & Samadi, 2016)
water	150.00	15.00	85.18	30.00	3.00	0.5	60.00	10.49	This work
water	150.00	15.00	85.18	30.00	3.00	0.5	60.00	10.73	(Kazemi & Samadi, 2016)

4.2 Optimization outcomes and cycle performance

The performance of a basic ORC, RORC, and TSORC with $C_9H_{14}NBF_4$ and water, each in the role of geothermal fluid, was compared and optimized using the same objective functions, thermodynamic, economic and thermo-economic (multi-objective function). The results of the optimization are shown in Table 4. 2 to Table 4. 5 at temperatures between 180 °C and 210 °C.

Table 4. 2: Thermodynamic, economic, and thermo-economic optimized results of $C_9H_{14}NBF_4$-R-600

optimization		Tgeo (ºC)	Tevap1 (K)	Tevap2 (K)	Treg (K)	D.S (K)	Δt pp (K)	energy (%)	exergy (%)	SIC ($/W)	α
basic ORC	Thermo.	180	410.71			0	5.00	13.25	54.92	4.35	
		190	410.71			0	5.00	13.24	60.49	4.73	
		200	409.83			0	5.00	13.21	67.59	4.11	
		210	410.02			0	5.00	13.22	82.35	4.89	
	Econo.	180	406.02			19.01	5.04	13.01	52.63	2.68	
		190	407.00			19.85	5.01	13.10	58.42	2.71	
		200	405.39			19.94	5.03	13.11	65.72	2.93	
		210	406.59			20.00	5.02	13.19	80.26	3.01	
	Thermo-Econo.	180	409.23			7.21	5.06	13.05	56.27	2.86	0.719
		190	408.83			8.11	5.00	13.14	61.78	3.19	0.806
		200	409.12			9.69	5.08	13.18	71.64	3.34	0.685
		210	409.76			10.58	5.01	13.20	84.70	3.67	0.821
RORC	Thermo.	180	408.60		325.14	0	5.02	14.06	54.88	4.62	
		190	410.57		325.12	0	5.00	14.16	59.36	3.98	
		200	409.93		325.02	0.01	5.02	14.13	63.90	4.53	
		210	410.08		325.09	0	5.00	14.14	71.96	4.79	
	Econo.	180	384.31		329.03	20.00	5.00	14.00	52.69	2.86	
		190	392.23		331.05	19.99	5.00	14.09	57.02	2.93	
		200	400.68		330.54	19.94	5.02	14.10	61.94	3.91	
		210	402.74		331.94	20.00	5.06	14.12	68.97	4.01	
	Thermo-Econo.	180	407.61		327.14	5.55	5.08	13.96	52.88	3.72	0.768
		190	409.87		326.12	6.38	5.11	13.89	56.36	3.51	0.654
		200	409.97		329.02	6.79	5.02	13.76	59.90	3.93	0.714
		210	409.08		331.09	7.51	5.08	13.92	69.96	3.87	0.691
TSORC	Thermo.	180	410.63	342.83		0.00	5.00	13.03	54.58	4.39	
		190	410.01	363.03		0.00	5.00	13.62	55.19	4.29	
		200	409.83	367.01		0.09	5.76	13.86	55.26	3.98	
		210	410.81	378.66		0.98	5.17	13.76	56.05	3.78	
	Econo.	180	409.32	330.26		20.00	5.00	13.00	52.52	2.76	
		190	409.11	346.58		19.98	5.01	13.35	53.63	2.65	
		200	408.76	347.08		19.99	5.00	13.49	53.89	2.89	
		210	409.83	357.42		20.00	5.13	13.51	54.35	2.98	
	Thermo-Econo.	180	409.93	343.62		5.21	5.00	13.00	52.37	2.89	0.736
		190	409.91	363.23		8.62	5.00	13.22	53.64	2.39	0.763
		200	409.63	367.41		7.49	5.01	13.36	53.29	2.68	0.718
		210	409.76	379.00		6.94	5.02	13.47	53.31	2.97	0.633

Table 4. 3: Thermodynamic, economic, and thermo-economic optimized results of $C_9H_{14}NBF_4$-R-600a

optimization		Tgeo (ºC)	Tevap1 (K)	Tevap2 (K)	Treg (K)	D.S (K)	Δt pp (K)	energy (%)	exergy (%)	SIC ($/W)	α
basic ORC	Thermo.	180	392.14			0	5.00	11.53	58.27	3.98	
		190	392.15			0	5.00	11.53	64.78	3.99	
		200	392.60			0.87	5.00	11.57	74.64	4.11	
		210	391.32			0.02	5.00	11.48	87.70	4.00	
	Econo.	180	370.25			20.00	5.03	11.42	56.03	2.96	
		190	373.64			19.98	5.00	11.49	62.65	2.88	
		200	372.68			20.00	5.01	11.50	72.94	3.27	
		210	370.96			19.99	5.02	11.40	85.87	3.57	
	Thermo-Econo.	180	392.07			5.98	5.02	11.23	53.47	2.90	0.632
		190	391.98			8.39	5.00	11.46	61.88	2.89	0.645
		200	391.86			6.47	5.08	11.49	70.94	3.21	0.683
		210	390.54			7.27	5.00	11.50	81.97	3.09	0.638
RORC	Thermo.	180	392.34		325.03	0	5.03	12.45	56.28	3.67	
		190	392.75		325.16	0	5.01	12.46	60.27	3.85	
		200	392.30		325.14	0	5.01	12.46	64.36	4.09	
		210	391.90		325.11	0.01	5.01	12.42	70.02	4.21	
	Econo.	180	379.11		321.43	20.00	5.00	12.26	54.89	2.89	
		190	380.03		321.68	20.00	5.01	12.28	58.37	2.94	
		200	379.68		323.25	19.97	5.03	12.29	62.25	3.61	
		210	381.24		322.65	19.96	5.01	12.36	68.11	3.70	
	Thermo-Econo.	180	392.04		327.03	8.31	5.00	12.15	52.98	2.57	0.653
		190	392.15		327.16	10.69	5.02	12.27	58.21	2.76	0.631
		200	392.29		327.54	5.97	5.01	12.34	61.35	3.34	0.628
		210	391.61		327.21	9.61	5.10	12.36	67.12	3.64	0.666
TSORC	Thermo.	180	392.62	355.27		0	5.27	12.03	51.97	4.11	
		190	392.60	355.07		0.01	5.00	12.32	52.40	4.23	
		200	392.51	353.35		0	5.00	12.85	53.12	4.62	
		210	392.27	374.12		0.02	5.20	12.71	55.27	4.78	
	Econo.	180	385.32	336.00		20.00	5.00	12.00	49.87	3.54	
		190	386.02	337.24		20.00	5.00	12.09	50.96	3.62	
		200	386.54	335.62		19.98	5.02	12.37	51.29	3.84	
		210	386.60	341.65		19.99	5.08	12.51	53.67	3.96	
	Thermo-Econo.	180	391.73	359.26		6.37	5.00	11.93	49.38	3.65	0.636
		190	392.00	358.87		8.94	5.00	12.02	50.82	3.95	0.735
		200	392.01	356.65		10.65	5.02	12.25	51.67	3.72	0.749
		210	391.97	375.42		9.73	5.09	12.11	54.71	3.24	0.807

Table 4. 4 : Thermodynamic, economic, and thermo-economic optimized results of water-R-600

optimization		Tgeo (ºC)	Tevap1 (K)	Tevap2 (K)	Treg (K)	D.S (K)	Δt pp (K)	energy (%)	exergy (%)	SIC ($/W)	α
basic ORC	Thermo.	180	408.74			1.20	5.00	13.16	52.83	5.11	
		190	410.07			0.05	5.00	13.14	57.17	5.21	
		200	409.06			0.94	5.00	13.18	60.98	5.00	
		210	408.14			1.20	5.00	13.13	65.37	5.26	
	Econo.	180	402.36			20.00	5.02	13.00	49.36	4.63	
		190	406.27			19.96	5.00	13.01	52.89	4.76	
		200	405.38			20.00	5.01	13.06	57.27	4.89	
		210	402.52			19.99	5.00	13.90	61.49	4.92	
	Thermo-Econo.	180	408.04			9.65	5.00	12.12	50.63	4.68	0.692
		190	409.87			8.35	5.02	12.24	55.13	4.53	0.677
		200	408.76			7.94	5.06	12.36	57.38	4.06	0.643
		210	408.00			7.68	5.09	12.46	62.32	4.81	0.687
RORC	Thermo.	180	409.64		322.40	0.57	5.00	14.03	54.36	5.01	
		190	410.71		322.28	0.02	5.00	14.07	58.06	5.00	
		200	410.84		322.00	0.37	5.04	14.07	62.08	5.03	
		210	410.45		322.16	0.02	5.01	14.05	67.13	5.13	
	Econo.	180	396.23		321.00	20.00	5.00	13.94	51.39	4.13	
		190	398.62		320.98	20.00	5.01	13.97	54.81	4.53	
		200	399.00		321.02	19.96	5.00	14.01	57.96	4.67	
		210	399.92		321.50	19.99	5.02	14.08	61.27	4.70	
	Thermo-Econo.	180	409.23		326.40	8.63	5.00	13.03	52.37	4.21	0.728
		190	410.38		325.28	7.69	5.03	13.07	55.86	4.32	0.686
		200	410.11		326.00	5.98	5.09	13.12	59.78	4.13	0.652
		210	409.95		325.16	10.63	5.00	13.65	64.10	4.63	0.636
TSORC	Thermo.	180	408.15	340.72		0.81	5.00	13.58	53.59	4.99	
		190	410.70	339.75		1.20	5.00	13.70	56.18	5.10	
		200	410.92	330.12		0.03	5.00	13.41	61.02	5.00	
		210	410.84	323.12		1.20	5.00	13.12	66.04	5.03	
	Econo.	180	392.32	324.00		20.00	5.01	13.18	51.36	4.12	
		190	393.00	325.35		20.00	5.03	12.97	52.25	4.36	
		200	394.62	322.95		19.96	5.00	13.27	56.85	4.40	
		210	394.85	320.11		19.98	5.10	13.02	59.34	4.52	
	Thermo-Econo.	180	407.95	344.34		9.67	5.01	12.28	50.88	3.69	0.771
		190	409.78	341.28		8.57	5.06	12.72	52.46	4.16	0.695
		200	410.02	336.42		10.11	5.09	12.81	59.42	4.02	0.666
		210	409.86	328.71		9.68	5.04	12.92	62.64	4.79	0.621

Table 4. 5: Thermodynamic, economic, and thermo-economic optimized results of water-R-600a

optimization		Tgeo (ºC)	Tevap1 (K)	Tevap2 (K)	Treg (K)	D.S (K)	Δt pp (K)	energy (%)	exergy (%)	SIC ($/W)	α
basic ORC	Thermo.	180	391.35			1.30	5.00	11.50	54.97	5.34	
		190	392.30			1.20	5.00	11.49	58.77	5.32	
		200	391.20			1.90	5.04	11.49	62.66	5.31	
		210	391.10			2.60	5.00	11.50	67.53	5.30	
	Econo.	180	386.23			20.00	5.00	11.02	51.63	4.34	
		190	387.11			19.98	5.02	11.10	55.37	4.42	
		200	386.96			19.96	5.00	11.26	57.69	4.69	
		210	386.21			20.00	5.04	11.34	62.00	4.73	
	Thermo-Econo.	180	390.45			10.68	5.01	10.65	51.97	4.07	0.763
		190	391.42			8.54	5.01	10.75	54.71	4.60	0.752
		200	391.00			7.68	5.00	10.78	59.66	4.70	0.688
		210	390.35			9.64	5.09	10.89	62.08	4.83	0.673
RORC	Thermo.	180	392.73		320.06	0.40	5.02	12.26	56.03	5.39	
		190	391.81		320.38	0.00	5.02	12.27	59.12	5.38	
		200	392.61		320.54	0.00	5.00	12.29	63.81	5.36	
		210	392.93		320.58	0.00	5.00	12.30	69.73	5.35	
	Econo.	180	379.64		320.00	20.00	5.00	12.06	53.63	4.69	
		190	381.63		320.16	18.96	5.03	12.17	55.82	4.71	
		200	381.96		320.39	19.11	5.01	12.00	59.18	4.75	
		210	382.05		320.46	19.69	5.10	12.01	62.98	4.79	
	Thermo-Econo.	180	391.62		326.48	6.56	5.06	11.32	53.92	4.31	0.804
		190	391.01		326.78	7.68	5.08	11.46	56.87	4.37	0.747
		200	392.11		327.14	10.63	5.00	11.59	61.02	4.62	0.700
		210	392.29		327.58	9.37	5.06	11.72	64.34	4.76	0.662
TSORC	Thermo.	180	392.34	326.18		0.21	5.00	11.70	56.03	5.67	
		190	391.80	325.01		0.75	5.01	11.69	59.12	5.62	
		200	391.62	325.14		0.00	5.00	11.50	63.81	5.55	
		210	392.48	321.07		0.72	5.05	11.34	69.73	5.76	
	Econo.	180	380.11	321.65		19.98	5.00	11.20	52.68	4.36	
		190	379.68	321.25		20.00	5.03	11.25	56.21	4.68	
		200	381.37	322.13		19.68	5.20	11.20	58.68	4.73	
		210	380.67	321.26		20.00	5.00	11.00	63.84	4.90	
	Thermo-Econo.	180	392.00	328.48		8.64	5.07	10.17	55.73	5.01	0.828
		190	391.21	327.91		9.46	5.04	10.29	58.82	5.12	0.817
		200	390.96	327.34		7.53	5.01	10.43	61.21	4.92	0.730
		210	391.68	324.72		8.35	5.00	10.57	66.67	5.32	0.745

4.3 Thermodynamic optimization

Comparisons of the cycle performances based on the thermodynamic objective function are evaluated and discussed in this section. Generally, the trends by which exergy efficiency varies with temperature for both geothermal fluids were found to be effectively similar when both working fluids, R-600 and R-600a, were utilized. R-600a was found to generate a slightly higher cycle performance than R-600 in all configurations except for the TSORC – $C_9H_{14}NBF_4$ combination (see Figure 4. 2 (a and b)). For $C_9H_{14}NBF_4$, the highest efficiency (87.70%) was obtained in the basic ORC at 210 °C while the lowest efficiency (51.97%) was in the TSORC at 180 °C, with R-600a as the working fluid in both instances. For water, the highest efficiency (69.73%) was obtained at 210 °C for the RORC configuration with R-600a as the working fluid while the lowest efficiency (52.83%) was in the basic ORC at 180 °C with R-600. In general, the performance of basic and regenerative ORC configurations, with water as a geothermal fluid, is relatively modest compared to $C_9H_{14}NBF_4$.

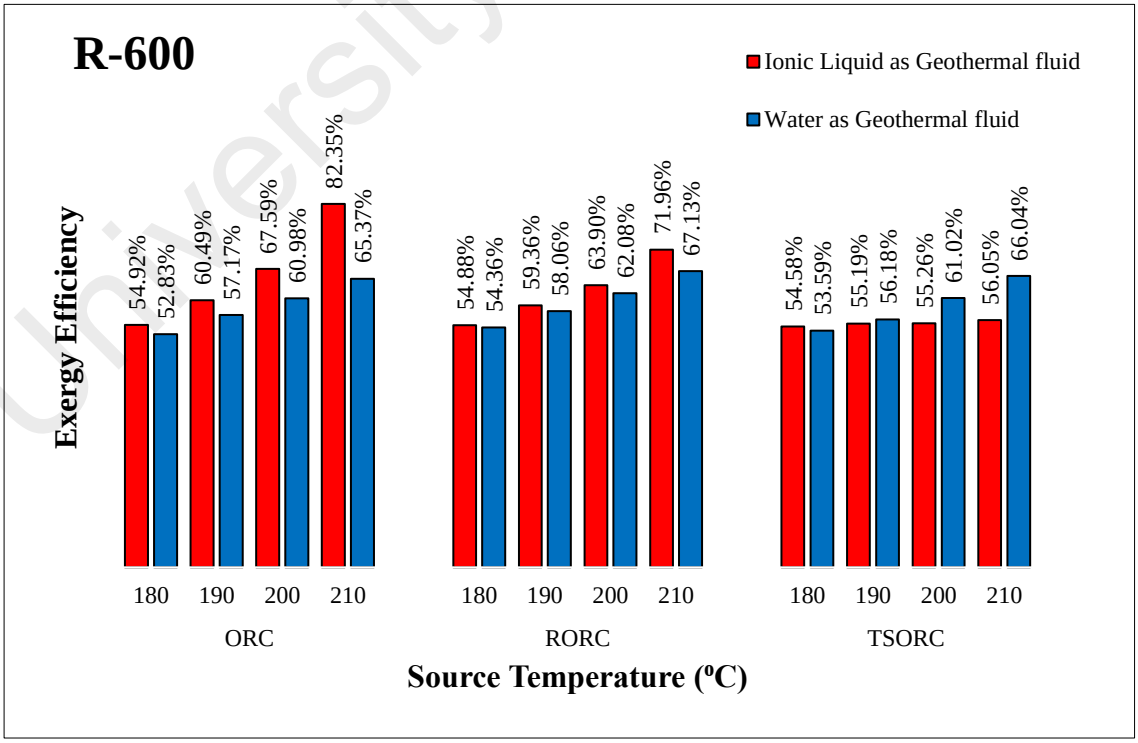

(a)

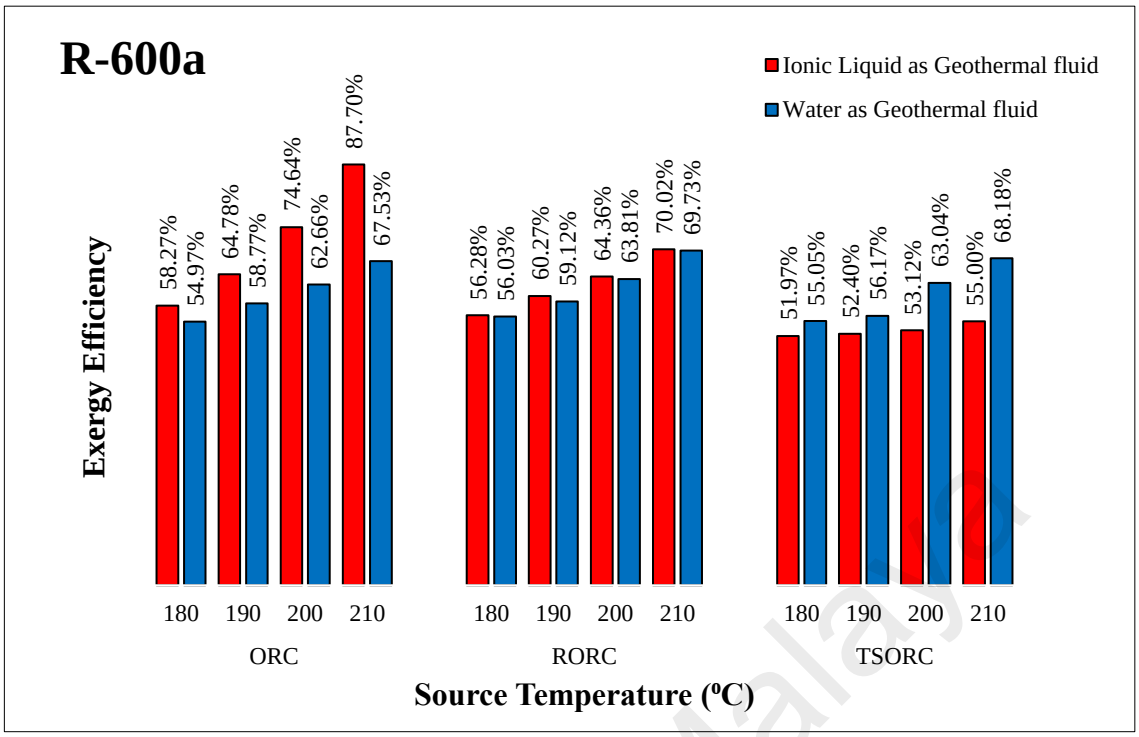

(b)

Figure 4. 2: Comparison of $C_9H_{14}NBF_4$ and water in three ORCs in terms of exergy efficiency with a) R-600 and b) R-600a

In addition, the best and the worst cycle performance, based on thermodynamic optimization, for both $C_9H_{14}NBF_4$ and water are illustrated in Figure 4. 3 (a and b). The best performance for $C_9H_{14}NBF_4$ occurs in the basic ORC cycle while the worst performance was found to be in the TSORC. On the other hand, when water was used as a geothermal fluid, the best cycle with the highest exergy efficiency is the RORC while the basic ORC exhibits the worst performance. Moreover, increasing $C_9H_{14}NBF_4$ temperature posed a significant rate of increase in exergy efficiency for basic ORC and RORC, while the rate of increase in the TSORC was relatively low. The difference in the rate of increase in exergy efficiency could most likely be due to the configuration of the cycles and the unique thermo-physical properties of ionic liquids.

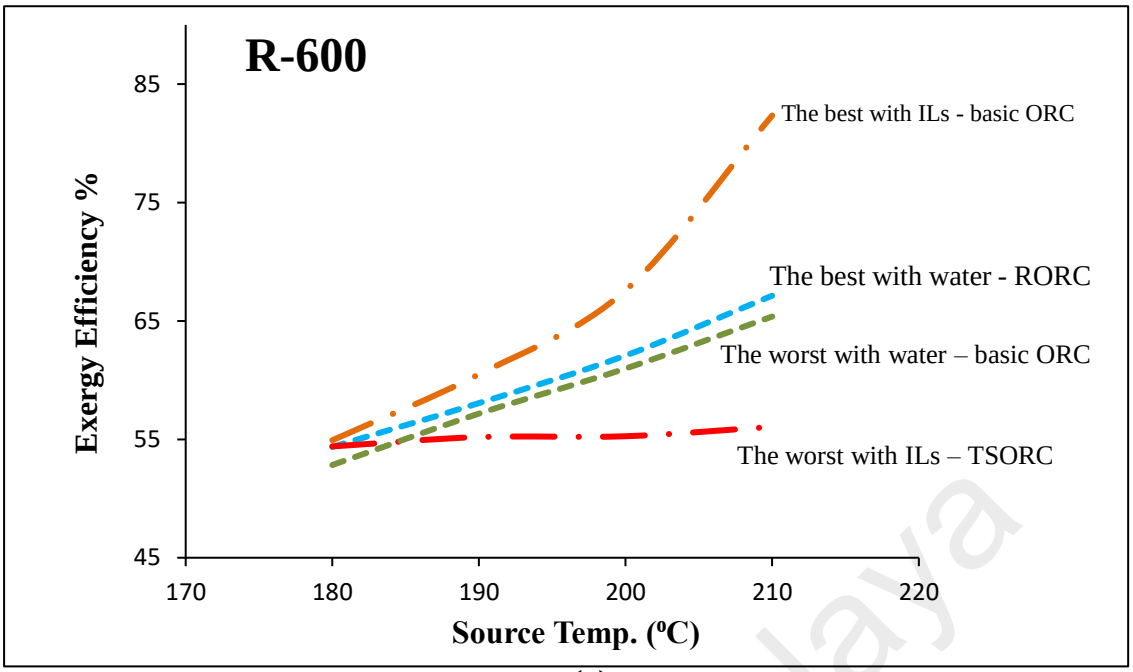

(a)

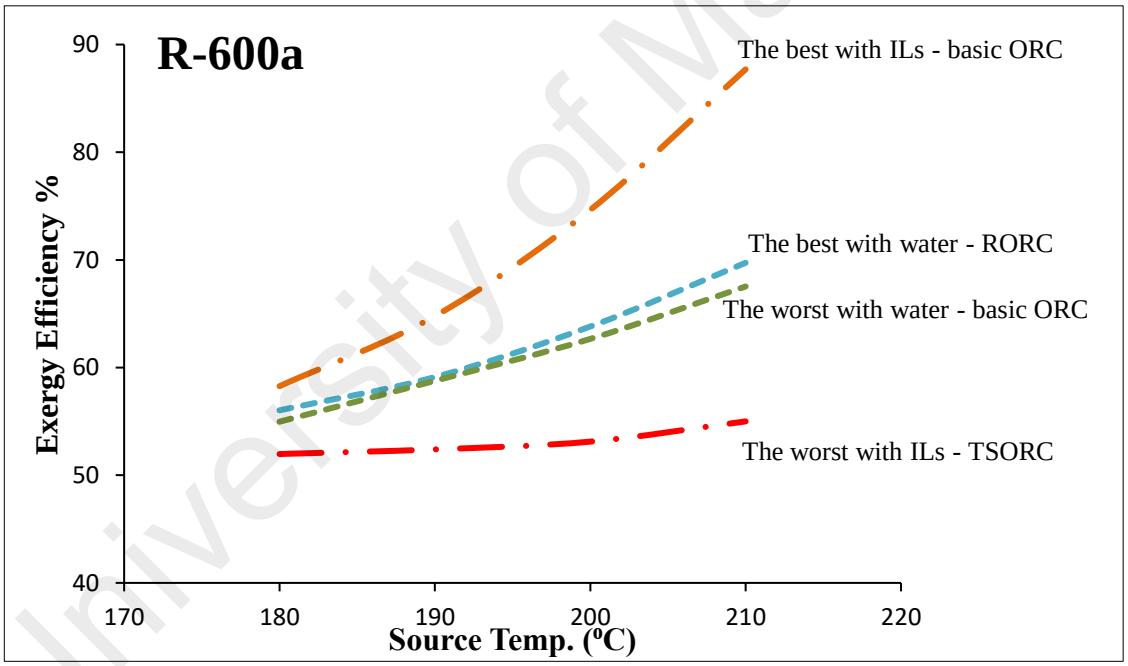

(b)

Figure 4. 3: The best and the worst cycle performance withwater and $C_9H_{14}NBF_4$ with a) R-600a and b) R-600a

The variation in the exergy efficiency of a basic ORC at varying pinch point temperature difference and the degree of superheat is shown in Figure 4. 4. It can be determined that both pinch point temperature difference and the degree of superheat do not facilitate the improvement of the cycle performance other than when these two operating parameters are at a minimum. The similar results were obtained in

thermodynamic models proposed by Kazemi and Samadi (2016) and Karimi and Mansouri (2018).

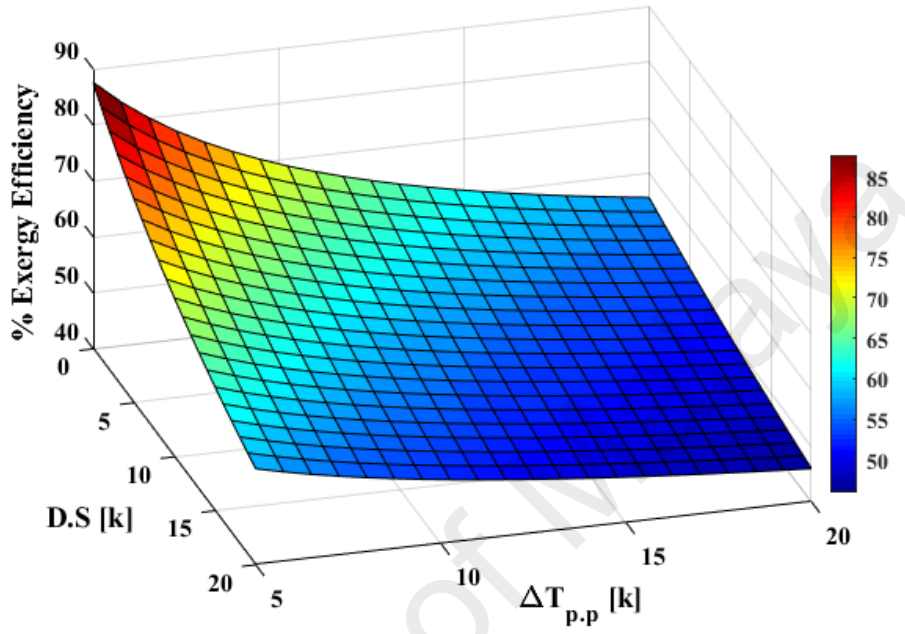

Figure 4. 4: The effect of pinch point temperature difference and degree of superheated on exergy efficiency in the basic ORC.

The variation in the efficiency of the basic ORC versus pinch point temperature difference and the evaporating temperature of R-600a is shown in Figure 4. 5. An increase in the evaporating temperature at a constant pinch point temperature difference gives rise to an increase in exergy efficiency. However, the pinch point temperature has no considerable effect on exergy efficiency.

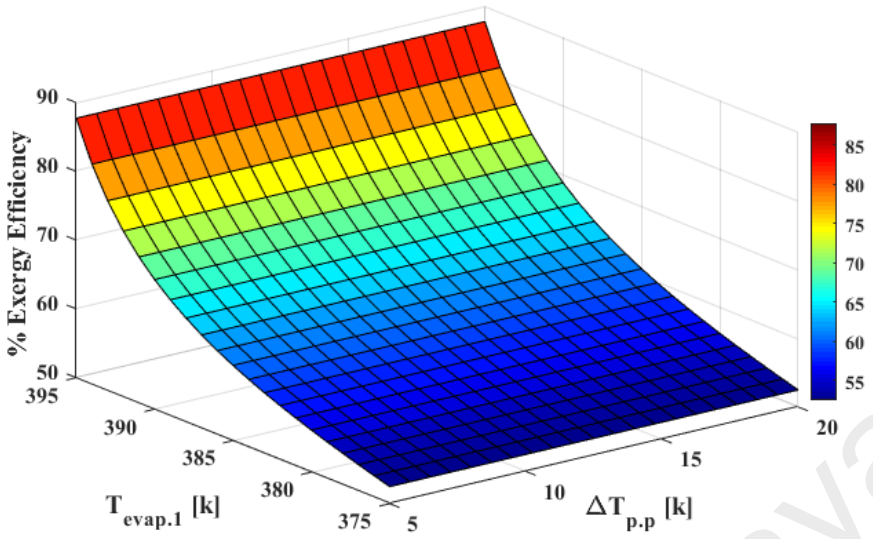

Figure 4. 5: The effect of pinch point temperature difference and evaporating temperature on exergy efficiency in the basic ORC

The variation of the mass flow rate of R-600a with respect to the degree of superheat and the evaporating temperature is illustrated in Figure 4. 6. The degree of superheat and the temperature of evaporator have an inverse impact on the flow rate of R-600a. The mass flow rate of the working fluid reaches a maximum value at minimum evaporating temperature. Considering the ORC is a closed-loop cycle, the working fluid (R-600/R-600a) was fed to the cycle once only. According to the processes 2-3 and 3-4 in the T-S diagram (Figure 3.3), the vapor is entered the turbine for electricity generation, and the remaining vapor in the turbine was liquified by the condenser to repeat the cycle. In this regards, due to the great performance of the $C_9H_{14}NBF_4$ as HTF in the evaporator, the maximum mass of the working fluid was superheated for electricity generation. Hence, as more and more the cycle is repeated, the working fluid mass flow rate in the cycle was decreased.

However, by increasing the degree of superheat, the working fluid mass flow rate is raised slightly. As mentioned earlier, the degree of superheat remained at lower bound in thermodynamic optimization, Tables 4.2 to 4.5. Therefore, this slight increase in the degree of superheat is not clearly visible through colors spectrum**.**

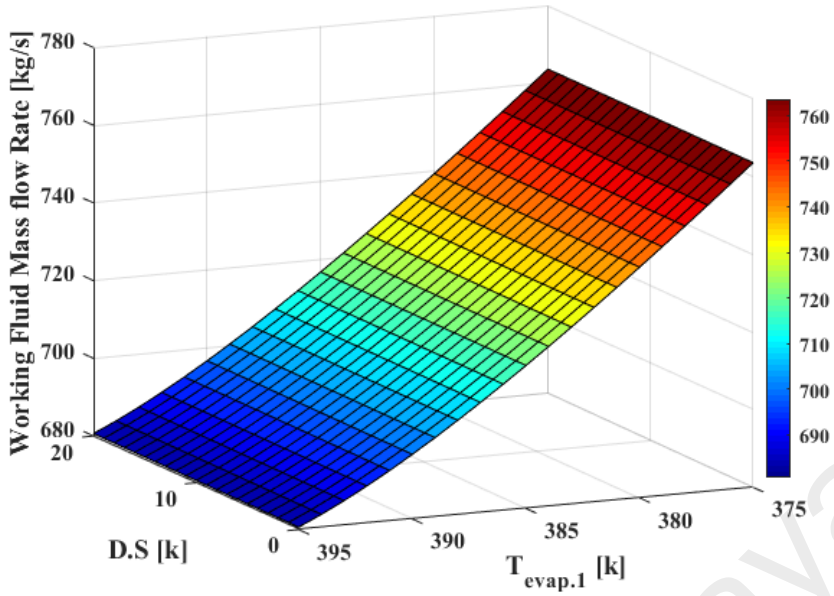

Figure 4. 6: The effect of the degree of superheat and evaporating temperature on working fluid mass flow rate in the **basic ORC**

The effect of the degree of superheat and evaporating temperature on exergy efficiency is shown in Figure 4. 7. A decrease in the evaporating temperature leads to a reduction in the performance of the cycle, while the effect of the degree of superheat on efficiency was found to be inconsequential.

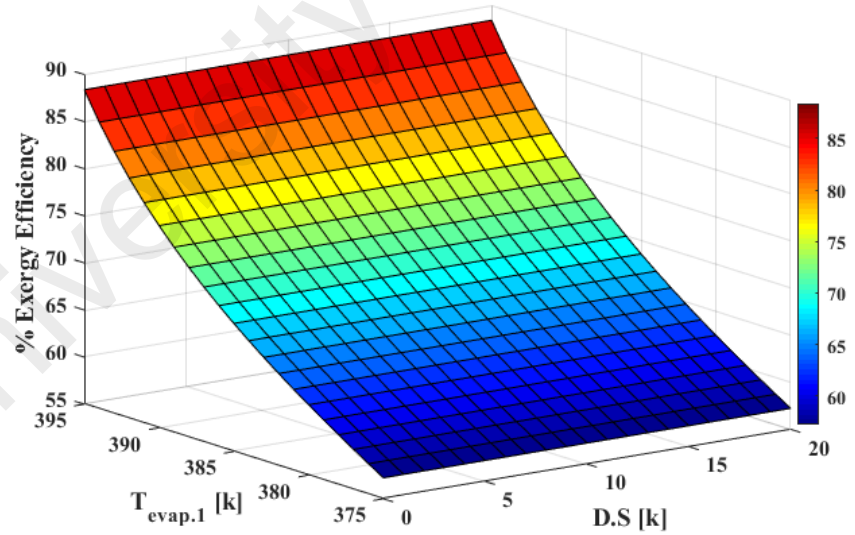

Figure 4. 7: The effect of the degree of superheat and evaporating temperature on exergy efficiency in a basic ORC

It is of interest to note that in thermodynamic optimization, when $C_9H_{14}NBF4$ was considered as a geothermal fluid, the highest exergy efficiency was obtained in a basic ORC configuration (87.70%) rather than the RORC or the TSORC. In contrast, with water as a geothermal fluid, the highest exergy efficiency was obtained in the RORC

configuration (69.73%). The almost 30% difference in efficiency when $C_9H_{14}NBF_4$ was utilized rather than water, compounded by the better performance being obtained in the simplest of the ORC configurations, signifies that the deliberation of ionic liquids as a geothermal fluid is well worth a closer look. Consequently, the use of an ionic liquid may be justifiable, not only from a thermodynamic point of view but also from an economic viewpoint since a basic ORC is more cost-effective and affordable.

4.4 Economic optimization

The optimized exergy efficiencies and specific investment costs (SIC) based on economic objective function with R-600a and R-600 as the working fluids are shown in Figure 4. 8. The exergy efficiencies for all three cycles using both geothermal fluids were found to increase with an increase in temperature. The relation between the heat source temperature and cycle's efficiency is in line with the research conducted by Li et al. (2019). As can be seen in Figure 4. 8, basic ORC and RORC demonstrated higher efficiencies when $C_9H_{14}NBF_4$ was used while TSORC performed better when water was utilized as a geothermal fluid. Overall, basic ORC with R-600a as the working fluid and $C_9H_{14}NBF_4$ as a geothermal fluid obtained the highest exergy efficiency.

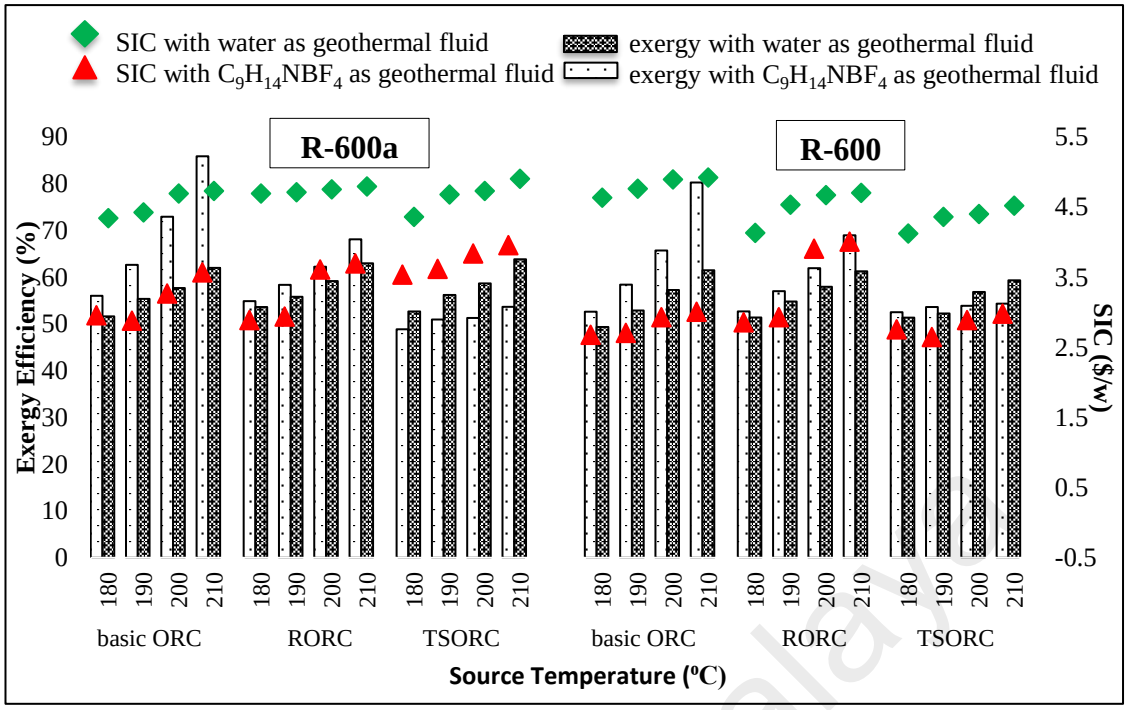

Figure 4. 8: Comparison of SIC and exergy efficiency obtained in economic optimization with water and C9H14NBF4

The required specific investment cost for all ORC – $C_9H_{14}NBF_4$ combinations were found to be lower than all ORC – water combinations. The lowest specific investment cost was obtained at 2.88 $/W for the basic ORC – $C_9H_{14}NBF_4$ combination with R-600a as a working fluid at 190 °C. Moreover, the optimized parameters in the economic optimization are in good agreement with the boundaries considered, where the evaporating temperatures are between the operating bounds and the pinch point temperature differences reached the minimum value of the optimization boundaries. On the other hand, the behavior of the degree of superheat under economic objective function is contradictory to that subjected under thermodynamic objective function. Under economic optimization, the degree of superheat tends to be a maximum, while it reaches a minimum in thermodynamic optimization. The trends of the optimized parameters resembled those of studied by Kazemi and Samadi (2016) and Karimi and Mansouri (2018).

4.5 Thermo-economic optimization

As there were opposing behaviors observed under thermodynamic and economic objective functions during optimization, a multi-objective function (thermo-economic objective function) was employed. As part of the thermo-economic optimization, coefficient of linear weighted evaluation function (α) was assessed (3.93.1), and its value for all configurations is shown in Table 4. 2 to Table 4. 5. A varying degree of superheat (D.S) was observed to be within a range of 0 – 20 °C. The variations observed in the D.S values are consequences of the opposing thermodynamic and economic behaviors. The varying D.S behaviour observed is similar to the observation made by Kazemi and Samadi (2016). In thermo-economic optimization, the exergy efficiencies obtained and the amount of specific investment cost (SIC) required, are shown in Figure 4. 9 (a and b). It can be observed that when $C_9H_{14}NBF_4$ utilized as a geothermal fluid, the thermodynamic performance of the basic ORC and RORC were better than TSORC. The observed results are similar to those obtained via economic optimization. In the thermo-economic optimization, comparatively higher exergy efficiencies were observed at 210 °C for basic ORC and RORC, with $C_9H_{14}NBF_4$.

However, water as a geothermal fluid was a better match for TSORC with the best performance at 210 °C which is in agreement with the work done by Karimi and Mansouri (2018) even though their heat source temperature was slightly lower. The highest exergy obtained for water was for the RORC configuration with R-600 as the working fluid.

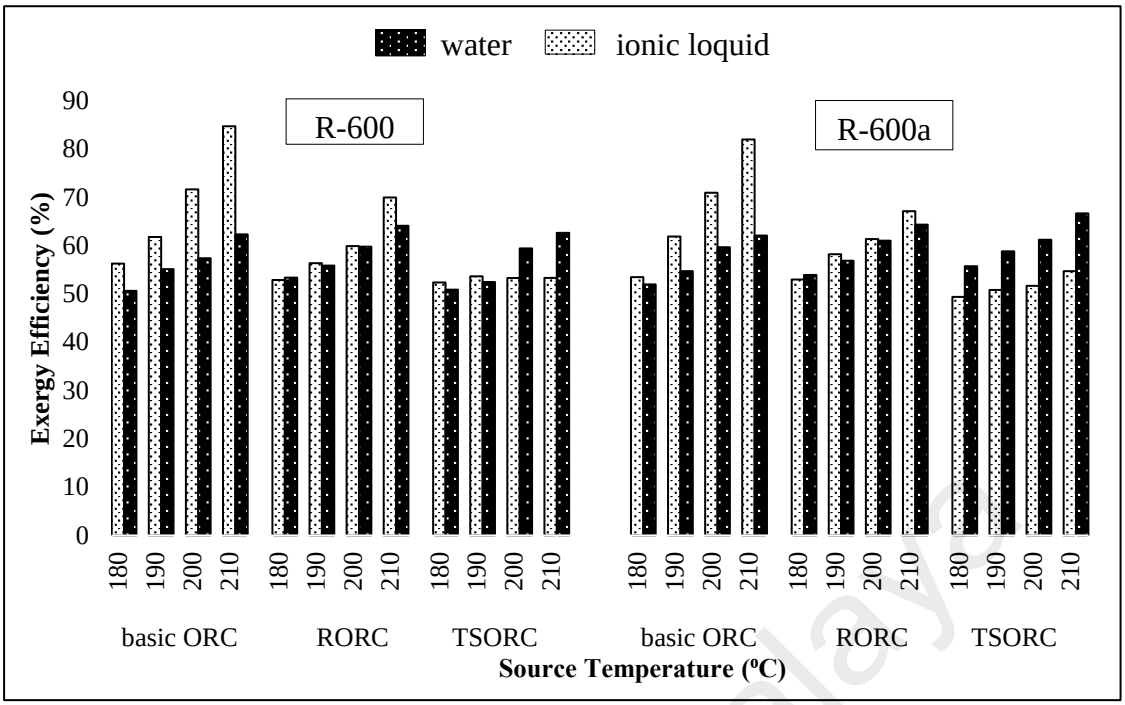

(a)

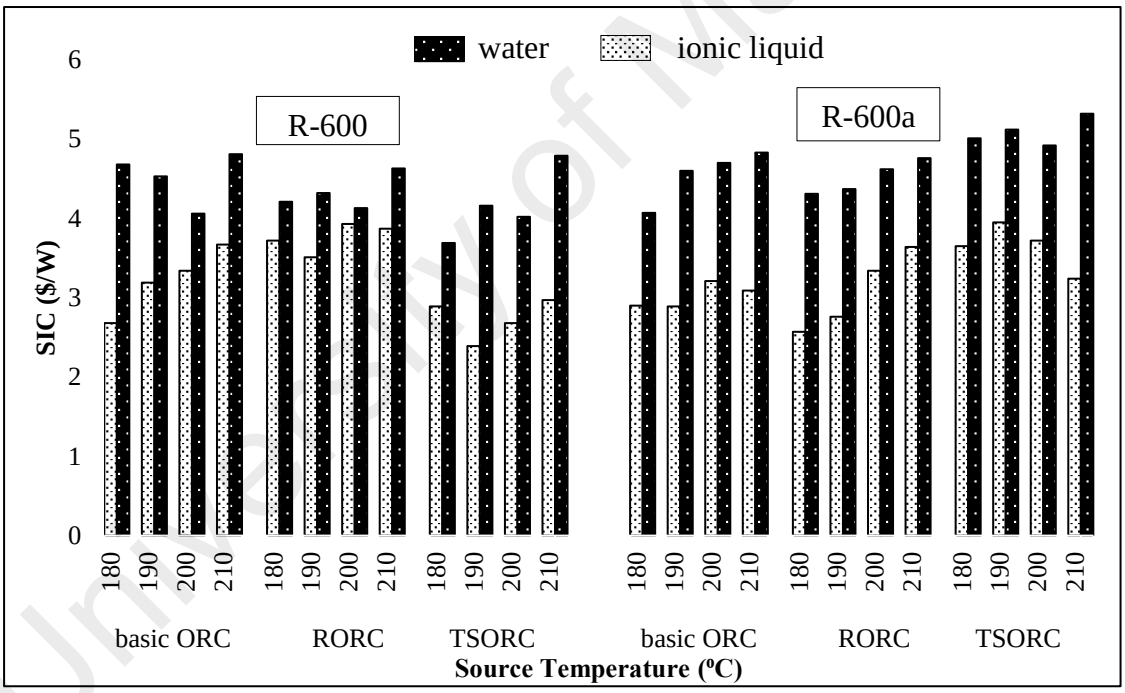

(b)

Figure 4. 9: Comparisons based on thermo-economic optimization, with water and $C_9H_{14}NBF_4$ as geothermal fluids, and R-600 and R-600a as working fluids for (a) exergy efficiency (b) SIC

Figure 4. 9 (b) indicates that the amount of SIC obtained for all ORC – $C_9H_{14}NBF_4$ combinations were lower than that for all ORC – water combinations. The two lowest SIC obtained are at 2.39 ($/W) in TSORC with $C_9H_{14}NBF_4$ and R-600, and 2.57 ($/W)

in RORC with $C_9H_{14}NBF_4$ and R-600a. However, a maximum SIC value was obtained at 3.93 ($/W) in RORC with $C_9H_{14}NBF_4$ and R-600, and at 3.95 ($/W) in TSORC with $C_9H_{14}NBF_4$ and R-600a. In this regard, in terms of thermo-economic optimization, ionic liquid plays a significant role in decreasing the SIC of TSORC with R-600 and RORC with R-600a. It is noteworthy that the total investment cost evaluated for TSORC – water was up to 2 $/W more expensive than TSORC – $C_9H_{14}NBF_4$ with R-600a.

On the whole, it is observed here that the cycle with the highest thermodynamic performance does not commensurate with the lowest investment cost. This work has shown that in most cases, cycles using the ionic liquid as a geothermal fluid performed considerably better than water. This could be due to the great performance of the $C_9H_{14}NBF_4$ as HTF, which led to minimizing the temperature difference in the evaporator (PPTD) to vaporize the working fluid. Thus, where the ionic liquid is concerned, the performance of a basic ORC is found to be substantially higher even though the required investment cost is roughly in the mid-range of the other two configurations.

In the present study, the optimal configuration with ionic liquid as a geothermal fluid is determined to be the basic ORC. It has been determined earlier that TSORC does not perform as well with ionic liquid. A comparison between the basic ORC and the RORC shows small differences in SIC values but a pronounced difference in exergy efficiencies as temperature increases. Hence, the basic ORC is determined to be the optimal choice of configuration. In terms of working fluids, R-600 was found to perform slightly better than R-600a but at a higher cost.

It is of interest to note here that under thermo-economic optimization, the basic ORC with $C_9H_{14}NBF_4$ and R-600 has higher exergy efficiencies compared to those obtained under sole thermodynamic optimization. Since thermo-economic optimization is a compromise between two opposing objective functions of thermodynamic and economic,

exergy efficiencies obtained under thermo-economic optimization were expected to be lower. However, the basic ORC – $C_9H_{14}NBF_4$ – R-600 combination was found to be an anomaly. For other combinations of ORC – geothermal fluid – working fluid, the exergy efficiencies obtained under thermo-economic optimization were indeed lower. In this regard, the performance of the cycle for three objective functions was evaluated and the factors for the anomaly were determined as follows. One significant factor is expressed in accordance with equations (3.2), (3.9), (3.46) and (3.69). In the mentioned equations, the mass flow rate of the working fluid has a direct relation with exergy efficiency. Therefore, in thermo-economic optimization, the increase in exergy efficiency is a result of an increase in the mass flow rate of the working fluid (R-600), shown in Figure 4. 10. In this regard, the increase in mass flow rate, in combination with the ionic liquid being a great heat transfer fluid and R-600 having the desired performance as a working fluid due to its properties, while running simulations at high geothermal heat source temperatures, most likely contributed to the anomalous behavior.

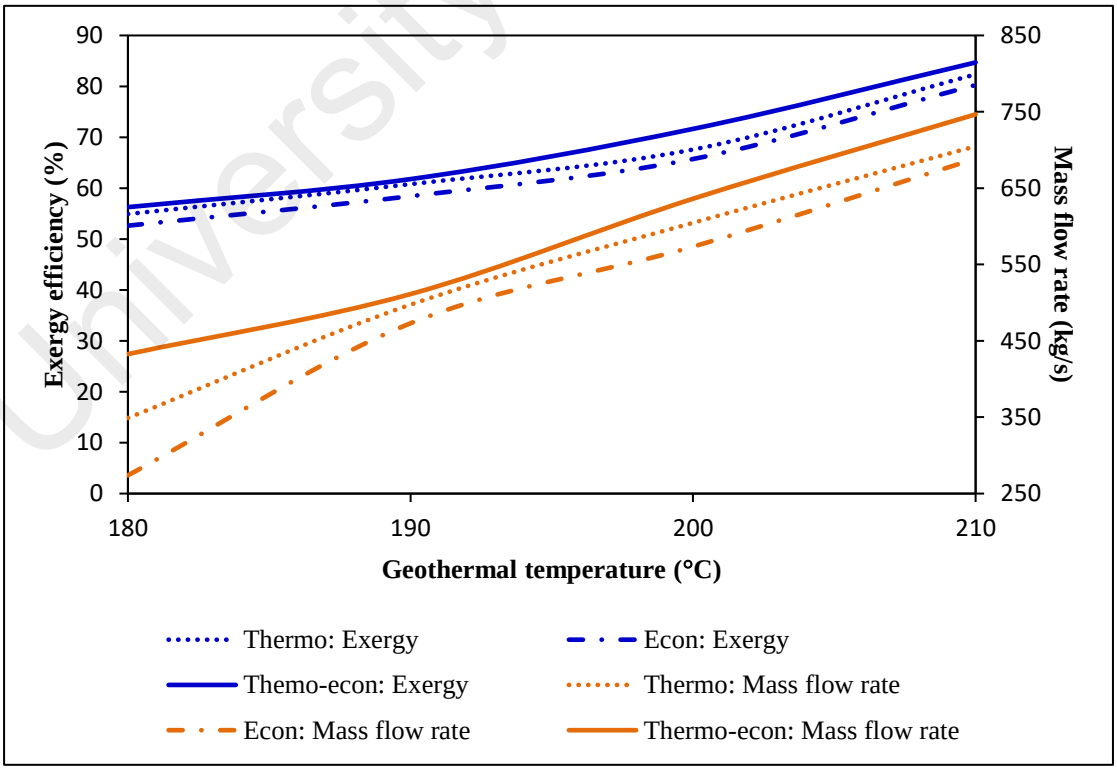

Figure 4. 10: Exergy efficiency of the basic ORC and mass flow rate of R-600 versus temperature, optimized under thermodynamic, economic and thermo-economic objective functions

CHAPTER 5: CONCLUSIONS AND RECOMMENDATIONS

In the present study, comprehensive thermodynamic and economic modeling was conducted on the basic ORC, RORC and TSORC. Then, the results of thermo-economic analysis are used to compare the simultaneous performance of three configurations from thermodynamic and economic viewpoints. The operating parameters, evaporative and regenerative temperatures, pinch point temperature difference of evaporators and the degree of superheat, are carried out to assess the performance of the considered cycles and the effect of these parameters on different objective functions are evaluated. The thermodynamic modeling includes the study of energy efficiency and exergy efficiency. Furthermore, thermo-economic optimization was carried out on each system to maximize exergy efficiency and minimize the cost per exergy unit for energy production. The main findings from this study are summarized below.

By taking advantage of the thermophysical properties of ionic liquids, improved cycle performance with $C_9H_{14}NBF_4$ was observed from thermodynamic and economic viewpoints. Based on thermodynamic optimization, the highest exergy efficiencies were obtained in the basic ORC rather than in the modified ORC architectures, with R-600 and R-600a as the working fluids. Pinch point temperature difference and the degree of superheat do not pose a significant impact on exergy efficiency and tend to a minimum value within their selected bands. However, under the economic objective function, the degree of superheat tended to a maximum. Under thermo-economic optimization, ionic liquid outperformed water for both basic ORC and RORC configurations. In all cases, the utilization of ionic liquid as a geothermal fluid also commensurate with lower specific investment costs. The optimum cycle under thermo-economic optimization was a basic ORC with $C_9H_{14}NBF_4$ as a geothermal fluid and R-600 as the working fluid. By custom, the efficiency of ORCs is typically raised at the expense of having to include additional unit operations such as an evaporator. In contrast, the present work determines that a

better cycle performance can be obtained by replacing water with an ionic liquid as a geothermal fluid (thermodynamically and economically) while keeping to the basics of the organic Rankine cycle. As the world trudges through a global water crisis, replacing water as a geothermal fluid may become a necessity.

Recommendations

Based on the present findings, it is recommended that the following areas can be further studied. The ionic liquid used in this study is 1-butylpyridinium tetrafluoroborate, $C_9H_{14}NBF_4$, a known green chemical and non-volatile compound with good thermal and chemical stability, and significant heat capacity is utilized as a geothermal fluid. It is highly recommended that other ionic liquids are examined to compare the efficiency of cycles. Besides, the performance of the dual-loop organic Rankine cycle can be considered for optimization with ionic liquid as a geothermal fluid. In the present work, medium to high heat source inlet temperatures are selected for optimization of organic Rankine cycles. It is recommended that the performance of ORC - ionic liquid combination be optimized for inlet geothermal temperatures that are outside of the range considered in this study. The working fluid considered in this study is R-600 and R-600a due to their characteristics and high efficiencies compared to other organic fluids. While these fluids were wisely selected based on their characteristics, it is suggested to evaluate other organic fluids to explore higher efficiency operation. An investigation into the effects of using a mixture of working fluids instead of a pure organic fluid, the performance of ORCs with ionic liquid could be further assessed.

At the current juncture, the viability of using the ionic liquid as a geothermal fluid may seem low due to the associated material costs. At this stage, the material price of ionic liquids is high because these materials are mainly used at the research stage, rather than having been fully commercialized. The emergence use of ionic liquids on an industrial

scale is being seen in sectors such as catalysis/ biocatalysis, electrochemistry, synthesis, materials science, and separation technology (Zhang, 2016). Therefore, the future lower pricing of ionic liquids is optimistic. It is envisioned that once ionic liquids are fully commercialized, the material price will, more often than not, become more cost-effective. Additionally, its use in the present work is in a closed loop; thereby, involving only the costs of replacing the materials in case of leakages. The upside to using an ionic liquid, in comparison to water, is that the investment cost is comparatively lower, with a higher level of energy production. In fact, the optimal configuration for ionic liquid is the basic ORC. In comparison with water that requires either RORC or TSORC for optimal energy production, basic ORC is the simplest of the three configurations and the cheapest to maintain. Thus, the savings accrued in the investment costs, and the additional profits obtained from higher energy production, may offset the costs of the ionic liquid.

REFERENCE

Abolhosseini, S., Heshmati, A., & Altmann, J. (2014). *A Review of Renewable Energy Supply and Energy Efficiency Technologies*. Retrieved from

Aneke, M., Agnew, B., & Underwood, C. (2011). Performance analysis of the Chena binary geothermal power plant. *Applied Thermal Engineering, 31*(10), 1825-1832.

Aparicio, S., Atilhan, M., & Karadas, F. (2010). Thermophysical Properties of Pure Ionic Liquids: Review of Present Situation. *Industrial & Engineering Chemistry Research, 49*(20), 9580-9595.

Ashouri, M., Razi Astaraei, F., Ghasempour, R., Ahmadi, M. H., & Feidt, M. (2017). Thermodynamic and economic evaluation of a small-scale organic Rankine cycle integrated with a concentrating solar collector. *International Journal of Low-Carbon Technologies, 12*(1), 54-65.

Astolfi, M., Romano, M. C., Bombarda, P., & Macchi, E. (2014a). Binary ORC (organic Rankine cycles) power plants for the exploitation of medium–low temperature geothermal sources – Part A: Thermodynamic optimization. *Energy, 66*, 423-434.

Astolfi, M., Romano, M. C., Bombarda, P., & Macchi, E. (2014b). Binary ORC (Organic Rankine Cycles) power plants for the exploitation of medium–low temperature geothermal sources – Part B: Techno-economic optimization. *Energy, 66*, 435-446.

Bao, J., & Zhao, L. (2013). A review of working fluid and expander selections for organic Rankine cycle. *Renewable and Sustainable Energy Reviews, 24*, 325-342.

Bertani, R. (2012). Geothermal power generation in the world 2005–2010 update report. *Geothermics, 41*, 1-29.

Bier, M., & Dietrich, S. (2010). Vapor Pressure of Ionic Liquids. *Molecular Physics - MOL PHYS, 108*, 211.

Bošnjaković, M., Stojkov, M., & JurjeviĆ, M. (2019). Environmental Impact of Geothermal Power Plants. *26*, 1515-1522.

Braimakis, K., & Karellas, S. (2017). Integrated thermoeconomic optimization of standard and regenerative ORC for different heat source types and capacities. *Energy, 121*, 570-598.

Braimakis, K., & Karellas, S. (2018). Energetic optimization of regenerative Organic Rankine Cycle (ORC) configurations. *Energy Conversion and Management, 159*, 353-370.

Brennecke, F., & Edward, J. M. (2001). Ionic Liquids: Innovative Fluids for Chemical Processing. *AIChE Journal, 47*, 2384 - 2389.

Chamorro, C. R., Mondéjar, M. E., Ramos, R., Segovia, J. J., Martín, M. C., & Villamañán, M. A. (2012). World geothermal power production status: Energy, environmental and economic study of high enthalpy technologies. *Energy, 42*(1), 10-18.

Chen, H., Goswami, D. Y., & Stefanakos, E. K. (2010). A review of thermodynamic cycles and working fluids for the conversion of low-grade heat. *Renewable and Sustainable Energy Reviews, 14*(9), 3059-3067.

Cox, K. R., & Chapman, W. G. (2001). The Properties of Gases and Liquids, 5th Edition By Bruce E. Poling (University of Toledo), John M. Prausnitz (University of California at Berkeley), and John P. O'Connell (University of Virginia). McGraw-Hill: New York. 2001. 768 pp. $115.00. ISBN 0-07-011682-2. *Journal of the American Chemical Society, 123*(27), 6745-6745.

Dai, C., & Chen, V. (2008). Classification of shallow and deep geothermal energy. *Transactions - Geothermal Resources Council, 32*, 270-273.

Dai, Y., Wang, J., & Gao, L. (2009). Parametric optimization and comparative study of organic Rankine cycle (ORC) for low grade waste heat recovery. *Energy Conversion and Management, 50*(3), 576-582.

Deshmukh, S., Bhattacharya, S., Jain, A., & Paul, A. R. (2019). Wind turbine noise and its mitigation techniques: A review. *Energy Procedia, 160*, 633-640.

Dincer, I. (2018). *comprehensive energy systems* (Vol. 1). University of Ontario, Institute of Technology, Oshawa,Canada.: Elsevier.

DiPippo, R. (2008a). Chapter 7 - Dry-Steam Power Plants *Geothermal Power Plants (Second Edition)* (pp. 135-156). Oxford: Butterworth-Heinemann.

DiPippo, R. (2008b). Chapter 8 - Binary Cycle Power Plants *Geothermal Power Plants (Second Edition)* (pp. 157-189). Oxford: Butterworth-Heinemann.

DiPippo, R. (2008c). Chapter 19 - Environmental Impact of Geothermal Power Plants *Geothermal Power Plants (Second Edition)* (pp. 385-410). Oxford: Butterworth-Heinemann.

DiPippo, R. (2013). Geothermal double-flash plant with interstage reheating: An updated and expanded thermal and exergetic analysis and optimization. *Geothermics, 48*, 121-131.

DiPippo, R. (2016a). Chapter 3 - Geothermal Well Drilling. In R. DiPippo (Ed.), *Geothermal Power Plants (Fourth Edition)* (pp. 49-59). Oxford: Butterworth-Heinemann.

DiPippo, R. (2016b). Chapter 5 - Single-Flash Steam Power Plants. In R. DiPippo (Ed.), *Geothermal Power Plants (Fourth Edition)* (pp. 107-142). Oxford: Butterworth-Heinemann.

DiPippo, R. (2016c). Chapter 6 - Double- and Triple-Flash Steam Power Plants. In R. DiPippo (Ed.), *Geothermal Power Plants (Fourth Edition)* (pp. 143-168). Oxford: Butterworth-Heinemann.

DiPippo, R. (2016d). Chapter 7 - Dry-Steam Power Plants. In R. DiPippo (Ed.), *Geothermal Power Plants (Fourth Edition)* (pp. 169-192). Oxford: Butterworth-Heinemann.

DiPippo, R. (2016e). Chapter 11 - Larderello Dry-Steam Power Plants, Tuscany, Italy. In R. DiPippo (Ed.), *Geothermal Power Plants (Fourth Edition)* (pp. 321-343). Oxford: Butterworth-Heinemann.

DiPippo, R. (2016f). Chapter 13 - Geothermal Power Plants of New Zealand. In R. DiPippo (Ed.), *Geothermal Power Plants (Fourth Edition)* (pp. 369-402). Oxford: Butterworth-Heinemann.

DiPippo, R. (2016g). Chapter 23 - Environmental Impact of Geothermal Power Plants. In R. DiPippo (Ed.), *Geothermal Power Plants (Fourth Edition)* (pp. 657-684). Oxford: Butterworth-Heinemann.

DiPippo, R. (2016h). Part 2. Geothermal Power Generating Systems. In R. DiPippo (Ed.), *Geothermal Power Plants (Fourth Edition)* (pp. 105-106). Oxford: Butterworth-Heinemann.

Domańska, U. (2006). Thermophysical properties and thermodynamic phase behavior of ionic liquids. *Thermochimica Acta, 448*(1), 19-30.

Dye, S. T. (2012). *Geoneutrinos and the radioactive power of the Earth* (Vol. 50).

El Haj Assad, M., Bani-Hani, E., & Khalil, M. (2017). Performance of geothermal power plants (single, dual, and binary) to compensate for LHC-CERN power consumption: comparative study. *Geothermal Energy, 5*(1), 17.

Fakeye, A., & Oyedepo, S. (2018). A Review of Working Fluids for Organic Rankine Cycle (ORC) Applications. *IOP Conference Series: Materials Science and Engineering, 413*, 012019.

Forero, L., & J, J. (2011). Wagner liquid–vapour pressure equation constants from a simple methodology. *The Journal of Chemical Thermodynamics, 43*, 1235–1251.

Franco, A., & Vaccaro, M. (2012). An integrated "Reservoir-Plant" strategy for a sustainable and efficient use of geothermal resources. *Energy, 37*(1), 299-310.

Franco, A., & Villani, M. (2009). Optimal design of binary cycle power plants for water-dominated, medium-temperature geothermal fields. *Geothermics, 38*(4), 379-391.

Fredlake, C. P., Crosthwaite, J. M., Hert, D. G., Aki, S. N. V. K., & Brennecke, J. F. (2004). Thermophysical Properties of Imidazolium-Based Ionic Liquids. *Journal of Chemical & Engineering Data, 49*(4), 954-964.

G. Montalbán, M., Collado-González, M. M., Díaz Baños, F. G., & Víllora, G. (2017). Predicting Density and Refractive Index of Ionic Liquids (pp. 339-368).

Gitonga., G. (2017). *Geothermal Power Plants for Medium and High Temperature Steam and An Overview of Wellhead Power Plants*. Paper presented at the Exploration and Development of Geothermal Resources, Lake Bogoria and Lake Naivasha, Kenya.

Goswami, D. Y. (2004). *The CRC Handbook of Mechanical Engineering*.

Guo, C., Du, X., Yang, L., & Yang, Y. (2015). Organic Rankine cycle for power recovery of exhaust flue gas. *Applied Thermal Engineering, 75*, 135-144.

Györke, G., Deiters, U. K., Groniewsky, A., Lassu, I., & Imre, A. R. (2018). Novel classification of pure working fluids for Organic Rankine Cycle. *Energy, 145*, 288-300.

Hærvig, J., Sørensen, K., & Condra, T. J. (2016). Guidelines for optimal selection of working fluid for an organic Rankine cycle in relation to waste heat recovery. *Energy, 96*, 592-602.

Hanbury, O., & Vasquez, V. R. (2018). Life cycle analysis of geothermal energy for power and transportation: A stochastic approach. *Renewable Energy, 115*, 371-381.

Harjanne, A., & Korhonen, J. M. (2018). Abandoning the concept of renewable energy. *Energy Policy, 127*.

Heberle, F., Schifflechner, C., & Brüggemann, D. (2016). Life cycle assessment of Organic Rankine Cycles for geothermal power generation considering low-GWP working fluids. *Geothermics, 64*, 392-400.

Holm, A., Blodgett, L., Dan., J., & and Gawell, K. (2010). *Geothermal Energy: International Market Update*. Retrieved from

Hung, T. C., Wang, S. K., Kuo, C. H., Pei, B. S., & Tsai, K. F. (2010). A study of organic working fluids on system efficiency of an ORC using low-grade energy sources. *Energy, 35*(3), 1403-1411.

Imran, M., Park, B. S., Kim, H. J., Lee, D. H., Usman, M., & Heo, M. (2014). Thermo-economic optimization of Regenerative Organic Rankine Cycle for waste heat recovery applications. *Energy Conversion and Management, 87*, 107-118.

Jalilinasrabady, S., Itoi, R., Valdimarsson, P., Saevarsdottir, G., & Fujii, H. (2012). Flash cycle optimization of Sabalan geothermal power plant employing exergy concept. *Geothermics, 43*, 75-82.

Kagel, A., Bates, D., & Gawell, K. (2005). *A guide to geothermal energy and the environment*. Retrieved from United States: https://www.osti.gov/servlets/purl/897425

Kanoglu, M., & Bolatturk, A. (2008). Performance and parametric investigation of a binary geothermal power plant by exergy. *Renewable Energy, 33*(11), 2366-2374.

Karimi, S., & Mansouri, S. (2018). A comparative profitability study of geothermal electricity production in developed and developing countries: Exergoeconomic analysis and optimization of different ORC configurations. *Renewable Energy, 115*, 600-619.

Kazemi, N., & Samadi, F. (2016). Thermodynamic, economic and thermo-economic optimization of a new proposed organic Rankine cycle for energy production from geothermal resources. *Energy Conversion and Management, 121*, 391-401.

Kazemi, S., Nor, M. I. M., & Teoh, W. H. (2020). Thermodynamic and economic investigation of an ionic liquid as a new proposed geothermal fluid in different organic Rankine cycles for energy production. *Energy, 193*, 116722.

Kern, D. (1986). *Process heat transfer* (i. S. ed. Ed.). McGraw-Hill: International Auckland Bogota.

Le, V. L., Feidt, M., Kheiri, A., & Pelloux-Prayer, S. (2014). Performance optimization of low-temperature power generation by supercritical ORCs (organic Rankine cycles) using low GWP (global warming potential) working fluids. *Energy, 67*, 513-526.

Le, V. L., Kheiri, A., Feidt, M., & Pelloux-Prayer, S. (2014). Thermodynamic and economic optimizations of a waste heat to power plant driven by a subcritical ORC (Organic Rankine Cycle) using pure or zeotropic working fluid. *Energy, 78*, 622-638.

Lee, J. H., Lee, J. W., & Kang, Y. T. (2016). CO2 regeneration performance enhancement by nanoabsorbents for energy conversion application. *Applied Thermal Engineering, 103*, 980-988.

Lemmon E, McLinden M, & D., F. (2011). *Thermophysical properties of fluid systems in NIST chemistry WebBook* (M. W. Linstrom PJ Ed.). Gaithersburg (MD).

Li, J., Ge, Z., Duan, Y., & Yang, Z. (2019). Effects of heat source temperature and mixture composition on the combined superiority of dual-pressure evaporation organic Rankine cycle and zeotropic mixtures. *Energy, 174*, 436-449.

Li, T., Wang, Q., Zhu, J., Hu, K., & Fu, W. (2015). Thermodynamic optimization of organic Rankine cycle using two-stage evaporation. *Renewable Energy, 75*, 654-664.

Li, T., Zhang, Z., Lu, J., Yang, J., & Hu, Y. (2015). Two-stage evaporation strategy to improve system performance for organic Rankine cycle. *Applied Energy, 150*, 323-334.

Li, X., Liu, T., & Chen, L. (2018). Thermodynamic Performance Analysis of an Improved Two-Stage Organic Rankine Cycle. *Energies, 11*(11).

Lin, W., Nilsson, L., & Malutta, R. (2017). *Waste Heat Recovery by Organic Rankine Cycle (ORC) for Moist Exhaust Gases From Paper Industry.* Paper presented at the ASME 2017 International Mechanical Engineering Congress and Exposition.

Liu, B.-T., Chien, K.-H., & Wang, C.-C. (2004). Effect of working fluids on organic Rankine cycle for waste heat recovery. *Energy, 29*(8), 1207-1217.

Liu, C., He, C., Gao, H., Xu, X., & Xu, J. (2012). The Optimal Evaporation Temperature of Subcritical ORC Based on Second Law Efficiency for Waste Heat Recovery. *Entropy, 14*(3).

Liu, W., Wieland, C. M., Meinel, D. M., & Spliethoff, H. (2016). *Optimal heat source temperature for supercritical organic rankine cycle*.

Lukawski, M., Tester, J., Bendall, B., Goldstein, B., Hiriart, G., Gutiérrez-Negrín, L., . . . Muraoka, H. (2018). Geothermal Energy, Nature, Use, and Expectations (pp. 35-46).

Mallakpour, S., & Dinari, M. (2012). Ionic Liquids as Green Solvents: Progress and Prospects. In A. Mohammad & D. Inamuddin (Eds.), *Green Solvents II: Properties and Applications of Ionic Liquids* (pp. 1-32). Dordrecht: Springer Netherlands.

Martínez-Gomez, J., Peña-Lamas, J., Martín, M., & Ponce-Ortega, J. M. (2017). A multi-objective optimization approach for the selection of working fluids of geothermal facilities: Economic, environmental and social aspects. *Journal of Environmental Management, 203*, 962-972.

Moran, E. F., Lopez, M. C., Moore, N., Müller, N., & Hyndman, D. W. (2018). Sustainable hydropower in the 21st century. *Proceedings of the National Academy of Sciences, 115*(47), 11891-11898.

Muhammad, A., Abdul Mutalib, M. I., Wilfred, C. D., Murugesan, T., & Shafeeq, A. (2008). Thermophysical properties of 1-hexyl-3-methyl imidazolium based ionic liquids with tetrafluoroborate, hexafluorophosphate and bis(trifluoromethylsulfonyl)imide anions. *The Journal of Chemical Thermodynamics, 40*(9), 1433-1438.

Mun, J., & Sim, H. (2012). *Handbook of ionic liquids : properties, applications, and hazards*. New York: Nova Science Publishers.

Navarro-Esbrí, J., Amat-Albuixech, M., Mota-Babiloni, A., Molés, F., Mateu-Royo, C., González, M., & Martí, J. (2019). *Small-Scale Organic Rankine Cycle for Domestic Biomass Fuelled Combined Heat and Power Applications*.

Nyambura., E. (2016). *DIRECT USE OF GEOTHERMAL ENERGY: MENENGAI DIRECT USE PILOT PROJECTS IN KENYA.* Paper presented at the 6th African Rift Geothermal Conference, Addis Ababa, Ethiopia.

Özkaraca, O., Keçebaş, P., Demircan, C., & Keçebaş, A. (2017). Thermodynamic Optimization of a Geothermal- Based Organic Rankine Cycle System Using an Artificial Bee Colony Algorithm. *Energies, 10*(11), 1691.

Pambudi, N. A., Itoi, R., Jalilinasrabady, S., Sirait, P., & Jaelani, K. (2015). Preliminary analysis of single flash combined with binary system using thermodynamic

assessment: a case study of Dieng geothermal power plant. *International Journal of Sustainable Engineering, 8*(4-5), 258-267.

Peng, D.-Y., & Robinson, D. B. (1976). A New Two-Constant Equation of State. *Industrial & Engineering Chemistry Fundamentals, 15*(1), 59-64.

Perry, R. H., Green, D. W., & Maloney, J. O. (1997). *Perry's chemical engineers' handbook* (7th ed. / ed.). New York: McGraw-Hill.

Perry Robert, H., Green Don, W., & Maloney James, O. (1997). *Perry's Chemical Engineers' Handbook* (Vol. 1-3). Technology & Engineering McGraw-Hill.

Peters, M., Timmerhaus, K., & West, R. (1968). *Plant design and economics for chemical engineers*. McGraw-Hill, New York.

Ravula, S., Larm, N., Mottaleb, M. A., Heitz, M., & Baker, G. (2019). Vapor Pressure Mapping of Ionic Liquids and Low-Volatility Fluids Using Graded Isothermal Thermogravimetric Analysis. *ChemEngineering, 3*.

Reddy, R. G., Zhang, Z., Arenas, M. F., & Blake, D. M. (2003). Thermal Stability and Corrosivity Evaluations of Ionic Liquids as Thermal Energy Storage Media. *High Temperature Materials and Processes, 22*(2), 87-94.

Rudiyanto, B., Illah, I., Pambudi, N. A., Cheng, C.-C., Adiprana, R., Imran, M., . . . Handogo, R. (2017). Preliminary analysis of dry-steam geothermal power plant by employing exergy assessment: Case study in Kamojang geothermal power plant, Indonesia. *Case Studies in Thermal Engineering, 10*, 292-301.

Rypkema, H. A. (2018). Chapter 2.1 - Environmental Chemistry, Renewable Energy, and Global Policy. In B. Török & T. Dransfield (Eds.), *Green Chemistry* (pp. 19-47): Elsevier.

Saleh, B., Koglbauer, G., Wendland, M., & Fischer, J. (2007). Working fluids for low-temperature organic Rankine cycles. *Energy, 32*(7), 1210-1221.

Saloux, E., Sorin, M., Nesreddine, H., & Teyssedou, A. (2018). Reconstruction procedure of the thermodynamic cycle of organic Rankine cycles (ORC) and selection of the most appropriate working fluid. *Applied Thermal Engineering, 129*, 628-635.

Samadi, F., & Kazemi, N. (2020). Exergoeconomic analysis of zeotropic mixture on the new proposed organic Rankine cycle for energy production from geothermal resources. *Renewable Energy, 152*, 1250-1265.

Saraswat, M., & Sharma, A. K. (2013). Genetic Algorithm for optimization using MATLAB. *International Journal of Advanced Research in Computer Science, 4*.

Shengjun, Z., Huaixin, W., & Tao, G. (2011). Performance comparison and parametric optimization of subcritical Organic Rankine Cycle (ORC) and transcritical power cycle system for low-temperature geothermal power generation. *Applied Energy, 88*(8), 2740-2754.

Shokati, N., Ranjbar, F., & Yari, M. (2015). Comparative and parametric study of double flash and single flash/ORC combined cycles based on exergoeconomic criteria. *Applied Thermal Engineering, 91*, 479-495.

Signanini, p., & Giancarlo, c. (2001). *HANDBOOK ON RENEWABLE ENERGY SOURCES*.

Sircar, A. (2009). Applications of Geothermal Energy. *3297*.

Smith, R. (2005). *Chemical process design and integration*. Chichester, West Sussex, England ;: Wiley.

Sui, D., Wiktorski, E., Røksland, M., & Basmoen, T. A. (2019). Review and investigations on geothermal energy extraction from abandoned petroleum wells. *Journal of Petroleum Exploration and Production Technology, 9*(2), 1135-1147.

Sun, W., Yue, X., & Wang, Y. (2017). Exergy efficiency analysis of ORC (Organic Rankine Cycle) and ORC-based combined cycles driven by low-temperature waste heat. *Energy Conversion and Management, 135*, 63-73.

Taylor, L., Water, M., & Susan., a. K. (2013, 17 -20 November). *Development of a Low Temperature Geothermal Organic Rankine Cycle Standard.* Paper presented at the Geothermal workshop Rotorua, New Zealand.

Tchanche, B. F., Lambrinos, G., Frangoudakis, A., & Papadakis, G. (2011). Low-grade heat conversion into power using organic Rankine cycles – A review of various applications. *Renewable and Sustainable Energy Reviews, 15*(8), 3963-3979.

Tiwari, D., Sherwani, A. F., Atheaya, D., & Arora, A. (2017). Energy and exergy analysis of solar driven recuperated organic Rankine cycle using glazed reverse absorber conventional compound parabolic concentrator (GRACCPC) system. *Solar Energy, 155*, 1431-1442.

Tubular Exchanger Manufacturers, A. (1999). *Standards of the Tubular Exchanger Manufacturers Association*. Tarrytown, N.Y.: Tublar Exchanger Manufacturers Association.

Turton, R., Bailie, R. C., Whiting, W. B., & J.A., S. (2009). *Analysis, synthesis, and design of chemical processes*: Pearson Education Inc.

Unverdi, M., & Cerci, Y. (2013). Performance analysis of Germencik Geothermal Power Plant. *Energy, 52*, 192-200.

Valkenburg, M. E. V., Vaughn, R. L., Williams, M., & Wilkes, J. S. (2005). Thermochemistry of ionic liquid heat-transfer fluids. *Thermochimica Acta, 425*(1), 181-188.

Vescovo, R., & Spagnoli, E. (2017). High Temperature ORC Systems. *Energy Procedia, 129*, 82-89.

Wang, J., Xu, P., Li, T., & Zhu, J. (2017). Performance enhancement of organic Rankine cycle with two-stage evaporation using energy and exergy analyses. *Geothermics, 65*, 126-134.

Wang, R., Jiang, L., Ma, Z., Gonzalez Diaz, A., Wang, Y., & Roskilly, T. (2019). Comparative Analysis of Small-Scale Organic Rankine Cycle Systems for Solar Energy Utilisation. *Energies, 12*.

Weiyao Tang, Zongmin Li, & Tu., Y. (2018). Sustainability Risk Evaluation for Large-Scale Hydropower Projects with Hybrid Uncertainty. *Sustainability, 10*(1).

Xi, H., Li, M.-J., Xu, C., & He, Y.-L. (2013). Parametric optimization of regenerative organic Rankine cycle (ORC) for low grade waste heat recovery using genetic algorithm. *Energy, 58*, 473-482.

Xiao, L., Wu, S.-Y., Yi, T.-T., Liu, C., & Li, Y.-R. (2015). Multi-objective optimization of evaporation and condensation temperatures for subcritical organic Rankine cycle. *Energy, 83*, 723-733.

Xu, W., Deng, S., Zhao, L., Su, W., Zhang, Y., Li, S., & Ma, M. (2018). How to quantitatively describe the role of the pure working fluids in subcritical organic Rankine cycle: A limitation on efficiency. *Energy Conversion and Management, 172*, 316-327.

Yadav, K., & Sircar, A. (2019). Application of low enthalpy geothermal fluid for space heating and cooling, honey processing and milk pasteurization. *Case Studies in Thermal Engineering, 14*, 100499.

Yang, M.-H., & Yeh, R.-H. (2015). Thermo-economic optimization of an organic Rankine cycle system for large marine diesel engine waste heat recovery. *Energy, 82*, 256-268.

Yue-feng, Y., Da, H., & Fang-zh, W. (2015, 19-25 April 2015). *Applications of the Screw Expander in Geothermal Power Generation in China.* Paper presented at the Proceedings World Geothermal Congress 2015, Melbourne, Australia.

Zeynali, A., Akbari, A., & Khalilian, M. (2019). Investigation of the performance of modified organic Rankine cycles (ORCs) and modified trilateral flash cycles (TFCs) assisted by a solar pond. *Solar Energy, 182*, 361-381.

Zhai, H., Shi, L., & An, Q. (2014). Influence of working fluid properties on system performance and screen evaluation indicators for geothermal ORC (organic Rankine cycle) system. *Energy, 74*, 2-11.

Zhang, S. (2016). Physicochemical properties of ionic liquid mixtures.

Zhao, Y., Lu, X., Zhu, J., Zhang, W., Hu, K., Xin, G., . . . Qin, Z. (2017). A study on selecting optimum flash and evaporation temperatures for four geothermal power generation systems under different geofluid's conditions. *Energy Procedia, 142*, 439-446.

Zheng, Y.-F., & Chen, Y.-X. (2016). Continental versus oceanic subduction zones. *National Science Review, 3*(4), 495-519.

LIST OF PUBLICATIONS AND PAPERS PRESENTED

PUBLICATION

Kazemi, S., Nor, M. I. M. and Teoh, W. H., 2020. Thermodynamic and economic investigation of an ionic liquid as a new proposed geothermal fluid in different organic Rankine cycles for energy production. Energy, 193, 116722.

SYMPOSIUM

Kazemi, S., Kazemi, N., Nor, M. I. M. and Teoh, W.H. (2019, October). Predicting the Refractive Index in Binary Systems of Ionic Liquids and Alcohol**.** Paper presented at 26th Regional Symposium of Chemical Engineering, Kuala Lumpur, Malaysia.